Neurogenesis and Oligodendrogenesis in the Adult Ventricular-Subventricular Zone During Pregnancy

Inauguraldissertation
zur
Erlangung der Würde eines Doktors der Philosophie
vorgelegt der
Philosophisch-Naturwissenschaftlichen Fakultät
der Universität Basel

von

Corina Gabriela Segalada

2022

Originaldokument gespeichert auf dem Dokumentenserver der Universität Basel
edoc.unibas.ch

Genehmigt von der Philosophisch-Naturwissenschaftlichen Fakultät

auf Antrag von:

Prof. Dr. Fiona Doetsch

Prof. Dr. Peter Scheiffele

Prof. Dr. Sebastian Jessberger

Basel, 22.03. 2022

The Dean of Faculty

Prof. Dr. Marcel Mayor

Table of Contents

List of Figures for Chapters 1 & 3 &4

List of Figures for Chapter 2 (manuscript)

Abbreviations

AOB	accessory olfactory bulb
CalB	calbindin
CalR	calretinin
Cc	corpus callosum
CldU	5-chloro-2'-deoxyuridine
DCX	doublecortin
DG	dentate gyrus
DLW	dorsolateral wedge
DMC	dorsomedial corner
GC	granule cell
GCL	granule cell layer
Gd	gestation day
GL	glomerular layer
IdU	5-iodo-2'-deoxyuridine
LV	lateral ventricle
LW	lateral wall
MBP	myelin basic protein.
MOB	main olfactory bulb
MOG	myelin oligodendrocyte glycoprotein
MW	medial wall
NG2	neural glial antigen2 = chondroitin sulphate proteoglycan 4
NSC	neural stem cell
OB	olfactory bulb
OPC	oligodendrocyte precursor cells
OSN	olfactory sensory neuron
PDGFRα	platelet derived growth factor alpha
PGC	periglomerular cell
Ppd	postpartum day
RE	rostral extension
RMS	rostral migratory stream
TAC	transit-amplifying cell
TH	tyrosine hydroxylase
V-SVZ	ventricular-subventricular zone

Abstract

Adult neurogenesis is an important form of brain plasticity, and mainly occurs in two regions of the adult rodent brain, the ventricular-subventricular zone (V-SVZ) and the subgranular zone of the hippocampal formation. Adult neural stem cells (NSCs) in the V-SVZ generate neurons and a small number of glia throughout life. They possess a regional identity, and depending on their location in the niche, give rise to different subtypes of olfactory bulb interneurons. The functional significance of such stem cell and interneuron diversity is not fully understood. Hunger and satiety were recently shown to regulate one distinct stem cell pool in the ventral V-SVZ. As such, physiological states may recruit different pools of stem cells. The result of increased stem cell activity is only seen with a delay of 14 days, as it takes this time for a newly-generated interneuron to mature. We therefore hypothesized that different physiological states could regulate stem cells "on demand" as a way to anticipate interneuron need in the near future. Here we describe that pregnancy induces the temporally coordinated recruitment of stem cells in different regional domains of the V-SVZ. Tightly controlled generation of new neurons during early pregnancy leads to the addition of distinct interneurons into different layers of the olfactory bulb, which become functional during onset of maternal care. Some subtypes of pregnancy-associated interneurons are short-lived, and their transient addition into the circuit might reflect temporary increased demand for their function. In the granule cell layer of the olfactory bulb, the transient increase in pregnancy-associated neurons in the perinatal care period is accompanied by a temporary rise in oligodendrocyte precursor cells. In short, dynamic stem cell recruitment during early pregnancy for the generation of diverse interneurons with different survival rates prepares the brain for maternal needs during the postpartum period.

Pregnancy has been demonstrated to increase oligodendrogenesis in the corpus callosum. It is unknown whether NSCs in the V-SVZ, which also generate oligodendrocytes, contribute to this increase. Here, we identify two cycling populations of oligodendroglial cells in the V-SVZ with unknown lineage relationship, branchy PDGFRα+ oligodendrocyte precursor cells and PDGFRα- transit-amplifying cells. Oligodendrogenesis increases during early pregnancy in both white and grey matter around the V-SVZ. In the corpus callosum, newborn oligodendroglial cells are predominantly found in the area above the V-SVZ, hinting at an origin in the germinal niche. There, however, neither PDGFRα+ oligodendrocyte precursor cells nor PDGFRα- transit-amplifying cells seem to be regulated by pregnancy in any of the analyzed domains.

In sum, different physiological states, including pregnancy, regulate neurogenesis but not necessarily oligodendrogenesis in the V-SVZ in a regional manner. Time, space and physiological context are key to understand the functional relevance of stem cell- and interneuron heterogeneity.

1 Introduction

1.1 Stem cells continuously give rise to new neurons in the adult brain

1.1.1 What is a stem cell?

Stem cells are unspecialized cells able to self-renew and give rise to progeny destined to differentiate into one or several specialized mature cell types (*1*). They can be found in development and in the adult body (*2*). Embryonic stem cells of the inner cell mass in the blastocyst are pluripotent, meaning they are capable of giving rise to all different tissues, organs and cell types in the body (*1*). With progressing embryonic development, stem cells derived from pluripotent stem cells become more and more committed towards different lineages, which is accompanied by long-lasting, heritable changes in gene expression. In the adult, most cells are fully differentiated and fulfill a specialized function. However, in many organs including the brain, uni- or multipotent precursor cells can be found, so called adult stem cells, with the potential to generate one or multiple different cell types (*3*). Activation and proliferation of stem cells are tightly regulated by cell-intrinsic mechanisms, but also by signals they receive from their environment, the stem cell niche (*4*, *5*). Adult stem cells maintain homeostasis by replacing cells undergoing cell death, and/or contribute to repair after disease or injury (*2*).

Further, so- called facultative stem cells have been identified. These are differentiated cells in the adult body that do have a specific function, but can act as stem cells upon injury (*3*). The existence of such facultative stem cells is implying that "stemness" is a property or state that can, though happening rarely, be reacquired by differentiated cells.

"Stem cell" is therefore a term describing cells of various potencies and specialization. Until today, there is not a unique marker gene whose expression would positively identify all known stem cell types (*1*).

1.1.2 The main classes of neural cells and their progenitors in the adult brain

The adult brain mostly consists of neurons, glia and vascular cells. Glia comprise three families: astrocytes that have a plethora of functions (reviewed in (*6*)), brain resident immune cells called microglia, and oligodendrocytes which ensheath and electrically insulate axons. Neurons and mature oligodendrocytes in the adult brain are post-mitotic, as are most types of astrocytes in the healthy brain. In contrast, subsets of astrocytes can reactivate proliferation upon injury (*7*).

Figure 1-1 Location of the two stem cell niches in the adult rodent brain.

In the adult, oligodendrocytes are made from NG2+ oligodendrocyte precursor cells distributed uniformly in grey and white matter (*8*). For decades, the generation of new neurons and neuronal replacement in the adult brain was believed to be impossible, but was eventually discovered in rats by Joseph Altman in 1963 . It took another 20 years and contributions of several more scientists until the occurrence of adult neurogenesis in specialized niches was acknowledged by the scientific community (reviewed in (*9*)). Today, we know of two main regions in the adult rodent brain in which neural stem cells reside and neurogenesis takes place: the subgranular zone that gives rise to neurons in the dentate gyrus (DG) in the hippocampus involved in learning and memory, and the ventricular-subventricular zone (V-SVZ) lining the lateral ventricles that generates interneurons for the olfactory bulb (Fig. 1-1)(*10*).

1.2 The adult ventricular-subventricular zone stem cell niche

1.2.1 Developmental origin of adult stem cells in the V-SVZ

Adult neural stem cells in the V-SVZ are derived from radial glia (RG). During brain development, RG and progenitors located in different regions of the developing ventricular zone sense differential morphogen expression, which induces them to switch on distinct transcription factor programmes. Consequently they generate different types of neurons (*11*). Some RG give rise to oligodendrocytes through intermediate precursor cells, but it is unknown whether a single RG can give rise to both neurons and oligodendrocytes. The ratio of neurons:glia generated is modulated by timing in development (*11*).

Towards the end of forebrain development, most RG terminally differentiate into astrocytes. Some RG however, specified between E13.5 and E15.5, retain apical contact with the brain ventricle and become quiescent (*12*, *13*). Quiescence is a reversible state of actively maintained cell cycle arrest, characterized by low metabolic activity and high sensitivity to signals in the niche, thought to protect from stem cell exhaustion, replicative senescence and accumulation of DNA damage. In the postnatal period and in the adult, upon the right signals, those stem cells set aside during development can activate and give rise to progeny (*14*).

1.2.2 Organization and regulators in the adult V-SVZ stem cell niche

The adult V-SVZ is an extensive stem cell niche found bilaterally in the brain around the entire length of the lateral ventricles (Fig. 1-2A). It is composed of the lateral wall of the ventricle, the medial wall adjacent to the septum, and the roof located below the corpus callosum (Fig. 1-2 A). Adult NSCs in the V-SVZ are a special type of astrocytes, expressing the intermediate filament glial fibrillary acidic protein (GFAP) (*15*). A monolayer of bi- and multiciliated ependymal cells is lining the ventricular wall, forming a barrier between the cerebrospinal fluid (CSF) and the neural tissue (Fig. 1-2B) (*16*, *17*). Cilia of ependymal cells propel the CSF in the ventricular system. Radial stem cells (also known as B1 cells) resemble RG in their apical basal polarity. They exist in quiescent and active states. On the apical side, they are in direct contact with the CSF, which includes factors secreted by the choroid plexus. Quiescent stem cells extend a primary cilium into the CSF (Fig.1-2B) (*16*, *18–20*). Strikingly, this contact happens at the center of the pinwheels formed by ependymal cells. One pinwheel mostly contains apical processes of one or two stem cells in the center, but large pinwheels with up to ten stem cells have been observed (*16*). On the basal side, radial stem cells are in contact with a unique type of planar vasculature with a blood brain barrier (BBB) permissive to small molecules (Fig.1-2B) (*21*). The neurovascular unit of a typical BBB is composed of a tube formed by endothelial cells held together by tight junctions, pericytes positioned on the abluminal surface of the tube, and astrocyte endfeet ensheathing the vascular tube (*22*). In the V-SVZ, astrocyte endfeet coverage and pericyte coverage are patchy, and stem cells often contact these sites with their basal processes (*21*). Extracellular matrix (ECM) can regulate stem cells on its own, or serve as a reservoir of secreted signals (*5*). In the V-SVZ, behind interstitial clefts in the ependymal cell layer, branched ECM structures called fractones composed of laminin, collagen IV, perlecan, agrin, nidogen and the glycosaminoglycan heparate sulphate proteoglycan can be found.

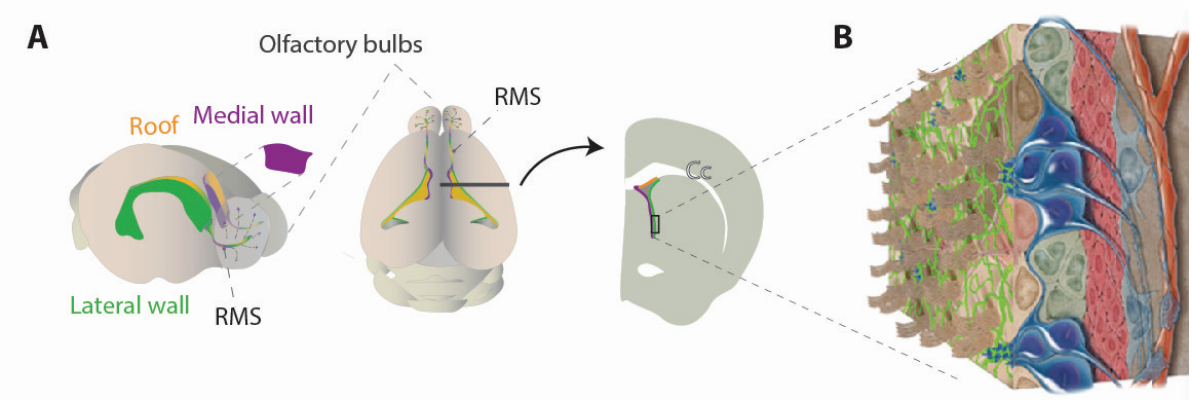

Figure 1-2 The V-SVZ stem cell niche

A The medial wall, lateral wall and the roof of the V-SVZ stem cell niche **B** Drawing of composition and organization within V-SVZ lateral wall. Source: (*23*) Reprinted with permission of Elsevier. **Abbreviations** RMS: rostral migratory stream; Cc: Corpus callosum

They regulate the bioavailability of growth factors in the niche by capturing heparin-binding growth factors released locally or diffusing from the cerebrospinal fluid through the clefts (*24–26*). Notably, the lateral wall is unusually stiff compared to surrounding non-neurogenic regions (*27*). The V-SVZ receives innervation and neural input from areas close-by and further away in the brain, including local choline acetyltransferase (ChAT) neurons (*28*), GABAergic medium spiny and aspiny neurons located in the neighbouring striatum (*29*), dopaminergic neurons in the substantia nigra (*30*) and ventral tegmental area (*31*), hypothalamic proopiomelanocortin (POMC) neurons (*32*), and serotonergic neurons originating in the dorsal raphe nucleus with their axons located on top of ependymal cells, on the luminal side (*23*). Taken together, the V-SVZ stem cell niche is extremely rich in signals regulating behavior of stem cells and their lineage, including the CSF, systemic signals, innervation, a unique ECM, and local signaling from niche cells.

1.2.3 Lineage of NSCs in the adult V-SVZ: neurons and glia

1.2.3.1 The neuronal lineage

Adult NSCs give rise to neurons and a small numbers of oligodendrocytes (*33*), and recently they were described to have the potential to generate astrocytes (*34*).

The main cell type generated in the V-SVZ are neurons. Upon activation, neural stem cells undergo symmetric divisions. 20% of the divisions serve self-renewal, and 80% are consuming divisions, resulting in two intermediate progenitors, also known as transit-amplifying cells or type C cells, expressing EGFR (Fig. 1-3) (*35*). Transit-amplifying cells usually divide three more times, giving rise to neuroblasts or type A cells. These immature neurons, characterized by expression of doublecortin (DCX) (Fig. 1-3), divide one or two times before leaving the V-SVZ (*36*). Within approximately five days, one consuming division of a B1 cell results in the generation of 32-64 new neurons. Importantly, at any moment, only a small fraction of cycling cells in the V-SVZ are dividing stem cells.

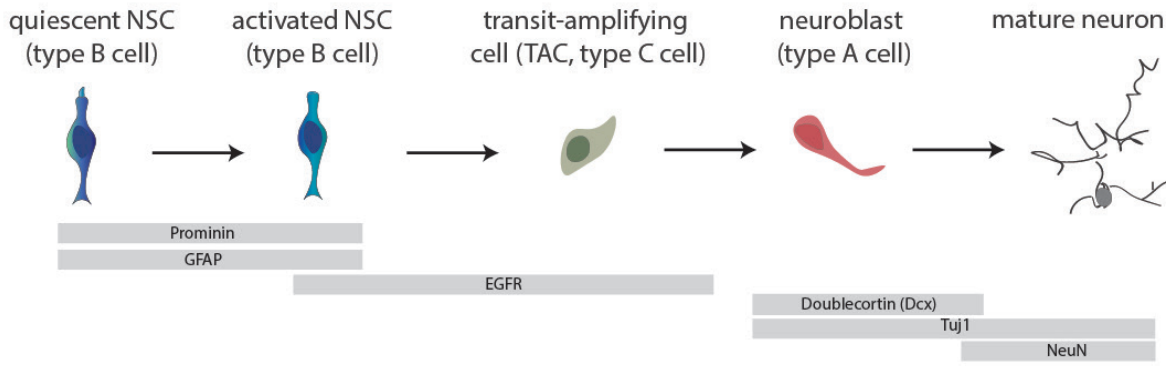

Figure 1-3 Neurogenic lineage of stem cells in the V-SVZ.

Each day, 10'000 new neurons are born bilaterally in the adult murine V-SVZ (*37*). Newly generated neurons are not used on site like in the dentate gyrus. Instead, they migrate along the V-SVZ and through a tunnel formed by astrocytes, the so called rostral migratory stream (RMS), to the olfactory bulb (OB) at the front of the brain, where they differentiate into mature interneurons (characterized by upregulation of NeuN (Fig. 1-3)) and integrate into the circuit in different anatomical layers (*38–40*).

1.2.3.2 The oligodendroglial lineage

New oligodendrocytes in the adult brain arise from chondroitin sulfate proteoglycan (CSPG4 or NG2) and platelet-derived growth factor receptor alpha (PDGFRα)-expressing oligodendrocyte precursors (OPCs) distributed evenly in grey and white matter (*8*, *41*). Moreover, this is complemented by oligodendrogenesis in the ventricular-subventricular zone and RMS (Fig. 1-4 A) (*42*, *43*). In the V-SVZ of healthy adult rodents, cells of the oligodendroglial lineage migrate dorsally and laterally to the corpus callosum located just above the V-SVZ (*42*, *43*), with the vast majority found within 1.5mm of the midline (*43*). Unlike neuroblasts, they do not migrate tangentially, but stay at the rostrocaudal level they originated in (*42*). V-SVZ-derived oligodendroglial cells differentiate into mature oligodendrocytes in the corpus callosum, as characterized by expression of CC1 (*42*).

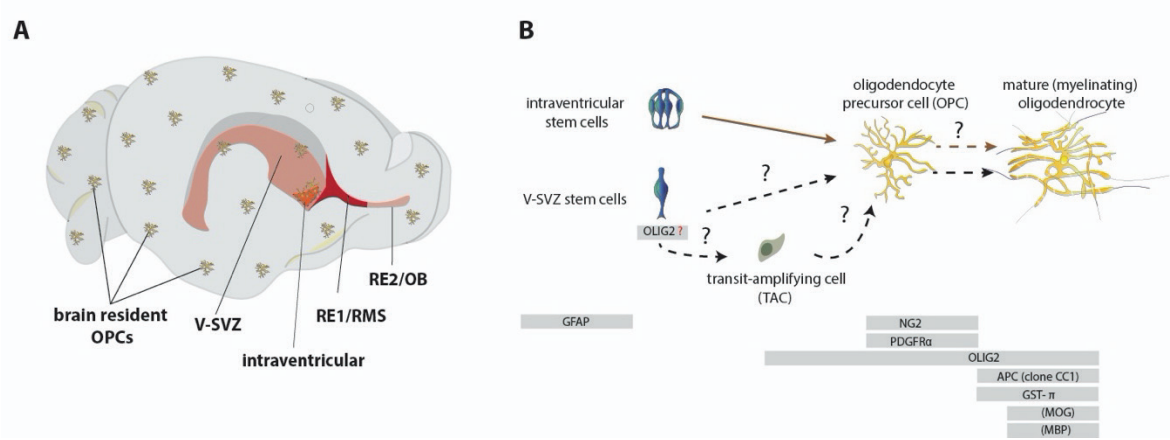

Figure 1-4 Oligodendrogenesis in the adult brain

A Domains with oligodendrogenesis in the adult brain **B** Unknown lineage of V-SVZ oligodendrogenesis and markers for oligodendrocyte progenitor cells and mature oligodendrocytes. **Abbreviations** OPC: oligodendrocyte precursor cells, RE: rostral extension, RMS: rostral migratory stream, OB: olfactory bulb

After drug-induced focal demyelination in the corpus callosum (*44*), multifocal demyelination in experimental autoimmune encephalomyelitis (EAE) mice (*45*) and seizures induced by pilocarpine-hydrochloride (*46*), generation of oligodendrocytes (and astrocytes) in the V-SVZ to the corpus callosum is increased, and, depending on the lesion, ectopic migration to atypical target sites such as the hippocampus (*46*), striatum and olfactory bulb (*45*) have been reported. Both in the healthy brain and in demyelination models it is controversial whether V-SVZ-derived oligodendrocytes contribute to myelination (*42*, *43*, *47*, *48*).

To the present day, the stem cell lineages giving rise to new oligodendroglial cells in the V-SVZ are still unclear (Fig. 1-4 B). In culture, isolated stem cells from the V-SVZ give rise to neurons, astrocytes and oligodendrocytes (*15*, *49*). Menn et al. (*42*) did a clonal analysis of FAC-sorted GFAP-GFP cells grown singly on cortical astrocytes. 80 % of the resulting colonies were purely oligodendrogenic, 10% consisted of both oligodendrocytes and neurons, and 8% consisted of neurons only. However, the behavior *in vivo* might differ from the behavior in a dish. Olig2+ stem cells are very rare (own observations), but a subpopulation of transit-amplifying cells expresses OLIG2, and these cells might become oligodendrocytes (*42*). Recently, GFAP+ stem cells were detected that give rise to previously undescribed intraventricular PDGFRα-expressing oligodendrocyte precursor cells nested between ependymal cilia and axons on the luminal side of the ventricular wall (Fig. 1-4 A&B) (*34*). It is still unknown if these cells stay resident or migrate away. Possibly, these intraventricular OPCs may be a source of SVZ-derived oligodendrocytes migrating to the corpus callosum.

1.3 The Olfactory Bulb

1.3.1 Function and connectivity in the olfactory bulb

The olfactory bulb (OB), composed of the main olfactory bulb (MOB) and accessory olfactory bulb (AOB), is the first relay center for olfactory information reaching the brain (Fig. 1-5). In the mouse, volatile odorants bind to olfactory receptors of olfactory sensory neurons (OSN) in the olfactory epithelium located in the back of the nasal cavity, each neuron expressing a single one of 1000 distinct olfactory receptors (*50*). Axons of OSNs travel through the cribriform plate to glomeruli in the outermost layer of the main olfactory bulb (Fig. 1-5). Odorants are also perceived by the vomeronasal organ, which sends information to the accessory olfactory bulb via the vomeronasal nerve (Fig. 1-5). Contrary to widespread belief, MOB and AOB do not have exclusive functions, but process similar chemosignals (reviewed in (*51*)).

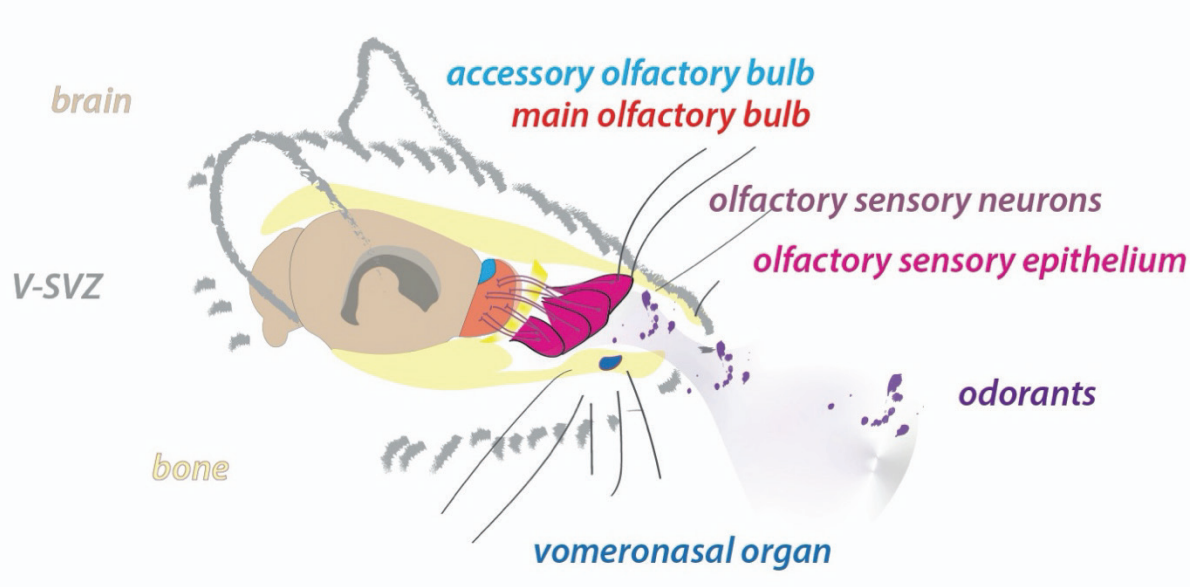

Figure 1-5 The mouse olfactory system

Drawing of the mouse olfactory sensory system and its connectivity to the main and accessory olfactory bulb. Odorants are perceived by neurons in the olfactory sensory epithelium and the vomeronasal organ. Their axons travel to the main and accessory olfactory bulb, respectively.

1.3.2 Organization of the olfactory bulb

The olfactory bulb is structurally composed of four layers. Listing beginning in the core of the bulb, these are the granule cell layer (GCL), mitral cell layer (MCL), external plexiform layer (EPL) and glomerular layer (GL) (Fig. 1-6 A) (*37*). One glomerulus only receives innervation from sensory neurons expressing the same olfactory receptor (*52*). The projection neurons in the olfactory bulb are tufted cells located in the external plexiform layer, and mitral cells in the mitral cell layer (Fig. 1-6B) (*52*). Both extend one long apical dendrite to a single glomerulus and lateral

dendrites into the external plexiform layer, while sending their axons to olfactory areas including the anterior olfactory nucleus, the piriform cortex, olfactory tubercle, cortical amygdala and to the gateway to the hippocampus, the lateral entorhinal cortex. OSN terminating in the glomeruli directly and indirectly regulate tufted cells and mitral cells. The response of tufted and mitral cells is modulated and sharpened by lateral inhibition in all layers in the OB, but mainly in the glomerular layer and external plexiform layer (Fig. 1-6B). In the glomerular layer, lateral inhibition is mediated by juxtaglomerular cells including periglomerular cells and superficial short axon cells. Granule cells located in the deep or superficial cell layer send processes into the external plexiform layer and form synapses with the lateral dendrites of mitral or tufted cells (*37*, *52*). Inhibitory cells in the MCL and EPL further sharpen mitral cell - and tufted cell output (Fig. 1-6B). Finally, the olfactory bulb receives centrifugal innervation from olfactory areas, but also non-olfactory areas (*52*, *53*).

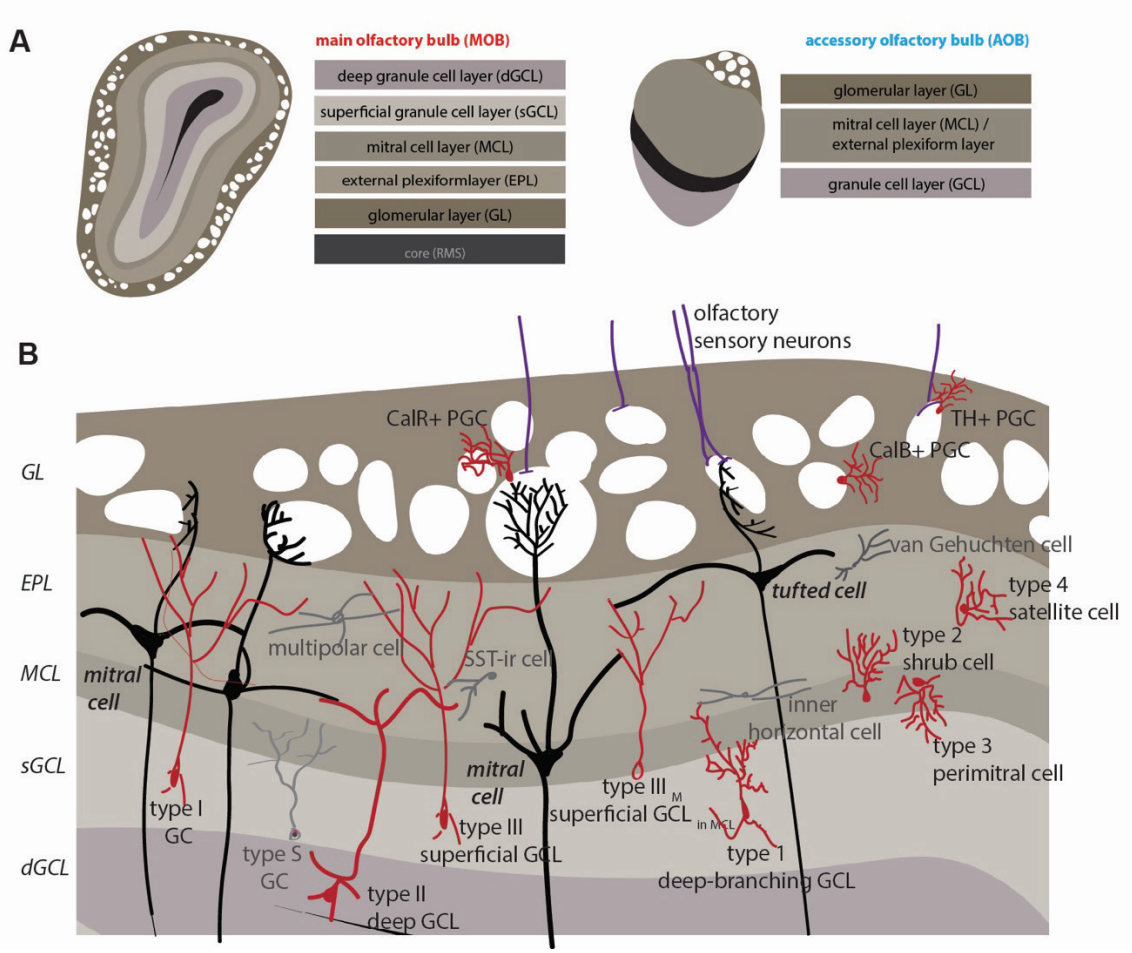

Figure 1-6 Layers and cell types in the olfactory bulb

A Main olfactory bulb and accessory olfactory bulb in cross-sections **B** Location of soma, dendrites and axons of main OB projection neurons (in black) and interneurons described by morphology and molecular markers (for PGCs). Interneurons in red are described to be generated via adult neurogenesis in the V-SVZ. Not depicted in this drawing are diverse types of short-axon cells and cells of non-neuronal lineage. **Abbreviations** GC: granule cell; PGC: periglomerular cell; TH: tyrosine hydroxylase; CalR: calretinin; CalB: Calbindin; SST-ir: somatostatin-immunoreactive. Review on these cell types:(*37*)

1.3.3 Lifelong generation of OB interneurons by V-SVZ stem cells

Mitral cells and tufted cells are generated only during development, but some types of granule cells in the granule cell layer, periglomerular cells in the glomerular layer, and some interneurons located in the mitral cell layer and external plexiform layer in the MOB are generated by adult NSCs (Fig. 1-6B). Neurogenesis is maintained throughout life, but the levels of neurogenesis decreases non-monotonously with ageing (*54*). Low levels of continuous neurogenesis are also observed in the accessory olfactory bulb (AOB) located caudally in the olfactory bulb (*39*, *55*).

1.3.4 Diversity of adult-born OB neurons

Already before single cell sequencing was performed at large scales, it was suggested that neurons in the OB were among the most diverse in the entire brain (*37*). Interneurons contribute greatly to this heterogeneity. They are diverse, as observed by integration site (layer), soma size, dendritic arborization, connectivity and molecular diversity including neurotransmitter/peptide used (Fig. 1-6B) (*37*, *56–61*).

Homeobox transcription factors Dlx1/2 are expressed by neuronal precursors and neuroblasts, and are required for differentiation into GABAergic OB interneurons (*62*). Analysis of Dlx1/2-CreER RosaYFP mice induced at P30 revealed ~75% of adult born neurons to be granule neurons. ~15% of YFP+ cells in the OB were periglomerular neurons, and only ~ 10% of newborn neurons were located in the mitral cell layer or external plexiform layer (*63*).

Based on their position (deep vs superficial granule cell layer, or mitral cell layer), dendrite extension, branching and connectivity with mitral cells or tufted cells, several types of granule cells were described (*56*, *58–60*), and most of them are also made in the adult brain (Fig. 1-6B) (*60*, *61*). Some of these granule cells express neurogranin, calretinin (CalR) or trophoblast glycoprotein (5T4) (*58*, *60*, *63*, *64*), but no unique markers are known yet that would allow molecular classification of all described subtypes.

In the glomerular layer, the juxtaglomerular neurons comprise GABAergic periglomerular neurons, superficial short axon cells and external tufted cells (*37*). Dopaminergic, Calbindin+ (CalB) and Calretinin+ (CalR) periglomerular cells get renewed in the adult (*63*) and make up the majority of juxtaglomerular cells (*37*). However, also a few glutamatergic (vGlut2+) short axon cells destined for the glomerular layer are made in the adult V-SVZ (*65*). The few neurons that integrate in the external plexiform layer were named satellite cells, and frequently, but not always, express CalR (*60*).

Thus, many distinct neuronal subtypes for the OB are generated in the adult V-SVZ.

1.3.5 Dynamics of adult neurogenesis in the OB: Activity-dependent survival or non-selective addition?

Two to three weeks after their birth in the V-SVZ, most newborn neurons have reached the main olfactory bulb, immunostain positive for NeuN and show a mature morphology including formed dendritic trees and synapses, thus have integrated into the preexisting circuit (*66*, *67*). Newborn neurons quietly integrate into the olfactory circuit, and acquire the ability to form action potentials only very late in their maturation (*68*). About 50% of adult-born granule cells, the principal neuronal type made in the adult, are rapidly lost between 20d and 45days after birth (*66*, *69*), at an age when they display dendritic arborizations and synapses, and are able to fire action potentials (*66*, *68*). After this initial fast drop, cell numbers stabilize. About 25% (*66*) to 50% (*70*) of the adult-born granule cells made stay long-term and can be found in the OB one year after their birth, or longer.

In the AOB, the peak of immature newborn neurons is observed earlier than in the MOB, already seven days after their birth. Like in the MOB, the initial high numbers of newborn neurons drop shortly after the arrival in the olfactory bulb (*55*).

In transgenic anosmic mice, in which mutated cyclic nucleotide–gated ion channels prevent Ca2+ influx and therefore the formation of action potentials in olfactory sensory neurons upon odorant binding, survival, but not the generation and maturation of OB neurons was reduced dramatically. This led to the proposition of an activity-dependent survival mechanism (*66*). This was confirmed with unilateral sensory deprivation experiments by naris cauterization, and the age of 14-28 days was defined as critical period in which newly generated granule cells are dependent on sensory experience for survival (*67*). This coincides with the period in which young neurons form synaptic contacts (*66*). In summary, the mentioned studies suggest that the surplus generation of neurons followed by activity-dependent survival serves as a mechanism for the formation of custom-built circuits based on olfactory experience.

Importantly, this model was recently challenged (*71*). In vivo two-photon imaging was used to study neuronal survival in the reported critical periods and beyond in both juvenile and adult mice. At both ages, cell death was minimal. In the adult, only 1.5% and 5.9% of the tracked periglomerular and granule cells died in the observed 7 week period after arrival in the olfactory bulb. Moreover, cell death was minimal when survival was observed over 6 months, and the authors reported continuous growth of the olfactory bulb over the first year of life, while its cell density stayed unchanged. Ultimately, it was demonstrated that the low survival rates observed by other groups (*66*, *69*, *70*) may have been due to the use of very high doses of thymidine analogue

(*71*). These findings are a change to the current dogma, and future research will show which one of the models, or possibly a combination of both, comes closer to reality, and under which circumstances.

1.4 Regional heterogeneity in the V-SVZ

1.4.1 Proliferation differs between and within different walls of the V-SVZ

Radial B1 stem cells are not evenly distributed in the V-SVZ, as assessed by counting B1 apical surfaces at the center of ependymal pinwheels. In the lateral wall, the highest density of stem cells is found ventrally in the most rostral aspect, and dorsal to the fusion area. Caudally, only few stem cells can be found (*16*, *72*). In the medial wall, the number of stem cells are also highest rostroventral, but the density is lower than in the lateral wall (*16*).

Single-cell analysis of the lateral and medial wall revealed that generally, the lateral wall of the V-SVZ is more proliferative than the medial wall (*73*). Within the lateral wall, proliferation is highest rostrally and dorsally, and decreases along the anterior-posterior axis and the dorsoventral axis (*74*). The medial wall tends to be more quiescent, with exception of the most rostral region (*73*).

1.4.2 Regional heterogeneity of stem cells

Different walls of the V-SVZ show varying levels of neurogenesis and gliogenesis. The lateral wall is more neurogenic than the medial wall, and the medial wall (especially in males) is more oligodendrogenic compared to the lateral wall (*73*). Moreover, within a wall, the ratio of oligodendrocytes/neurons generated changes along the rostrocaudal axis (*42*). The generation of neurons decreases greatly from anterior to posterior. In the rostral V-SVZ, 30 times more neurons than oligodendrocytes are generated, whereas in the caudal V-SVZ it is only three times more. Oligodendrocytes, however, are born in similar numbers in the V-SVZ along the anterior-posterior axis (*42*). Multipotent progenitors also exist in the rostral migratory stream (RMS), or rostral extension (RE) of the V-SVZ. In culture, cells isolated from the caudal RMS (RE1) are highly more oligodendrogenic compared to stem cells isolated from the V-SVZ (Fig. 1-4A) (*49*).

In vivo, analysis of the neurogenic and gliogenic potential of stem cells in different domains is limited to activated neural stem cells. Transgenic reporter mice in which stem cells are released from quiescence and genetically labelled allow to look at the lineage unbiased from the activation state. Study of these mice led to the detection of intraventricular OPC-generating stem cells. Further, this approach allowed to identify stem cells with oligodendrogenic potential in the medial wall of the rostral V-SVZ, especially in the dorsomedial corner. Stem cells in the rostral

intermediate and ventral V/SVZ, but not in the dorsal or caudal V-SVZ, generated special types of astrocytes (*34*).

1.4.3 Developmental origin and position of V-SVZ stem cells as determinant of interneuron subtypes generated

Which type of interneuron adult NSCs generate is not arbitrary, but analogous to development, depends on the position and transcription factor expression by the neural stem cells (Fig. 1-7A) (*11*). Regional pools of stem cells were labelled by stereotactical adenoviral delivery of Cre recombinase to reporter mice that express GFP upon recombination. Variations of the injection site along the dorsoventral and rostrocaudal axes of the V-SVZ followed by lineage tracing for 28 days resulted in a fate map of adult NSCs in the ventricular zone and their progeny in the olfactory bulb (*60*, *61*). Together with other lineage tracing experiments this showed that diverse postnatal/adult-born interneuron types have different origins along the dorsoventral and rostrocaudal axes.

Progenitors in the dorsal V-SVZ produce mostly superficial granule cells and TH+ periglomerular cells (*61*, *75*), and Pax6 is essential for the generation of these subtypes (Fig.1-7A, B) (*76*, *77*). TH+ cells are also made in the subcallosal zone (*61*) and in the RMS (*76*). In contrast, stem cells in the ventral V-SVZ generate deep granule cells and CalB+ periglomerular cells (*61*). They derive from Nkx2.1 and Gsh2 positive stem cells, respectively (Fig.1-7A,B) (*78*, *79*). The domain generating TH+ cells extends almost the entire length of the V-SVZ, whereas the region generating CalB+ cells spans only the first half of the rostrocaudal axis (Fig.1-7B) (*61*). CalR+ interneurons (both periglomerular cells and granule cells) are generated almost exclusively in the RMS and the medial wall of the anterior V-SVZ (Fig.1-7B) (*60*, *61*), a few derive from the dorsolateral wall (*61*, *80*). Transcription factors associated with progenitors of CalR+ interneurons are Emx1 and Gsx2 (*79*, *80*). Type 1-4 interneurons are generated in the medial and lateral wall in the anterior ventral V-SVZ (Fig.1-7B) (*60*). Nkx6.2+ stem cells contribute to their production, and type 1 (deep-branching granule cells) and type 3 (perimitral cells) are potentially derived from Zic+ stem cells in the medial wall (Fig.1-7A,B) (*60*). Glutamatergic short axon cells are generated by Neurogenin2/Tbr2+ stem cells in the dorsal V-SVZ (*65*). In sum, NSCs in the adult V-SVZ have a positional identity inherited from development that specifies the type(s) of OB neurons made. Importantly, transcription factor domains are overlapping, and the combination of transcription factor expressed may ultimately determine the interneuron subtype made. Moreover, these studies imply that for generating a full repertoire of OB interneurons, molecularly distinct stem cells in regionally distinct domains need to become activated.

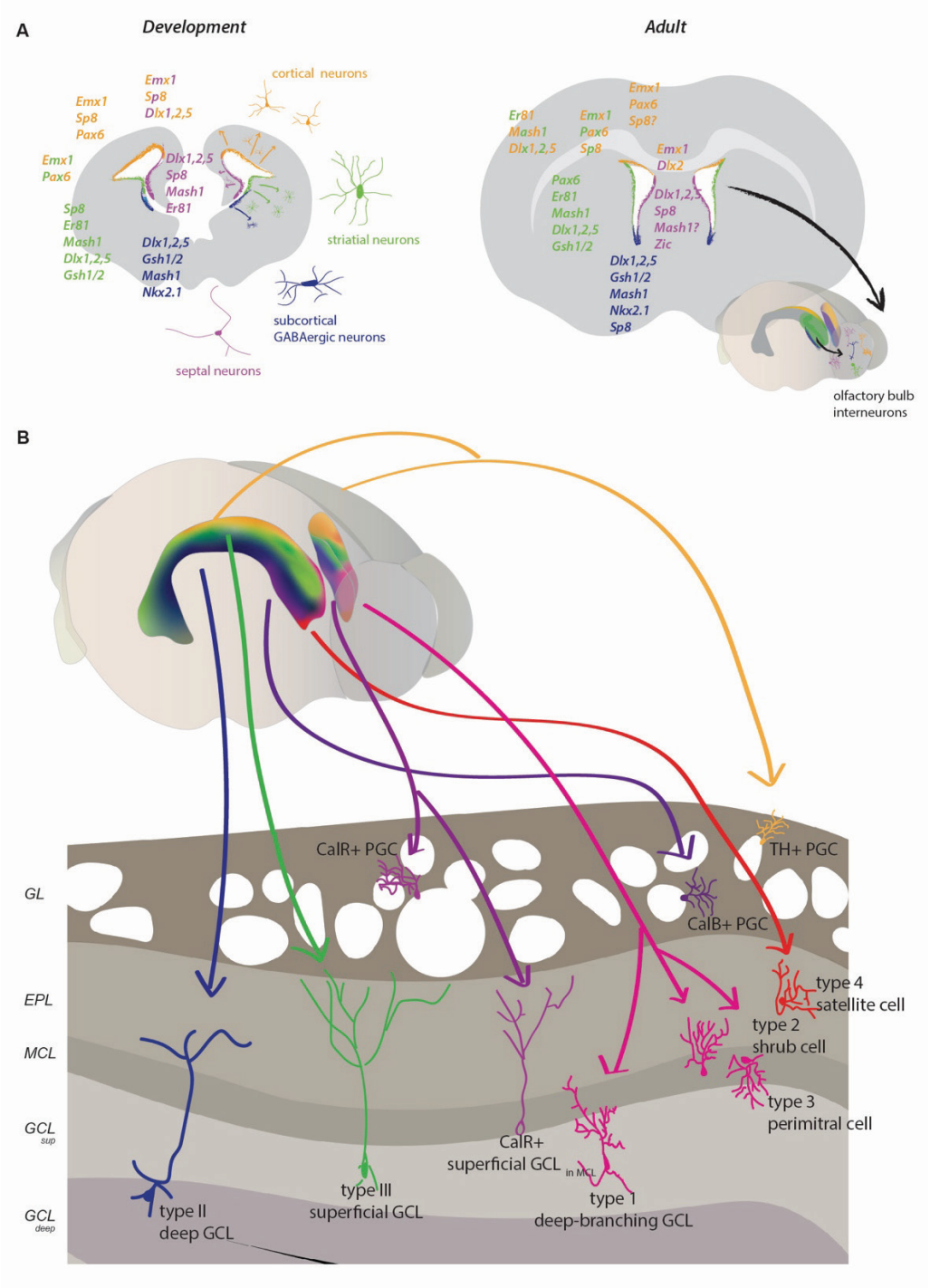

Figure 1-7 Regional stem cell identity retained from development specifies types of olfactory bulb neurons made

A *Left side* Cross-section through the embryonic forebrain with focus on the germinal zone around the future ventricles. Orange: Pallium; magenta: septum; green: lateral germinal eminence, blue: medial germinal eminence. Radial glia in the different zones initiate different transcription factor programmes (listed) and consequently generate different types of neurons. *Right side* Cross-section through the adult forebrain, with view on the V-SVZ stem cell niche lining the lateral ventricles. Orange: roof; magenta: medial wall of the V-SVZ; green: lateral wall of the V-SVZ; blue: ventral tip of the V-SVZ. Neural stem cells have retained

their transcription factor identity from development and generate diverse interneurons destined for the olfactory bulb. Data compiled from (*11*, *60*, *81*). **B** Regionalized transcription factor expression instructs type of olfactory bulb neurons generated in the adult V-SVZ. Schema based on (*33*, *60*, *61*). **Abbreviations** GL: glomerular layer; EPL: external plexiform layer; MCL: mitral cell layer; GCL: granule cell layer.

1.5 Temporal dynamics in stem cell recruitment

1.5.1 OB interneuron composition changes over life

Neurogenesis for the olfactory bulb is high during the first postnatal days, and then gradually decreases to lower levels in adulthood (*63*, *82*). While perinatally-born OB interneurons preferentially integrate into the superficial GCL and MCL (*82*), adult-born neurons show limited cell replacement in the superficial GCL, and predominantly integrate into the deep GCL (*83–85*). Moreover, while granule cells born in neonates survive long-term with virtually unchanged numbers, adult-born granule cells (potentially) have lower survival rates and frequently get replaced by younger neurons (*82*, *83*). Thymidine-analog pulse chase experiments, temporal genetic fate mapping, and long-term time-lapse imaging in reporter mice revealed that the relative abundance of newborn OB interneuron subtypes fluctuated from late development to the postnatal period and into adulthood, as well as during adulthood (*63*, *70*, *86*). These studies imply that regionally distinct stem cells are dynamically regulated over time.

1.5.2 Life experiences and physiological states as modulators of V-SVZ neurogenesis

In this thesis, physiological state is used as term to describe the condition or state of the body or bodily functions, including the feelings that neurophysiological changes induce. Examples of such states are hunger and satiety, sleep and wakefulness, body temperature, pain, stress, anxiety, depression, arousal, pregnancy, as well as mating season and hibernation in seasonal animals. Various studies addressed the effects of different physiological states or life styles on neurogenesis in the V-SVZ and the dentate gyrus. In rodents, dentate gyrus neurogenesis is modulated by various states including chronic pain, chronic sleep deprivation, voluntary exercise and sexual activity. V-SVZ neurogenesis is unaffected by most of these, except sexual activity (*87–92*), but these negative results have to be taken with a grain of salt, as regional stem cell heterogeneity was rarely considered in these studies. Strikingly, pheromones of the opposite sex, sexual activity in males and females, pregnancy and even pseudopregnancy positively impact V-SVZ neurogenesis (*90*, *92–95*).

1.5.3 Regionalized recruitment of stem cells in response to hunger and satiety

A few years ago, opioid ligand beta-endorphin was identified as an activator of quiescent neural stem cells in culture. In the mouse brain, beta-endorphin is expressed in POMC neurons located in the hypothalamus, which increase their activity upon feeding. Strikingly, these neurons regionally innervate just the ventral domain of the rostral V-SVZ, and upon ablation of POMC neurons, or fasting, the activity of just these ventral stem cells is reduced. In turn, the production of deep granule cells, but not other OB interneurons, decreases (*32*). Importantly, this demonstrates that stem cell recruitment in the V-SVZ can be regionalized, and suggests that different pools of stem cells might be regulated by distinct physiological states, for the generation of specific interneurons.

1.6 Functional heterogeneity of OB interneurons

A tightly regulated production of interneurons in response to physiological states suggest a functional map may underlie stem cell heterogeneity. Neural stem cells in the V-SVZ in neonate and adult mice generate distinct types of neurons with distinct positions, connectivity and survival rates (*63*, *85*). This implies that on a population level, juvenile-born and adult-born neurons play different roles in odour processing. The function of OB interneurons is traditionally tested by either ablating cycling stem cells and their dividing progeny over several days using targeted irradiation or anti-mitotic drugs, or by the use of transgenic mice for conditional ablation of proliferating or differentiating newborn neurons. The effect of the intervention is then assessed with behavioral tests two to four weeks later.

For basic olfactory functions such as odour detection, odour discrimination and formation of short-and long-term olfactory memories, neither the ablation of juvenile- nor adult-born OB neurons alone results in functional deficits (*69*, *83*, *84*, *93*, *96*, *97*), suggesting that the presence of either juvenile-born or adult-born neurons alone is sufficient to maintain basic olfactory function. However, continuous neurogenesis is required for more difficult tasks, such as flexible association learning (*84*). Moreover, increasing stem cell proliferation through acute overexpression of Cdk4/cyclinD1 increases neurogenesis, and supernumerary neurons are generated that lower the threshold for detection and discrimination of faint and highly similar odours (*98*).

Age-dependent functions of OB interneurons appear when looking at affiliative and sexual behaviors that both heavily depend on olfaction: Interactions between females and spontaneous maternal care in nulliparous mice do depend on juvenile neurogenesis (*96*), while these and other affiliative (but non-sexual) behaviors such as social recognition, male-male interactions are still intact in absence of adult neurogenesis (*69*, *96*, *99*). On the other hand, sexual behaviors including

male mounting behavior, male aggression towards intruders, female mate choice preference, mate recognition and maternal behaviors in primiparous mothers are disturbed with reduced or absent adult neurogenesis (*93*, *95*, *97*, *99*, *100*). Occasional discrepancies between findings can be explained by the use of different ablation methods with varying specificity (systemic, local, cell type-specific) and efficiency (chemical ablation, irradiation or transgenic approaches), time frame of analysis and the use of different behavioral tests.

Taken together, juvenile- and adult-born OB interneurons differ in composition, which makes them, on a population level, relevant for different aspects of olfaction.

1.7 V-SVZ neurogenesis during pregnancy

1.7.1 Pregnancy increases V-SVZ neurogenesis in a prolactin-dependent manner

Almost 20 years ago, Shingo et. al (*94*) assessed neurogenesis in the V-SVZ in timed-pregnant mice on gestation days (Gd) 7 and 14; at partum (P0) and on postpartum days (Ppd) 7, 14 and 21 by injecting BrdU 5x/day every 2hours. BrdU incorporation and Ki67 (cell cycle marker) expression was studied 30 minutes after the last injection. Compared to virgins, significantly more BrdU+ and Ki67+ cells were found in the V-SVZ on Gd7 and Ppd7, but not on any of other days studied. Mice pulsed at Gd7.5 and Ppd7.5 sacrificed four weeks later had significantly more labelled mature neurons (BrdU+ NeuN+) in the granule cell layer and glomerular layer of the olfactory bulb, confirming that the increase in proliferation in the stem cell niche lead to an increase in newborn neurons added to the olfactory bulb.

The increase in proliferation in the V-SVZ during pregnancy was also seen in females mated with sterile males, albeit to a lesser degree (65% vs 42% increase in BrdU+ cells) (*94*). Mated female mice undergo a hormonal response lasting 10-13 days that is induced by sexual stimulation, and required for successful initiation and maintenance of pregnancy. Females mated with sterile males also undergo this hormonal response, which is called pseudopregnancy (*101*, *102*). As pseudopregnancy also increased proliferation in the V-SVZ, it seemed likely that pregnancy hormones played a role in mediating neurogenesis (*94*). In virgin females, subcutaneous and intraventricular infusions of prolactin but not progesterone or estrogen in virgin females increased neurogenesis (*94*). Furthermore, prolactin increased proliferation of isolated NSCs in culture, and even males infused with prolactin showed increased proliferation in the V-SVZ, but to a lower extent than virgin females infused with prolactin. Immunostaining revealed that prolactin receptor expression in the V-SVZ was restricted to the dorsolateral wedge. Finally, they showed that in Prlr+/- mice, the pregnancy-associated increase in neurogenesis is reduced (*94*). In sum, pregnancy increases neurogenesis in rodents, and prolactin is a mediator.

1.7.2 An intact main olfactory system is required for proper maternal care

An intact main olfactory system in primiparous mice and sheep is required for proper maternal care: anosmia induced irrigation of the nasal epithelium using zinc sulfide resulted in pup-killing in mice (*103*), whereas sheep showed delayed onset of maternal behavior. Licking times and maternal bleats were reduced (*104*). Multiparous mice and sheep, however, do not show disturbed maternal behavior despite nasal mucosa irrigation, showing that experience compensates the loss of olfactory information (*103*, *104*). The exception was selective care: sheep depend solely on smell for lamb recognition (*105*), and anosmia prevented selective care for an ewe's biological lamb (*104*). Furthermore, vomeronasal nerve section or removal of vomeronasal organs did not disturb maternal behavior or selective care, indicating that the accessory bulb system is not required for adequate maternal care (*104*, *106*). Thus, maternal behavior heavily relies on olfaction and the main olfactory system.

1.7.3 Role of adult neurogenesis in maternal behaviour

In Nestin-CreER^{T2};NSE-DTA mice, adult-generated neurons are ablated when they are maturing. In these females, odour sensing and discrimination are intact, but they show decreased fertility and impaired nurturing behavior, and most of their pups die within a day (*99*). In contrast, focal irradiation of the V-SVZ resulting in a 63% decrease in neurogenesis did not result in altered maternal behavior, and mothers were able to discriminate between own and unfamiliar pups (*97*). On first sight these results may seem contradictory, but the approaches used had different specificity and efficiency. The use of Nestin-CreER^{T2};NSE-DTA mice also affects neurogenesis in the hippocampus, but at the same time, compared to irradiation, is the more efficient way to reduce OB neurogenesis, reportedly resulting in a 90% decrease in neurogenesis (*83*).

Sheep also display adult neurogenesis in the V-SVZ. A 70% reduction in OB neurogenesis induced by infusion of the anti-mitotic dug AraC into the lateral ventricle did not reduce suckling time in the first two hours of postpartum. However, ewes undergoing the Ara-C treatment displayed slight behavioral deficits: they vocalized less low-pitched bleats, so called maternal bleats, which have calming effects on neonate lambs and promote contact with the young and nursing. In addition, similar to anosmia, ewes showed deficits in discrimination of familiar and unfamiliar lambs (*107*). Together, these studies indicate that adult neurogenesis may play a role in mediating maternal behaviour.

1.7.4 Suppressing the prolactin-mediated increase in neurogenesis during early pregnancy impairs maternal behaviour in the postpartum period

As newborn neuron needs about 14-20 days to migrate and fully integrate into the olfactory bulb circuit, and a mouse pregnancy lasts 19 days, neurons generated at Gd7.5 would become functional in the first few days of the postpartum period.

Larsen et al. speculated that pregnancy-associated neurogenesis would play an important role in maternal behavior (*95*). First, they confirmed that pregnancy-associated neurogenesis is mediated by prolactin. During early pregnancy, serum prolactin levels peak twice daily, before onset of dark period, and to a lesser extent before light period. Prolactin is secreted from the anterior pituitary gland. To prevent the nocturnal surge of prolactin, but maintain high enough levels to allow progression of pregnancy, they administrated controlled doses of dopamine D2 agonist bromocriptine during the first three days of gestation. This led to a reduction of cell proliferation in the V-SVZ at Gd7.5. Consistently, this caused reduced numbers of newborn cells in the olfactory bulb on postpartum day 2. Interestingly, bromocriptine-treated mice displayed higher anxiety during pregnancy. At first sight, maternal behavior remained intact despite the subdued neurogenesis, but deficits became apparent when the mother was stressed (*95*). Importantly, neurogenesis in the dentate gyrus is not affected by this approach, as it is not modulated by prolactin (*94*, *95*).

Similarly, inhibition of just the pregnancy-induced surge of neurogenesis (but not a complete arrest) with the mitotic inhibitor methylazoxymethanol acetate (MAM), impaired maternal behavior compared to control mothers when mother and nest were placed in an unknown and therefore stressful environment (*95*). Together, this shows that V-SVZ-derived pregnancy-associated neurons play a role in mediating some aspects of maternal behaviour.

1.8 Gliogenesis during pregnancy

The first indications that pregnancy might alter oligodendrogenesis came from multiple sclerosis patients. Relapse rates are lowered during pregnancy, especially during the third trimester, followed by higher relapse rates during the first three months of postpartum, before decreasing to pre-pregnancy levels (*108*).

In mice, early pregnancy (Gd7.5) leads to a prolactin-mediated increase in oligodendrocyte precursor proliferation and OPC cell number in the corpus callosum and the spinal cord, two highly myelinated brain regions (*109*). At gestation day 18, the increase in OPC division during earlier gestation days lead to increased number of new mature (GST π+) oligodendrocytes in both regions. Most of these cells also express the myelin protein MBP. Myelination in the corpus

callosum, as measured by western blot analysis, increases steadily from early pregnancy to postpartum day 14 (*109*). Whether V-SVZ oligodendrogenesis contributes to this effect, or if it is only due to local oligodendrocyte precursor cell proliferation, is still unclear. In the spinal cord, remyelination after lysolecithin-induced focal demyelination in the dorsal funiculus is improved in pregnant mice (*109*). Thus, pregnancy does exert an proliferative effect on OPCs located in two different white matter areas, the spinal cord and the corpus callosum. However, whether and to what extent V-SVZ oligodendrogenesis in a non-pathological condition contributes to the observed pregnancy-induced effects in the corpus callosum, is not resolved.

1.9 Aim of this thesis

1.9.1 Working hypothesis

The functional significance of adult NSC intrinsic heterogeneity and resulting interneuron diversity (and glial cells) is still poorly understood. With many adult-born OB interneuron subtypes only described by morphology and connectivity, but no specific markers, there is only limited understanding about the contribution of each individual interneuron subtype to olfactory processing and olfactory memory formation. Since physiological states modulate adult V-SVZ neurogenesis, the context in which neurons are made might be the key to understanding their function.

We hypothesize that adult V-SVZ neural stem cells comprise a mosaic of cells, and that different physiological states regulate stem cells in regionally distinct domains, modulating neuro- and gliogenesis. Importantly, modulating adult neurogenesis in the niche is a slow form of brain plasticity: consequences of altered stem cell activation only take effect with a delay of two weeks, the time needed for newborn neurons to migrate to the OB and become mature. We propose that dynamic regulation of stem cell activity and interneuron production by life experiences may be a mechanism of adaptive brain plasticity, in which specific OB interneurons are made in anticipation of future need. In the case of hunger and satiety, for example, feeding or energy uptake may lead to increased generation of deep granule cell interneurons in anticipation of times in which food is scarce and energy intake is low. Then, the previously generated additional neurons may help rodents locate food. In the case of pregnancy-induced neurogenesis, interneurons born during the first week of pregnancy would become mature just in time for perinatal care, which relies on olfaction.

The key study on pregnancy and V-SVZ neurogenesis (*94*) was published before the concept of regional stem cell heterogeneity had emerged. *In vivo*, it has not been shown if pregnancy modulates the behavior of stem cells, or of its lineage. Similarly, in the olfactory bulb, neither the types of

neurons generated during pregnancy nor their survival have not been studied in detail. Importantly, becoming a mother is a long transformative journey. In mice, the milestones include the copulatory plug after mating, embryo implantation, immense hormonal changes to maintain pregnancy, birth, and lactation in the postpartum period. To this day, a detailed analysis of adult V-SVZ neurogenesis and oligodendrogenesis over the course of pregnancy has not been performed.

1.9.2 Aims

The aims of this thesis were therefore

1)

- to study the effect of pregnancy on neural stem cells in different spatial domains in the V-SVZ at different moments of gestation
- to characterize the types of OB interneurons made during pregnancy, and to study the dynamics of their addition and survival
- to shed light on the roles of pregnancy-associated interneuron subtypes in maternal behaviour

and

2)

- to study V-SVZ gliogenesis during pregnancy, with a focus on the oligodendrocyte lineage

2 Spatio-temporal recruitment of adult neural stem cells in the V-SVZ for transient neurogenesis

2.1 Manuscript: Spatio-temporal recruitment of adult neural stem cells during pregnancy for transient neurogenesis

One sentence summary

Dynamic response of adult neural stem cells during pregnancy prepares the olfactory bulb for early motherhood

Authors: Zayna Chaker[1*], Corina Segalada[1*], Jonas A. Kretz[2], Ana C. Delgado[1], Valerie Crotet[1], Andreas E. Moor[2] and Fiona Doetsch[1#]

Affiliations:

[1]Biozentrum, University of Basel, Basel, Switzerland

[2] Department of Biosystems Science and Engineering, ETH Zurich, Basel, Switzerland

 # Corresponding author

Fiona Doetsch
Biozentrum, University of Basel
Spitalstrasse 41
CH 4056 Basel
Switzerland
Telephone: +41 61 207 22 30
Email: fiona.doetsch@unibas.ch

[*]These authors contributed equally to this work

Short title:

Pregnancy triggers transient neurogenesis

Abstract:

Neural stem cells (NSCs) in the adult mouse brain contribute to lifelong plasticity. In the adult ventricular-subventricular zone, NSCs are heterogeneous and, depending on their location in the niche, give rise to different subtypes of olfactory bulb interneurons. Here we show that, during pregnancy, multiple regionally-distinct NSCs are recruited on different gestation days. Coordinated temporal activation of these adult NSC pools generates sequential waves of short-lived olfactory bulb interneurons that are temporarily needed during early perinatal care. Spatial transcriptomics revealed layer-specific olfactory bulb remodeling during motherhood, and identified neuropeptide Y interneurons as a new type of adult-generated neuron, which dynamically change in pregnancy. Thus, pregnancy triggers transient neurogenesis under tight spatial and temporal control, highlighting the functional significance of adult stem cell heterogeneity for on-demand brain plasticity.

Main text:

Stem cells in the adult mouse brain dynamically integrate and respond to environmental signals lifelong (*110*, *111*). Ventricular-subventricular zone (V-SVZ) NSCs residing along the lateral ventricles are radial glial fibrillary-acidic protein (GFAP) expressing cells and are found in quiescent or activated states (*111*). NSCs in distinct spatial domains of the V-SVZ give rise to different subtypes of olfactory bulb (OB) interneurons (*111*) which, once integrated, persist long-term (*66*, *112*). In addition to constitutive neurogenesis, regionally-distinct adult NSCs can be modulated by physiological state, namely hunger and satiety (*32*). However, whether other physiological states dynamically control distinct pools of stem cells, and the functional relevance of such regulation, is still unknown. The timing of recruitment of spatially-distinct stem cells and the temporal delay between the generation of adult-born neurons in the V-SVZ and their integration in the olfactory bulb may provide a powerful substrate for plasticity, in preparation for upcoming changing physiological demands.

Pregnancy induces important structural changes in the brain, including increased adult neurogenesis in the olfactory bulb (*94*, *113*). Proliferation in the V-SVZ selectively increases at gestation day 7 and again at postpartum day (Ppd) 7 in a prolactin-dependent manner (*94*, *95*). Perturbing adult V-SVZ neurogenesis results in defects in maternal behavior (*95*, *99*, *107*, *114*). However, depending on the timing of manipulation during gestation, and the phase of

motherhood at which newborn neurons were examined, differing results were obtained (*95*, *97*, *99*, *107*, *114*). Importantly, the process of becoming a mother consists of a succession of physiological phases, including mating, conception, blastocyst implantation, gestation, birth, perinatal care, lactation, and weaning. In light of the discovery of adult neural stem cell regional heterogeneity (*110*, *111*) we investigated whether spatially-distinct neural stem cells are recruited at different times during pregnancy, and in turn affect the dynamics of adult neurogenesis in the olfactory bulb during motherhood.

We first quantified stem cell proliferation (GFAP+ Ki67+) at several timepoints of gestation, and Ppd 7.5 (Fig. 1A, B, Fig. S1A). Pregnancy did not evenly enhance proliferation of stem cells, but only of those residing in certain domains. Intriguingly, V-SVZ domains that tend to be more quiescent, such as the ventromedial wall (Fig. 1C, E and Fig S1A) and the roof (Fig. 1D, F and Fig S1A), were activated during pregnancy, as was the less proliferative dorsomedial corner (DMC, Fig. S1A and B). Stem cells residing in the proliferative dorsolateral wedge (DLW, Fig. 1D, F and Fig S1A) and the ventrolateral wall (Fig. 1C, E and Fig S1A) were also more recruited during pregnancy. In contrast, the dorsolateral wall and intermediate V-SVZ were not more active during pregnancy (Fig. S1A, S1C-D). Notably, pregnancy-related domains displayed distinct temporal dynamics of recruitment (Fig. 1G). Dividing NSCs in the roof and the ventral V-SVZ increased at Gd 4.5 (the day of implantation) or Gd7.5, respectively (Fig 1E and F). In contrast, in the dorsolateral wedge and in the dorsomedial corner, NSC proliferation had more complex dynamics and increased at several gestation days (Fig. 1F, Fig. S1B). All changes were transient, and stem cell proliferation decreased to virgin levels at Gd12.5 and Gd18.5. Stem cell division in mothers at Ppd 7.5 was similar to virgin females in most domains, with the exception of NSCs in the dorsolateral wedge (Fig. 1F).

To more broadly survey domains recruited throughout the entire V-SVZ, we analyzed proliferation in whole mount preparations. Heatmaps of MCM2 cell density (Fig. 1H, Fig. S2C) and fold change intensity (Fig. S1G, S2D) revealed that regions that tend to be more quiescent in virgin mice were activated in pregnant females and exhibited regionally-distinct temporal dynamics. In the rostral medial wall, proliferation started to increase already at Gd0.5, peaking at Gd2.5 and again at Gd7.5 (Fig. 1H). In the caudal two-thirds, cell division progressively increased through Gd7.5 (Fig. 1H, S1E-G). In the lateral wall, the increase was less pronounced, but was highest rostrally at Gd7.5 and caudally at Gd4.5 (Fig. S2A-D). Pregnancy therefore leads to the coordinated recruitment of multiple stem cell pools in different spatial domains at specific gestation days in the entire V-SVZ.

Adult-born neurons are already functionally integrated about two to three weeks after their generation (*66*, *68*), which coincides with key phases of motherhood, just after birth and during early perinatal care. To investigate whether the temporally coordinated recruitment of spatially-distinct NSCs during pregnancy resulted in the addition of specific interneuron subtypes to the olfactory bulb, we analyzed olfactory bulbs twenty days after pulsing once with a thymidine analog on different gestation days (Gd 0.5, 2.5, 4.5 or 7.5) (Fig. 2A, B). Most adult-generated neurons integrate into the granule cell layer of the main olfactory bulb (MOB), with a bias toward the deep granule cell layer (*37*) and have a different connectivity than those in the superficial granule cell layer (*85*). New neurons also integrate into the glomerular layer (GL) (*110*) and more rarely into the mitral cell layer (*60*). During the perinatal care period, neurogenesis was globally increased in the olfactory bulb of mothers, but strikingly the distribution of neurons within layers differed depending on their day of birth (Fig. S3A, B). In the granule cell layer, only newborn neurons (thymidine analogue+ NeuN+) labeled at Gd4.5 and 7.5 increased in mothers (Fig. 2C to F, Fig. S3C). Moreover, the increase was highest in the superficial granule cell layer (Fig. S3A, D), in both Calretinin (CalR) positive and negative cells (Fig. S3E and F). In the glomerular layer (GL), CalR+ and Calbindin+ (CalB) neurons born at Gd 4.5 and 7.5, and Tyrosine hydroxylase+ (TH) neurons at Gd 7.5, were increased in number (Fig. S4A to E). Notably, increased neuronal addition also occurred in mothers in the mitral cell layer, which was the only layer where more new neurons were already generated at Gd 0.5 and 2.5 (Fig. 2C-F). Neurogenesis in the accessory olfactory bulb (AOB) (Fig. 2B-F), where adult born-neurons have been implicated in social and reproductive behaviour (*115*), was also increased, but only those in the granule cell layer generated on Gd 4.5 and Gd 7.5 (Fig. S3G and H). Thus, pregnancy results in the generation of neurons at different days of gestation that are added to distinct olfactory bulb layers during early motherhood.

To investigate whether pregnancy-related neurons are transient or long-lasting, we assessed their survival 10 days later (30 dpi), when pups are progressively feeding on solid food and mothers are less engaged in maternal care (Fig. 2A). Strikingly, in all layers in which neurogenesis was enhanced in mothers, except the GL (Fig. S5A-C), the number of newborn neurons decreased between 20 dpi and 30 dpi (Fig. 2G-I). This decrease in newborn neurons was not observed in matched virgin controls. Interestingly, neurons born on different gestation days and integrated into different layers exhibited distinct survival rates. While granule cell layer interneurons had been culled by 30 dpi (Fig. 2H), in the mitral cell layer (Fig. 2G) and in the AOB (Fig. 2I) some neurons born on Gd7.5 still persisted through weaning in mothers.

The short-term addition of pregnancy-related olfactory bulb interneurons suggested that they may be transiently needed in the perinatal period. We first examined whether they were already functionally integrated into the OB circuitry at 20dpi, as measured by c-fos expression (Fig. 3A-C). In both the granule cell and mitral cell layers, Gd4.5 and Gd7.5 pulsed mothers had more c-fos+ analog+ neurons as compared to virgins or virgins exposed to pups during perinatal care (Fig. 3A-C). A similar trend was also observed in the AOB (Fig. S6A). Interestingly, in the MOB of mothers, c-fos expressing analog+ granule neurons were predominantly located in the superficial layer (Fig. S6B). Next, to investigate whether the survival of transient neurons generated during pregnancy could be prolonged, we performed cross-fostering experiments to extend the early perinatal care period. Foster mothers had their biological pups removed at Ppd6 and were given newborn pups twice, at six- or seven-day intervals, and analyzed at the time point corresponding to the weaning of their biological pups (30dpi) (Fig. 3D). Strikingly, foster-mothers maintained granule cell layer interneurons born at Gd4.5 and Gd7.5 (Fig. 3E), but the survival of those integrated in the mitral cell layer (Fig. 3F) or AOB (Fig. S6C) was not prolonged. Notably, after pup removal at birth (donor mothers), the increase in newborn interneurons in the mitral cell layer (Fig. 3F) and AOB was absent during perinatal care (Fig S6C), whereas granule cell layer interneurons were unaffected (Fig 3E). Thus, while maintenance of pregnancy-associated granule cell layer neurons beyond the first days of perinatal care requires active involvement in maternal care, mitral cell layer interneuron survival depends on the continuous presence of the mother's own pups. Together these data reveal the physiological relevance of pregnancy-associated neurons and functional heterogeneity among adult-born mitral cell and granule cell layer interneurons.

To identify global and layer-specific molecular changes in the olfactory bulb of mothers, and to identify potential markers for pregnancy-associated interneurons, we performed 10x Visium spatial transcriptomics (Fig. S7A-E). This approach allowed us to map transient and longer-lasting changes in the olfactory bulb occurring during perinatal care and peri-weaning, as compared to virgins, while preserving spatial information. Unbiased clustering of the transcriptomic data revealed 11 clusters, which corresponded to anatomical layers in the MOB and AOB, including separate clusters for the superficial and deep granule cell layers in the MOB (Fig 4A, Fig, S7B). Markers for each cluster in the MOB and AOB were confirmed using the Allen Brain Atlas in situ database, validating the power of this approach (Fig. S7F and G).

Comparison of the whole olfactory bulb transcriptome (MOB and AOB pooled) of mothers during perinatal care and virgins revealed up-regulation of GO processes related to circadian clock (*Per1*), neuronal generation and dendritic remodeling (*Elp3, Klf9, Nr4a3*), and neuronal activity (*Egr1, Egr3*)) (Fig. S8A, B, Table S1 and Table S2). RNAscope of selected candidate genes validated this upregulation (Fig. S8C). The majority of up-regulated genes during perinatal care were maintained in mothers through peri-weaning (136 / 161 genes) (Table S2, Tab4) and were related to ribosome biogenesis and translation (*RPL*, *RPS, Etf1*), and mitochondrial function (*Cox* and mitochondrial genes) (Fig. S9A-D Table S2, Tab6). In contrast, genes transiently upregulated during perinatal care (25 / 161 genes) (Fig. S9A, Table S2, Tab3) belonged to GO processes of neuronal development, differentiation and cell migration (Fig. S9C, D, Table S2, Tab5), again highlighting the transient nature of pregnancy-associated neurogenesis in the olfactory bulb. Moreover, pair-wise comparison of differentially expressed genes in each cluster (Fig. S10A, Table S3) showed that some processes were enriched in specific layers (Figure S10B and C, Table S4), whereas others were increased globally (Fig. S10C, Table S4). Furthermore, these layer-based maps differed between perinatal care and weaning (Fig. S10C, D). Altogether, the spatial transcriptomic analysis highlights multiple modes of remodeling occurring in the olfactory bulb during motherhood, from synaptic plasticity to the generation of new cells.

Importantly, two clusters (4 and 9) were enriched in mothers compared to virgins, but not uniquely related to discrete anatomical layers of the olfactory bulb (Fig. S11A). 10x Visium slide analysis showed that cluster 4 was primarily localized to the outer layers, and cluster 9 to the inner layers of the olfactory bulb (Fig. S11A). Allen Brain ISH for top markers in both clusters confirmed this spatial distribution (Fig. S11B). Genes up-regulated in clusters 4 and 9 (Table S4, Tab1) included doublecortin (*DCX*) and *Dlx2*, markers of newly generated neurons (Fig. 4B, Fig. S11C), and CalR (*Calb2*), of which there were increased analog+ neurons in the superficial granule cell layer and GL (Fig S3D and E). Moreover, Cluster 4 and 9 enriched genes contributed to GO processes related to neurogenesis (*Dlx2, Dcx*), gliogenesis, behavior and blood vessel remodeling (Fig. 4B, Table S4, Tab3 and Tab4). As such they were ideal clusters to identify markers for transient pregnancy-related interneurons, especially for those in the mitral cell layer and superficial granule cell layer, for which few molecular markers are known (*60*). Strikingly, Neuropeptide Y (NPY) was transiently up-regulated in mothers in Cluster 4 (Fig. 4B, TableS4, Tab1 and Tab2), and quantification of thymidine analog+ cells in both the mitral cell and superficial granule cell layers showed that the increase in new neurons born at Gd 4.5/Gd7.5 was largely due to NPY+

interneurons (Fig. 4C-E). Thus, we identify NPY+ interneurons as a new type of adult-born olfactory bulb interneurons that are dynamically modulated during pregnancy.

Here we show that pregnancy triggers the coordinated recruitment of regionally-distinct stem cells in response to specific physiological phases during gestation, leading to a tightly controlled temporal addition of distinct interneuron subtypes into different layers of the olfactory bulb at key moments in motherhood. These pregnancy-related interneurons are short-lived, and their temporary addition and culling may be key contributors to on-demand olfactory bulb plasticity during motherhood. As such, dynamic stem cell recruitment for the generation of diverse neurons during early pregnancy prepares the maternal brain in anticipation of changing physiological needs. In songbirds and chickadees, seasonal neurogenesis has been linked to seasonal song-learning and food-caching (*116*, *117*). The general principle of transient neurogenesis at different time scales upon physiological demand may be conserved across evolution, including in humans, such as during pregnancy where the sense of smell can transiently but dramatically change. In sum, different physiological states, including pregnancy and hunger and satiety (*32*), regulate spatially-distinct NSC pools, revealing an underlying logic for adult NSC heterogeneity in the V-SVZ. Time, space and physiological context are key to fully decode this functional stem cell map.

Acknowledgements:
We thank members of the Doetsch lab, P. Scheiffele, D. Thaler and S. Jessberger for discussion and/or comments on the manuscript; and the Biozentrum Imaging Core Facility for help with image acquisition and analysis, especially S. Herbert and K. Schleicher. **Funding**: This work was supported by Swiss National Science Foundation 31003A_163088 (F.D), European Research Council Advanced Grant (No 789328) (F.D.), the University of Basel, Biozentrum PhD Fellowship University of Basel (C.S.) and the Doris Dietschy und Denise Dietschy-Frick-Stiftung (C.S.). A.E.M. was supported by an SNSF Eccellenza Professional Fellowship from the Swiss National Science Foundation (PCEFP3_181249). **Author Contributions:** Conceptualization: F.D., Z.C. and C.S.; Performed experiments: Z.C., C.S., J.A.K., A.C.D. and V.C.; Data Analysis: Z.C., C.S. and J.A.K; Supervision: F.D. and A.E.M; Manuscript writing: Z.C., C.S. and F.D.
Competing Interests: The authors declare no competing interests.

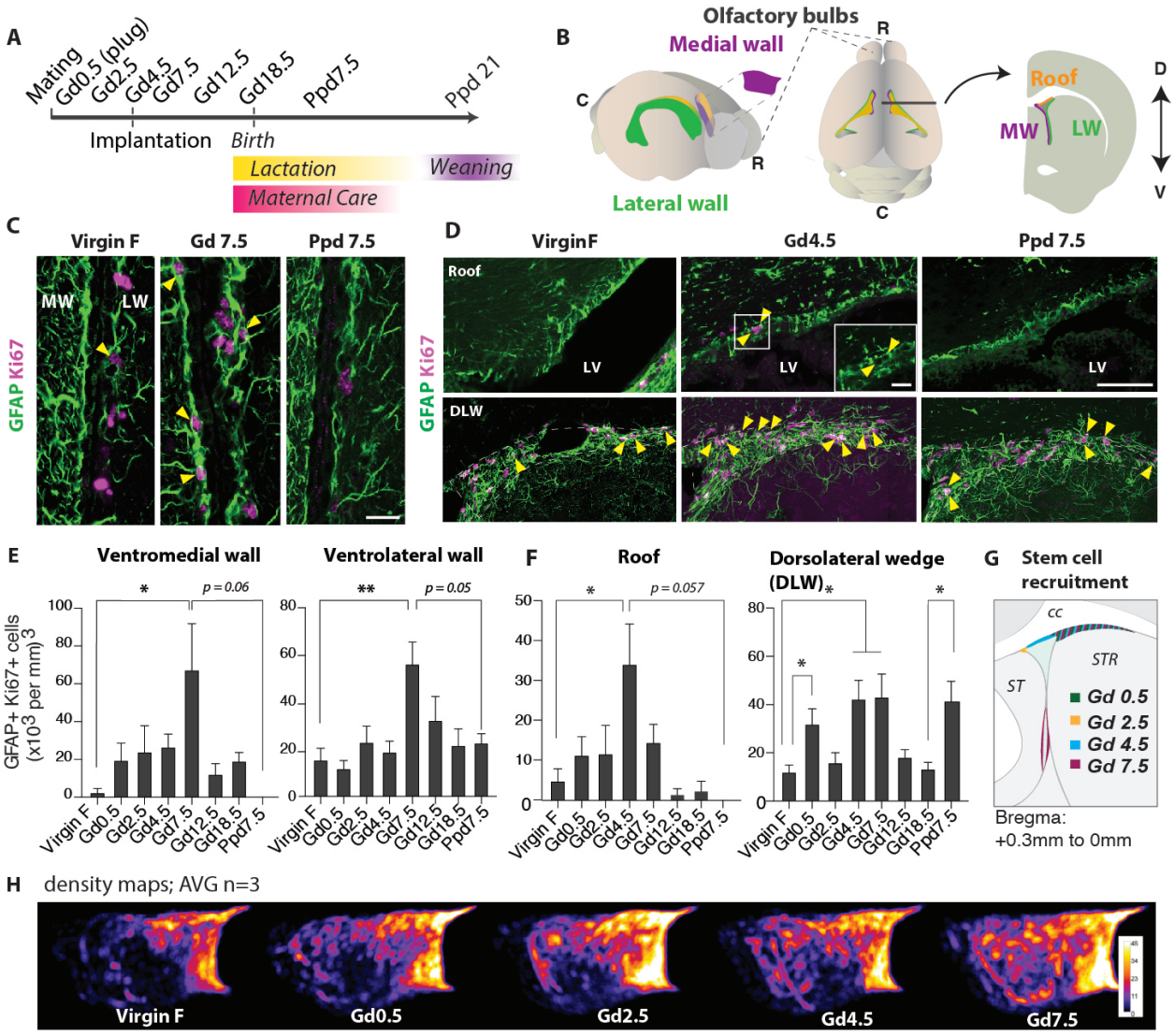

Fig. 1 Dynamic spatial and temporal response of adult V-SVZ NSCs to pregnancy

(**A**) Timeline of gestation (Gd) and post-partum (Ppd) period. (**B**) *Left:* Schema of a mouse brain showing the location of the V-SVZ stem cell niche, with the lateral wall in green, the medial wall in magenta and the roof of the lateral ventricle in orange. *Middle:* Top-down view of mouse brain showing the V-SVZ. Black bar indicates level of coronal section on *right*. **(C and D)** Representative images of dividing NSCs (arrowheads) with GFAP in green and Ki67 in magenta in ventrolateral and ventromedial V-SVZ **(C)** and the roof and dorsolateral wedge (**D**). See Fig. S1D for more domains. (**E** and **F**) Quantification of dividing stem cells. (**G**) Summary schema of temporal and spatial recruitment of V-SVZ stem cell domains during pregnancy. **(H)** Averaged MCM2 density maps on the medial wall for each timepoint (n=3). Scale indicates intensity. Scale bars: **C,** 20μm, **D,** 50μm, Box in **D** 10μm, I: 50μm. LV: lateral ventricle. MW: medial wall, LW: lateral wall, C: caudal, R: rostral, D: dorsal, V: ventral, DLW: dorsolateral wedge, cc: corpus callosum, ST: septum, STR: striatum

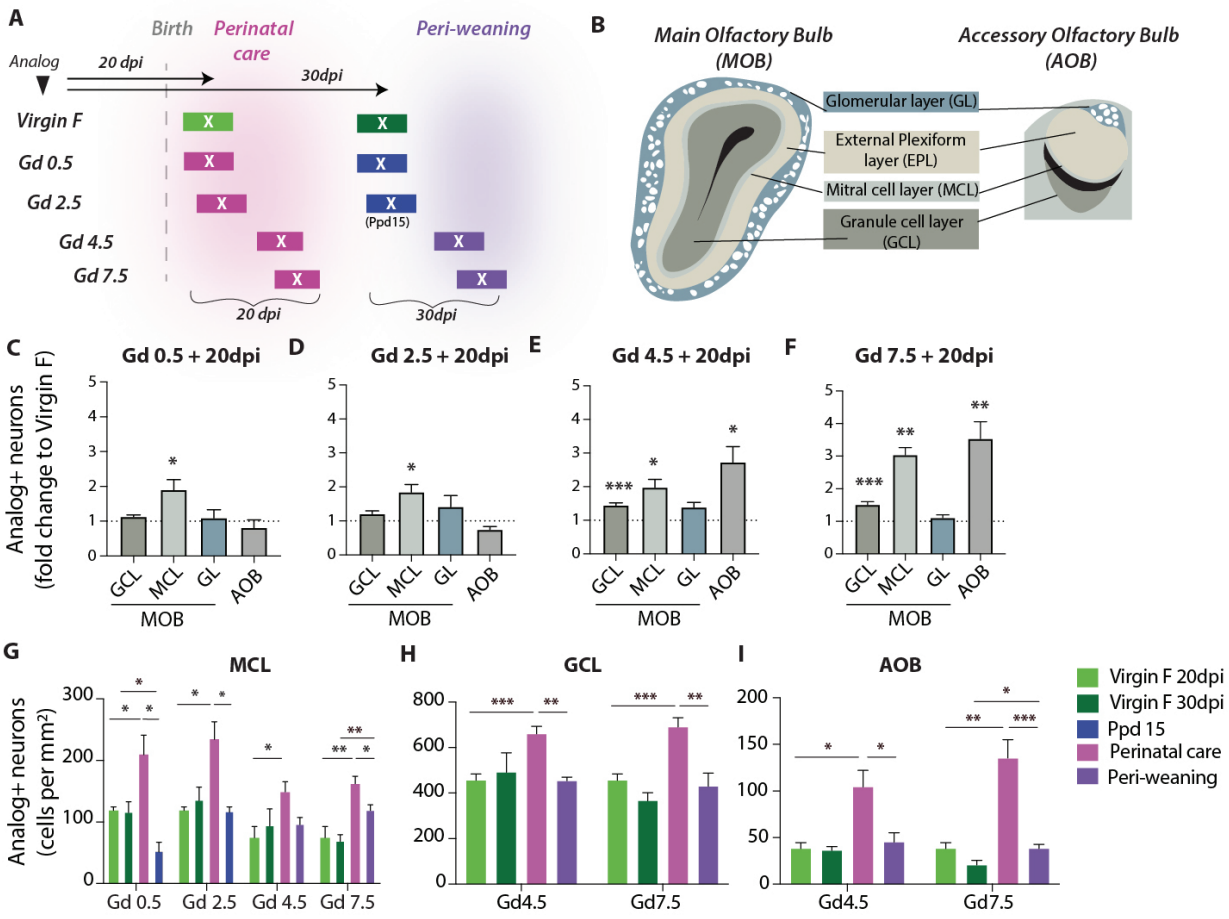

Fig. 2 Waves of distinct OB interneuron subtypes are generated during pregnancy

(**A**) Schema of pulse-chase experiment on different gestation days (Gd) during pregnancy, and physiological phases corresponding to 20 and 30 dpi. (**B**) Schema of different layers in MOB and AOB. (**C** to **F**) Quantification of fold-change of Analog+ neurons generated at different gestation days in distinct OB layers compared to matched virgin controls. (**G** to **I**) Quantification of newly-generated neurons born on different Gd at 20 dpi and 30 dpi in the MCL (**G**), GCL (**H**), AOB (**I**).

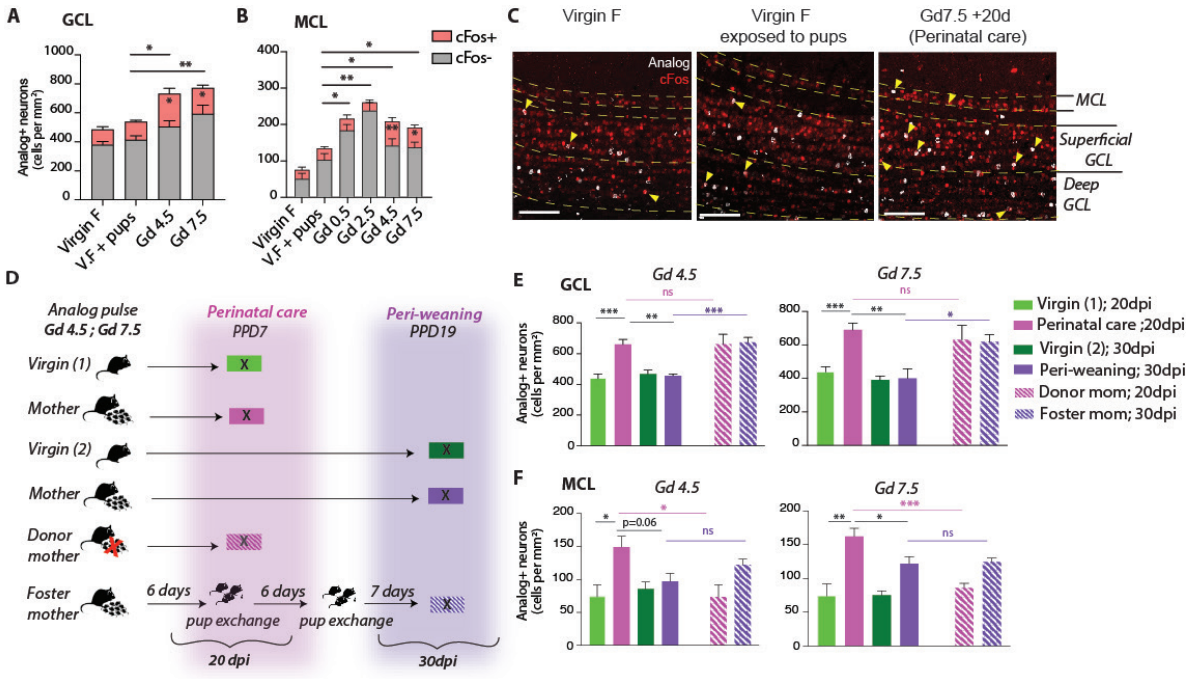

Fig. 3 Pregnancy-generated neurons are functional and differentially involved in perinatal care

(A-C) c-fos expression in newborn neurons in the GCL **(A)**, and in the MCL **(B)** of the MOB. Stars above refer to comparisons between virgin exposed to pups and mothers. Stars inside pink bars show significant differences in c-fos+ analog+ cell number. (**C**) Representative images of analog+ c-fos+ cells in the MOB of mothers pulsed at Gd 7.5, and virgin females with or without pups. Arrowheads indicate co-labeled cells. **(D)** Cross-fostering experimental design. (**E-F**) Effect of cross-fostering or pup removal on dynamics of Gd4.5- and Gd7.5-born neurons in the GCL (**E**) and MCL (**F**) of the MOB. Gd: gestation day, MCL: mitral cell layer, GCL: granule cell layer, PPD: post-partum day. Scale bars, 100µm.

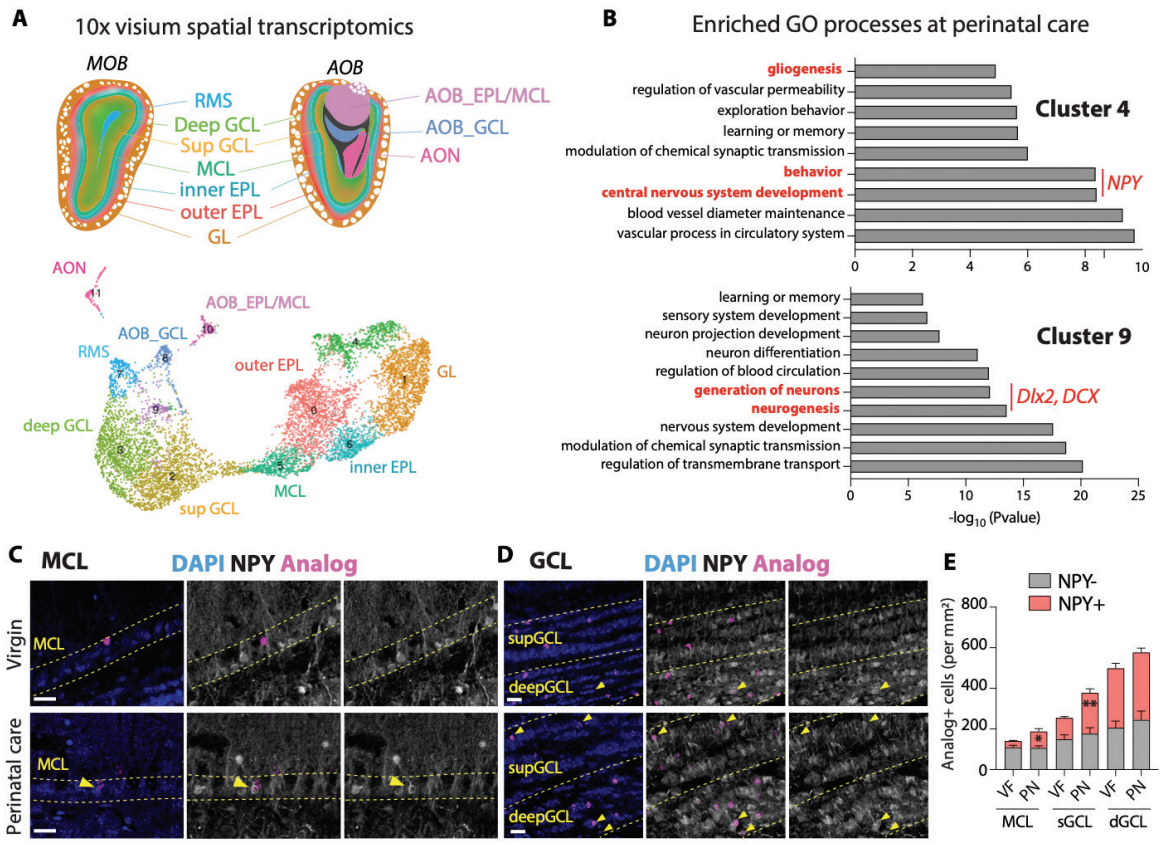

Fig. 4 Spatial transcriptomic analysis of olfactory bulb remodeling in mothers

(**A**) 10x Visium spatial transcriptomics of MOB and AOB. Color-coded schema of olfactory bulb anatomical layers in MOB and AOB matching colours in UMAP plot from unbiased clustering. (**B**) GO process analysis for genes enriched in clusters 4 and 9 transiently at perinatal care. Selected genes are highlighted in red. (**C, D**) Immunostaining for NPY (grey) and analog (magenta) in the MCL (C) and GCL (D). Yellow arrowheads show co-labeled analog+ NPY+ cells. (**E**) Quantification of analog+ and NPY co-labeled cells in MCL, superficial and deep GCL. MOB: main olfactory bulb, AOB: accessory olfactory bulb, RMS: rostral migratory stream, supGCL/sGCL: superficial granule cell layer, deepGCL/dGCL: deep granule cell layer, MCL: mitral cell layer, EPL: external plexiform layer, GL: glomerular layer; AON: anterior olfactory nucleus. Scale bars 20µm.

2.2 Supplemental Materials

Supplementary Materials for

SPATIO-TEMPORAL RECRUITMENT OF ADULT NEURAL STEM CELLS DURING PREGNANCY FOR TRANSIENT NEUROGENESIS

Zayna Chaker[1*], Corina Segalada[1*], Jonas A. Kretz[2], Ana C. Delgado[1], Valerie Crotet[1], Andreas E. Moor[2] and Fiona Doetsch[1#]

Correspondence to: Fiona Doetsch, fiona.doetsch@unibas.ch

This PDF file includes:

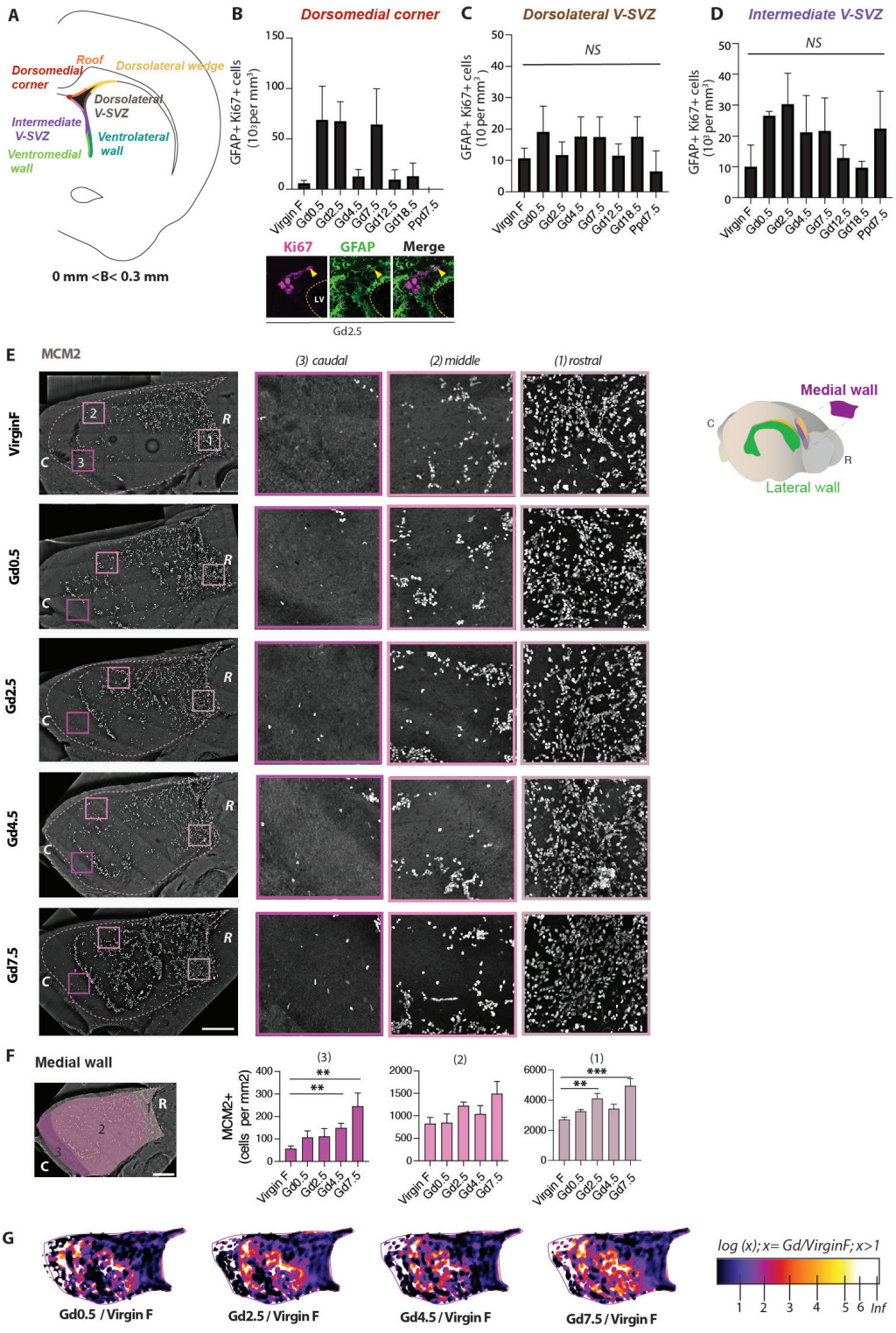

Fig. S 1 Regional dynamics of adult NSCs and their progeny in the V-SVZ during pregnancy

(**A**) Schema illustrating different V-SVZ domains analyzed. (**B-D**) Quantification of GFAP+ Ki67+ cells in the dorsomedial corner and corresponding GFAP/Ki67 images at Gd 2.5 (**B**), in the dorsolateral V-SVZ (**C**), and intermediate V-SVZ (**D**). (**E**) Whole mount immunostaining for

MCM2 in the medial wall. Schema on far right shows medial wall in magenta. Left hand column shows low power magnification of MCM2+ cells in entire medial wall. Boxes in magenta are shown at higher power on the right. (**F**) Quantification of MCM2+ cells in the three areas of the medial wall depicted in the schema. (**G**) Maps displaying the fold change in proliferation at each analyzed pregnancy day compared to virgin females on a log scale. Colored areas are those in which pregnant mice showed higher MCM2 density compared to virgin females. Black regions include non-changing regions and domains in which virgin females had higher proliferation than pregnant mice. R, rostral, C, caudal. scale bars in E and F: 500μm

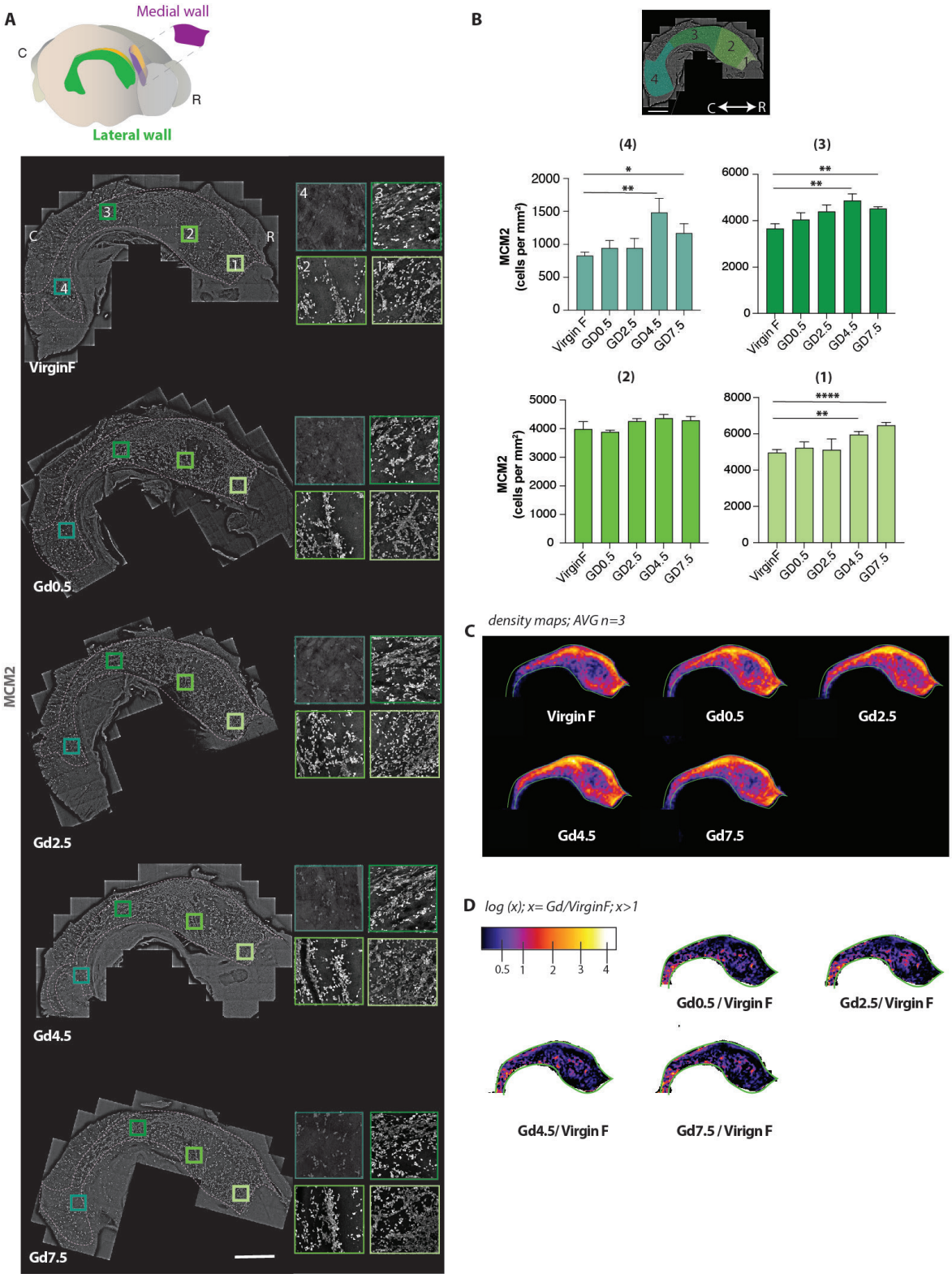

Fig. S 2 Analysis of cell proliferation during the first week of pregnancy in the lateral wall

(A) Schema of Lateral wall in green (top). Whole mount immunostaining for MCM2 in the lateral wall. Boxes in green are shown at higher magnification on the right. **(B)** Quantification of MCM2+ cells in the lateral wall were binned in the four shaded areas shown in schema at top.

(C) Maps showing MCM2+ cell density in the lateral walls on different gestation days based on a nearest neighbor analysis. (**D)** Maps displaying the fold change in proliferation at each analyzed pregnancy day compared to virgin females on a log scale. Colored areas are those in which pregnant mice showed higher MCM2 density compared to virgin females. Black regions include non-changing regions and domains in which virgin females had higher proliferation than pregnant mice. Scale bars in A and B: 1000μm.

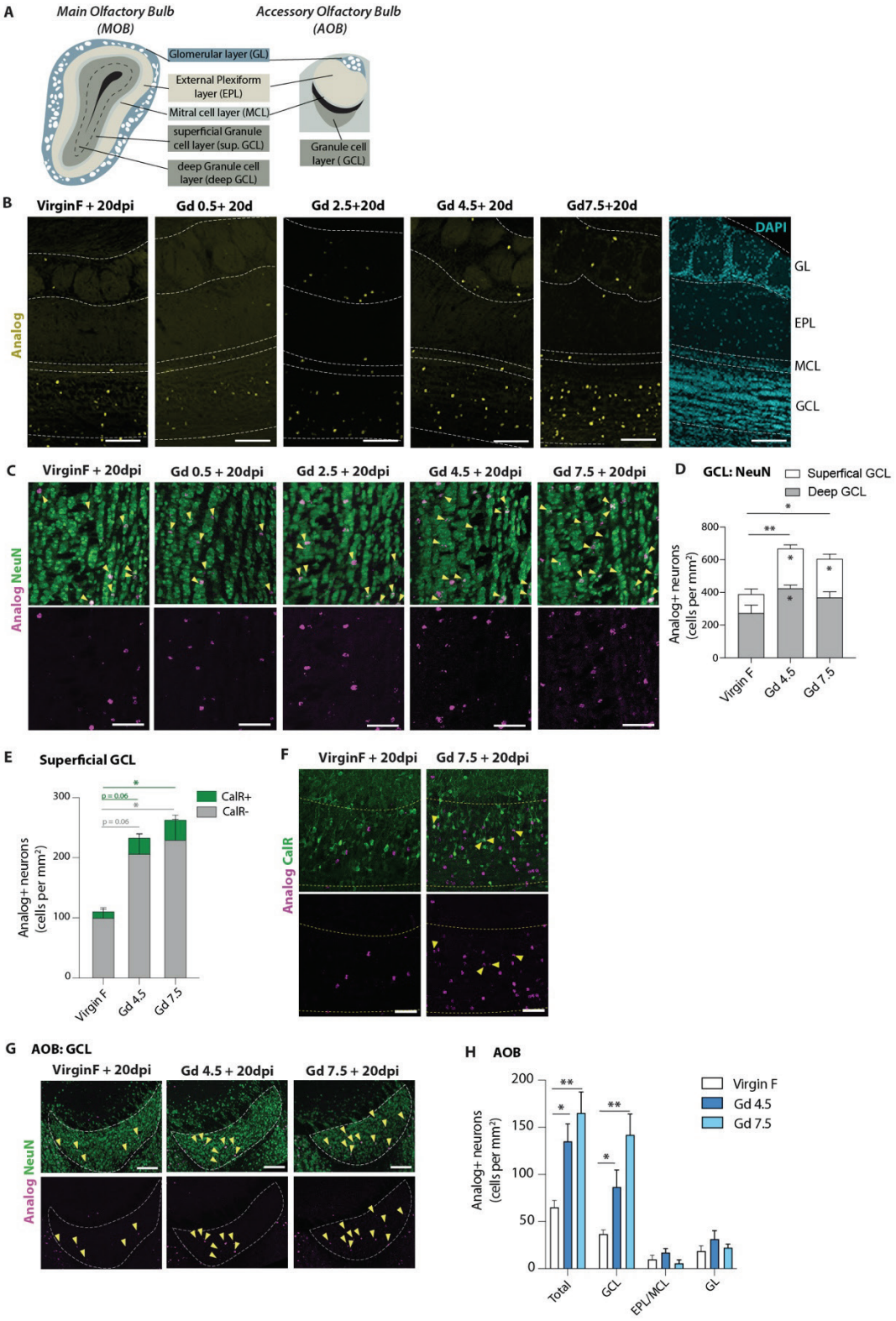

Fig. S 3 Characterization of newborn neurons in the main olfactory bulb and accessory olfactory bulb at 20 dpi

(A) Schema of layers in the main and accessory olfactory bulb. (**B**) Right panel: Low power image of representative DAPI stained main olfactory bulb showing different layers. Left panels: Images

of thymidine analog+ cells in the MOB of virgin mice and mothers pulsed at Gd 0.5, Gd 2.5, Gd 4.5 or Gd 7.5. (**C** to **F**), Characterization of newborn neurons in the GCL. (**C**) Representative images of GCL showing NeuN in green and analog in magenta. (**D**) Quantification of analog+ NeuN+ neurons in both superficial and deep GCL at Gd 4.5 and Gd 7.5 + 20 dpi. (**E**) Quantification of total NeuN+ analog+ neurons and the fraction that is CalR+ in the superficial GCL at Gd 4.5 and Gd 7.5 + 20 dpi. (**F**) Representative images of (**E**), showing CalR in green and analog in magenta. (**G** and **H**) Characterization of newborn neurons in the AOB. Representative pictures (**G**) show NeuN in green and analog in magenta. Arrowheads indicate double-labeled cells. (**H**) Quantification of newborn neurons (NeuN+ analog+) generated at Gd 4.5 and 7.5 in each AOB layer. MOB: Main olfactory bulb; AOB: Accessory olfactory bulb; GL: Glomerular layer; EPL: External plexiform layer, MCL: Mitral cell layer, GCL: Granule cell layer. Scale bars: (**B** and **G**): 100μm. (**C** and **F**): 50μm

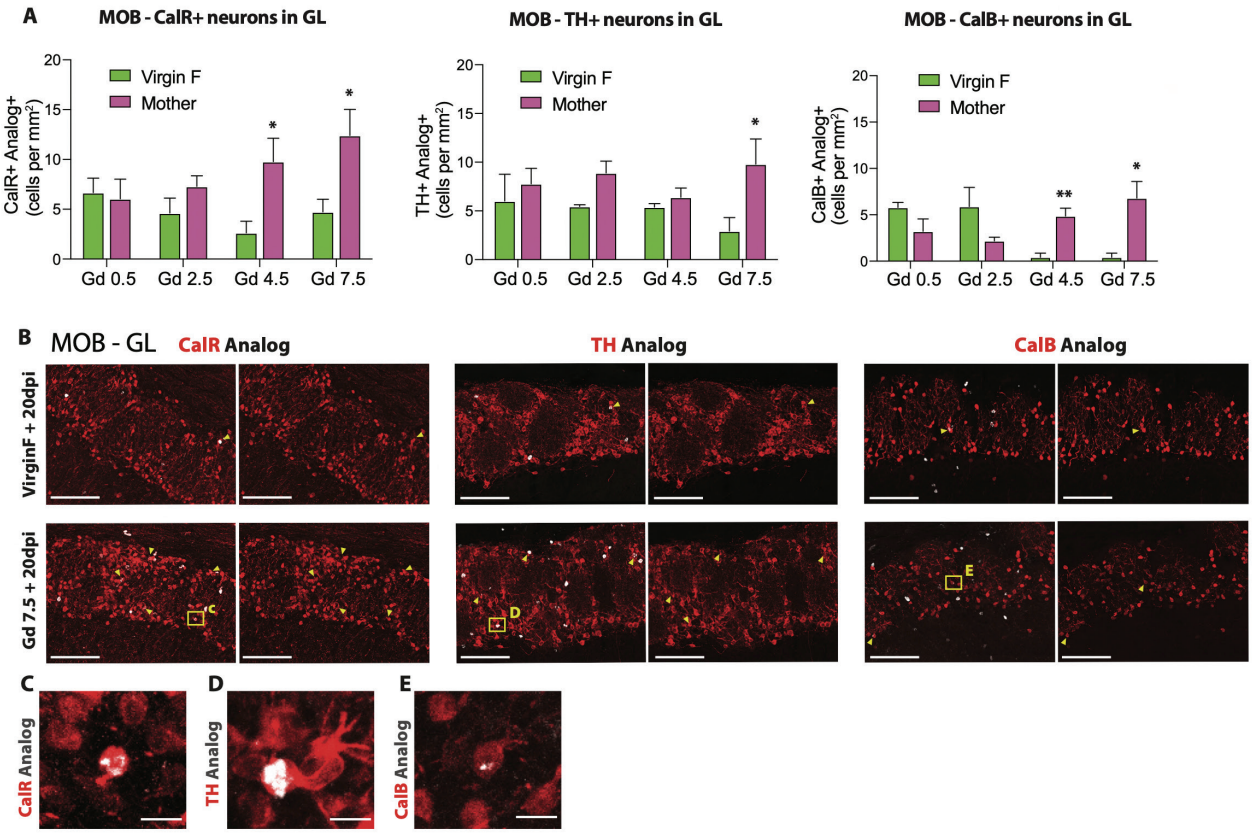

Fig. S 4 Characterization of newborn neurons in the glomerular layer of the main olfactory bulb at 20dpi

(**A**) Quantification of analog+ Calretinin (CalR+), Tyrosine hydroxylase (TH+) and Calbindin (CalB+) cells in mothers and their corresponding matched virgin controls. (**B**) Representative images of analog+ CalR+, TH+ and CalB+ subtypes in the GL comparing virgin females (top panels) and Gd 7.5 + 20 dpi (bottom panels). (**C** to **E**), High-power images of CalR+, TH+ and CalB+ analog double-positive cells shown in boxes in (**B**). MOB: Main olfactory bulb; GL: Glomerular layer. Scale bars: (**B**) 100µm, (**C** to **E**) 10µm.

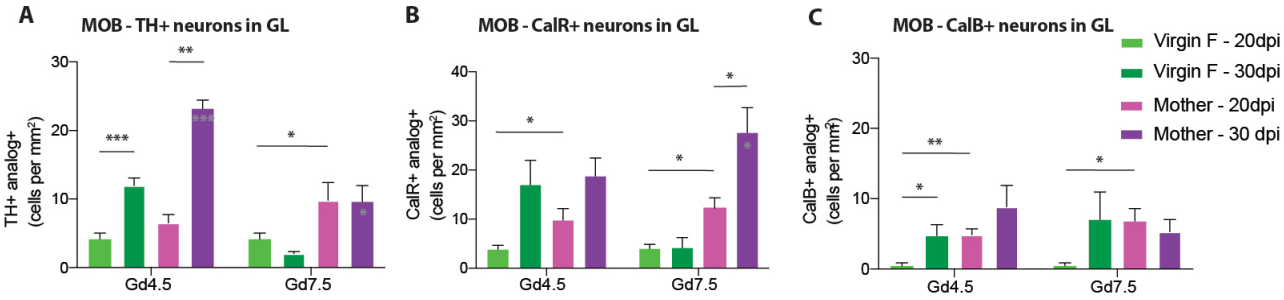

Fig. S 5 Neuronal addition dynamics in the glomerular layer of the main olfactory bulb

(**A** to **C**) Quantification of dynamics of analog+ Tyrosine hydroxylase (TH+), Calretinin (CalR+) and Calbindin (CalB+) newborn neurons in the GL at Gd 4.5/Gd 7.5 + 20dpi and 30dpi. Grey stars inside the purple bars show significant differences as compared to the virgins 30dpi. MOB: main olfactory bulb; GL: glomerular layer.

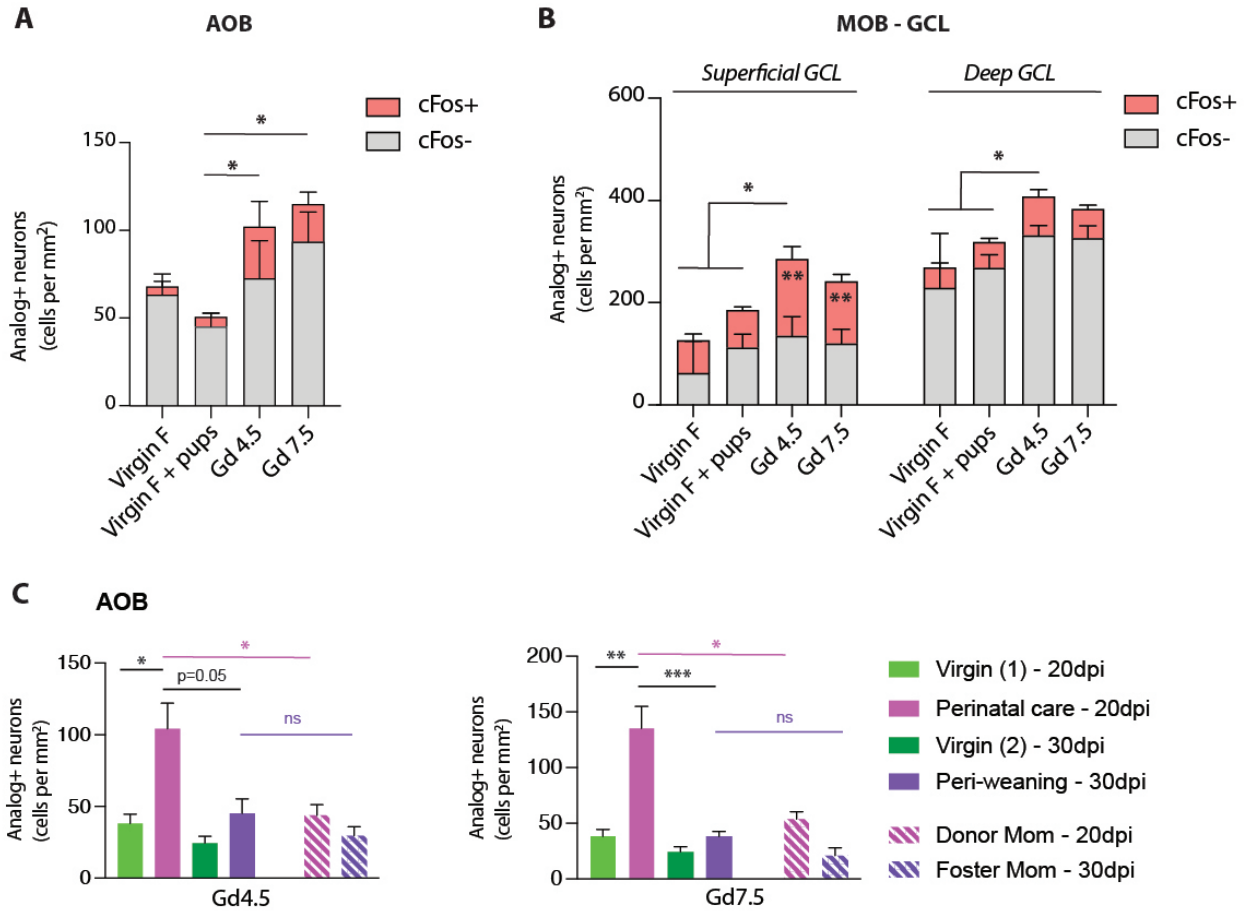

Fig. S 6 Dynamics of newborn neurons in the main and accessory olfactory bulbs

(**A**) Proportion of c-fos+ analog+ neurons in the AOB at Gd 4.5/7.5 + 20 dpi. Stars shows significant increase in total analog+ cell number in mothers compared to virgins exposed to pups. (**B**) Quantification of c-fos+ analog+ neurons in superficial and deep GCL at Gd 4.5/7.5 + 20 dpi. Stars inside pink bar graphs show significant differences in c-fos+ analog+ cell number between virgins exposed to pups and mothers. **(C)** Quantification of cross-fostering experiment in AOB. MOB: main olfactory bulb; AOB: accessory olfactory bulb; GCL: granule cell layer.

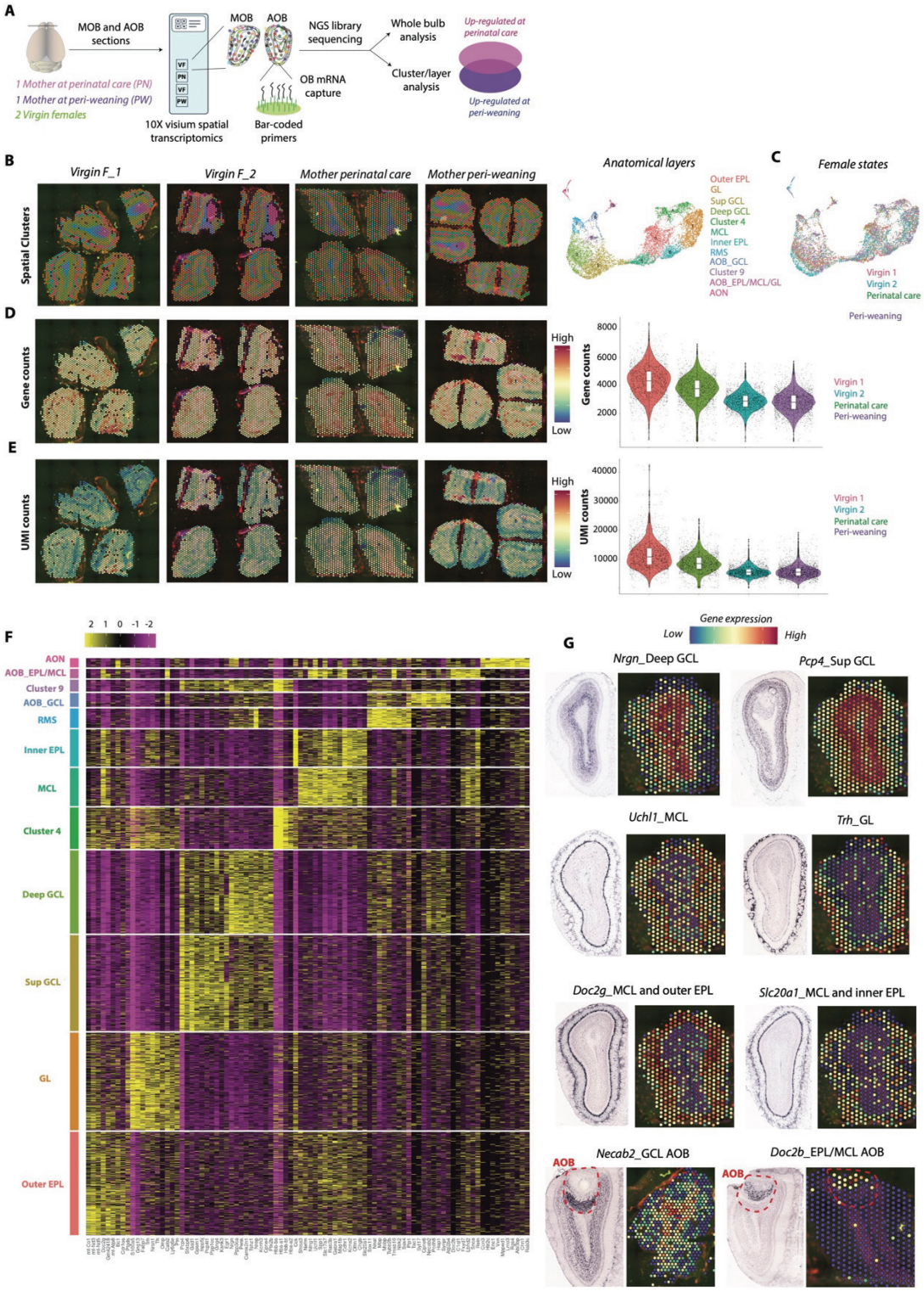

Fig. S 7 10x Visium spatial transcriptomics of the olfactory bulb

(**A**) Flowchart of the 10x Visium spatial transcriptomic experimental design. **(B)** Visium sequencing slides highlighting spatial OB clusters (*left*), and the corresponding UMAP plot of transcriptomic data clusters (*right*). (**C**) UMAP plot of clustered data highlighting sample origin.

(**D**) Visium slides and corresponding violin plots of the gene counts. (**E**) Visium slides and corresponding violin plots of the UMI counts. (**F**) Heatmap showing the top genes for each cluster. This clustering method allows unbiased segregation of deep and superficial GCL, as well as inner and outer EPL, and AOB layers. (**G**) Allen Brain in situ hybridization images showing enriched markers for each OB layer, with corresponding gene expression on experimental Visium slides (maximal cutoff: *Nrgn* = 3, *Pcp4* = 4, *Uclh1* = 3, *Trh* = 3, *Doc2g* = 3.2, *Slc20a1* = 2.4, *Necab2* =2.9, *Doc2b* = 1.8). Deep GCL: deep granule cell layer; Sup GCL: superficial granule cell layer; MCL: mitral cell layer; EPL: external plexiform layer; AOB: accessory olfactory bulb; RMS: rostral migratory stream; AON: anterior olfactory nucleus.

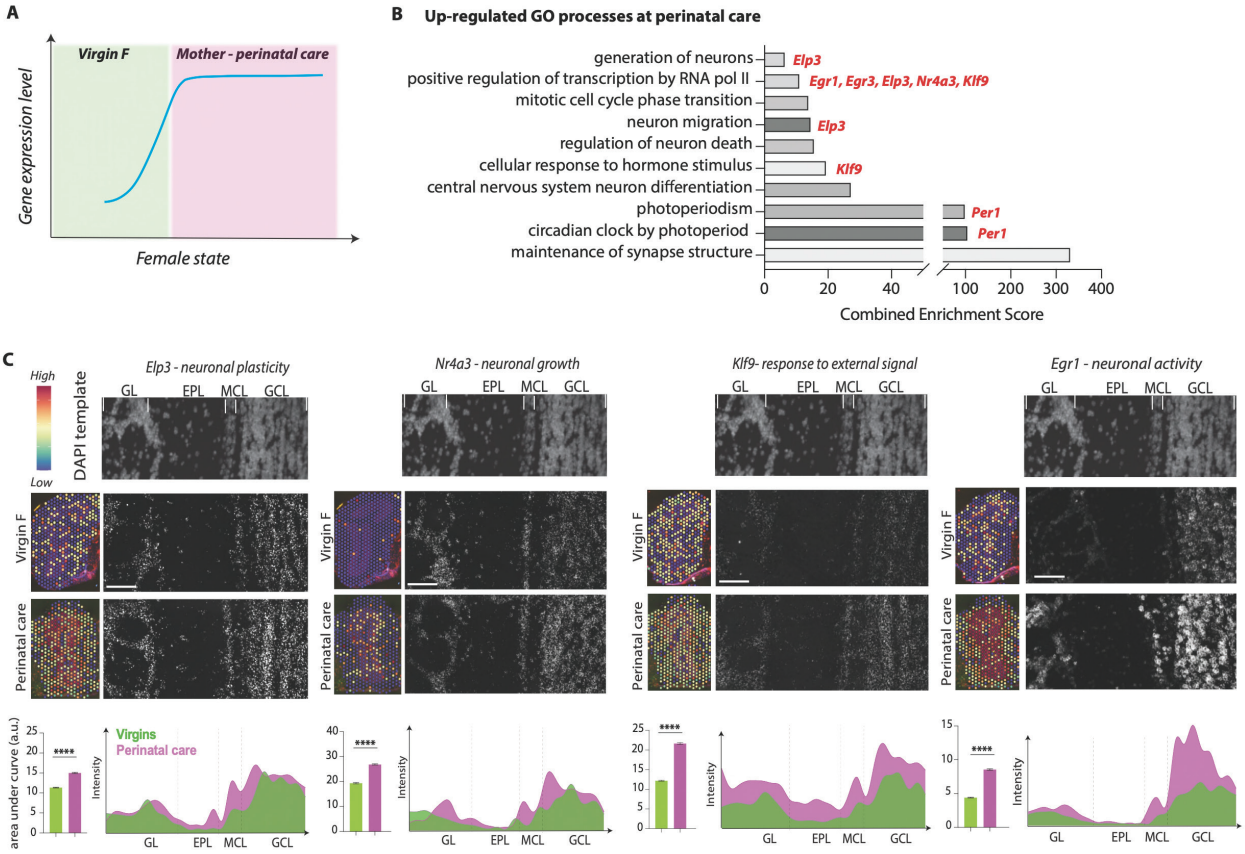

Fig. S 8 Whole olfactory bulb analysis of spatial transcriptomic data reveals OB remodeling in mothers during perinatal care

(**A**) Whole bulb sequencing analysis comparing perinatal care mothers with Virgins. Cutoffs: Log2FC > 0.10, Adj-P-value < 0.05. (**B**) GO process analysis using EnrichR, highlighting genes belonging to specific biological functions. (**C**) RNAscope validation of selected gene expression in the olfactory bulb of mothers during perinatal care and virgins (n = 3). *Top*: DAPI image of olfactory bulb layers shown in RNAscope images below. *Left*: gene expression on Visium slides (maximal cutoff: *Elp3* = 2, *Klf9* = 2.5, *Nr4a3* = 1.3, *Erg1* = 2). *Bottom Right:* RNAscope signal quantification using line profile intensity along olfactory bulb anatomical layers. Bar graphs show quantification of area under curves. GL: glomerular layer, EPL: external plexiform layer, MCL: mitral cell layer, GCL: Granule cell layer.

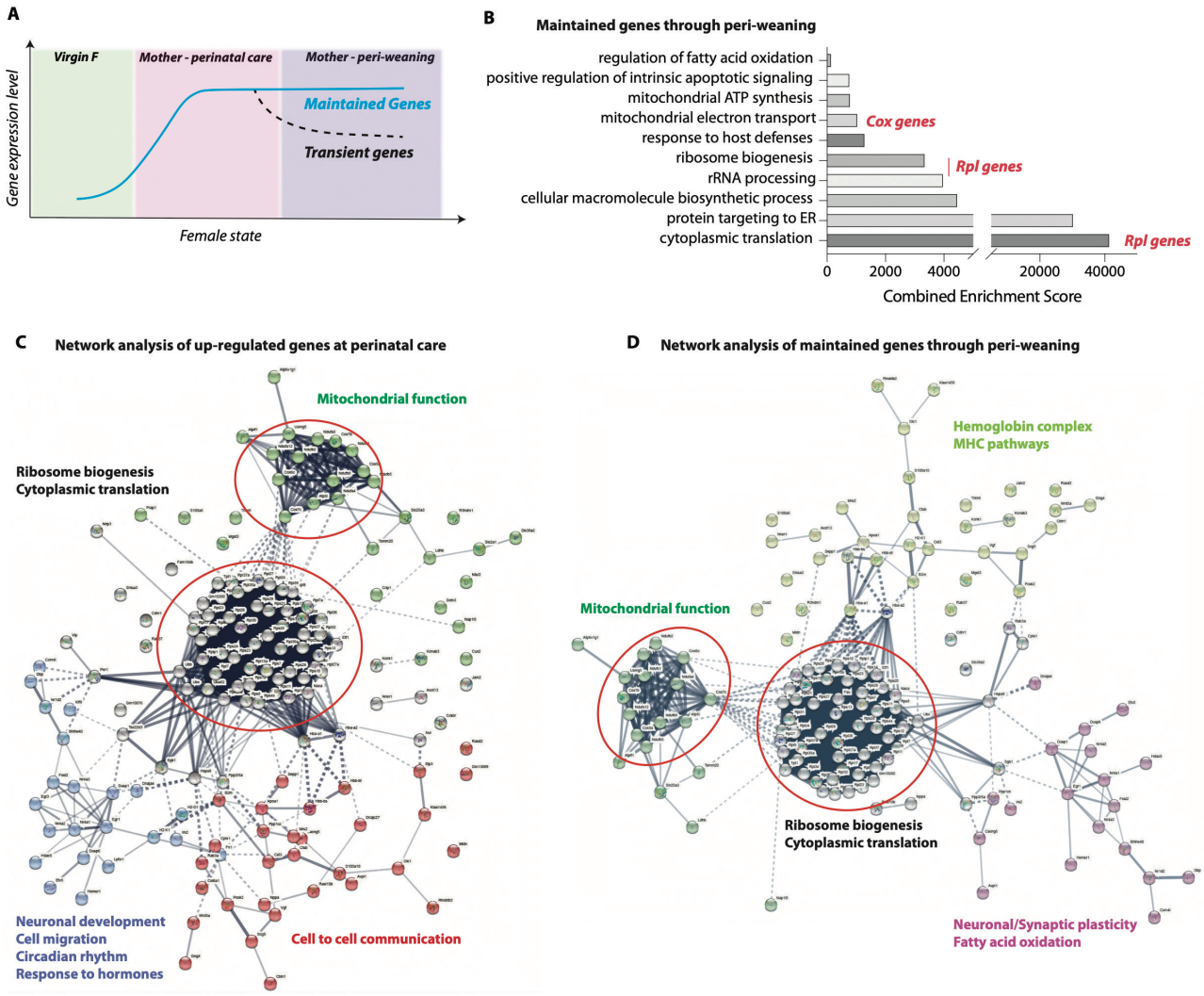

Fig. S 9 Whole bulb analysis of spatial transcriptomic data identifies transient and maintained changes in mothers through peri-weaning

(**A**) Pair-wise comparison of virgins and mothers reveal both genes maintained through peri-weaning and transient genes. Cutoffs: Log2FC > 0.10, Adj-P-value < 0.05. (**B**) Corresponding GO process analysis using EnrichR of the maintained set of genes. (**C and D**) Network analysis generated using STRING, for all genes up-regulated at perinatal care (**C**) and for those maintained through peri-weaning (**D**). In C and D: k-means clustering highlights 4 groups of genes. Dashed lines link connected genes belonging to two distinct clusters. Line thickness represent interaction strength. Red circles highlight the two main processes maintained through peri-weaning.

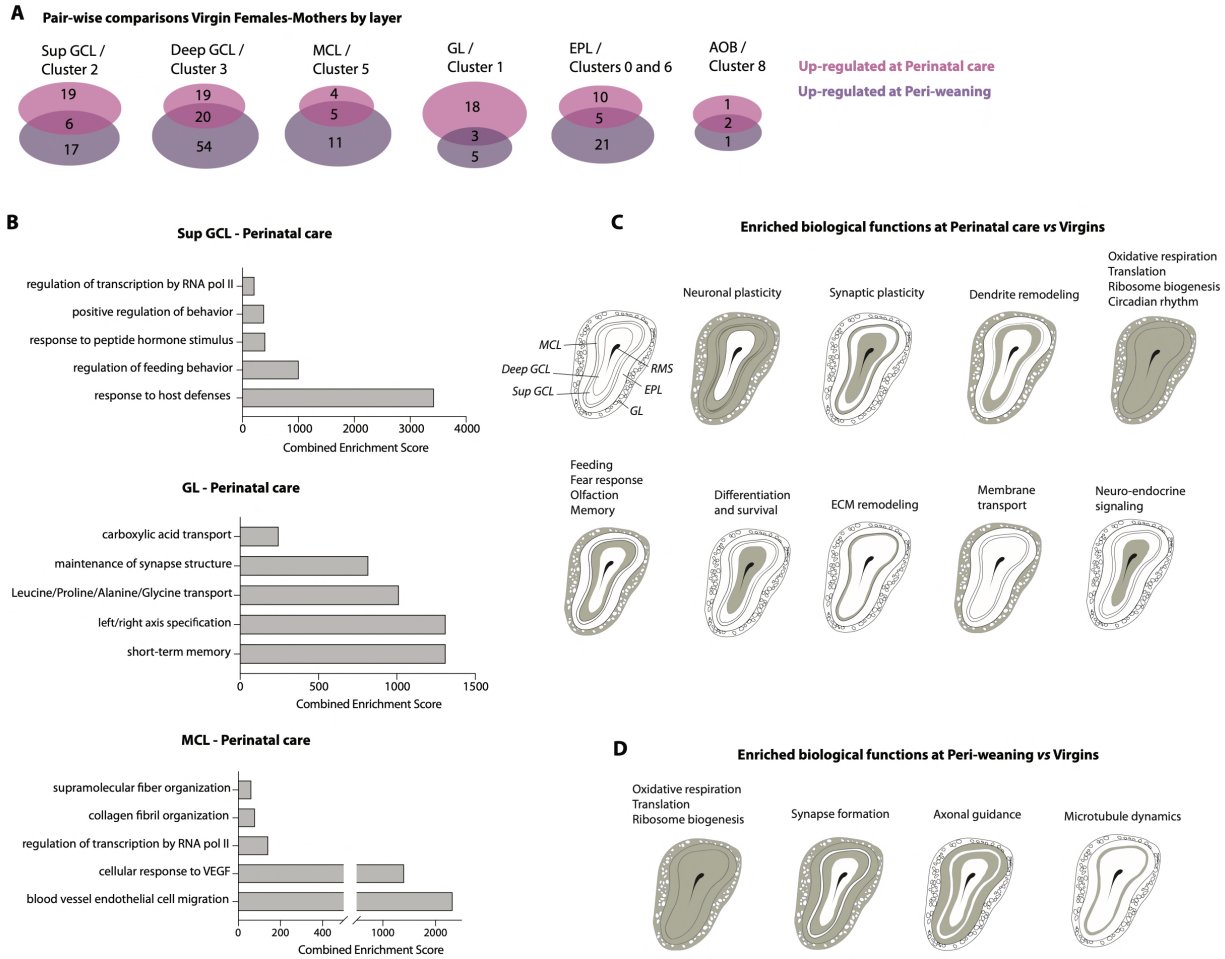

Fig. S 10 Cluster-based comparison between virgins and mothers reveals layer-specific remodeling of the OB during motherhood

(**A**) Pair-wise comparisons of gene sets up-regulated in mothers at perinatal care and peri-weaning was performed for each cluster/anatomical layer of the OB. (**B**) GO process analysis was performed on gene sets specifically up-regulated at perinatal care in the Superficial GCL, GL, and MCL using EnrichR. (**C and D**) Summary schemas of the biological processes changing in each OB layer, at perinatal care (**C**), and peri-weaning (**D**), compared to virgin controls.

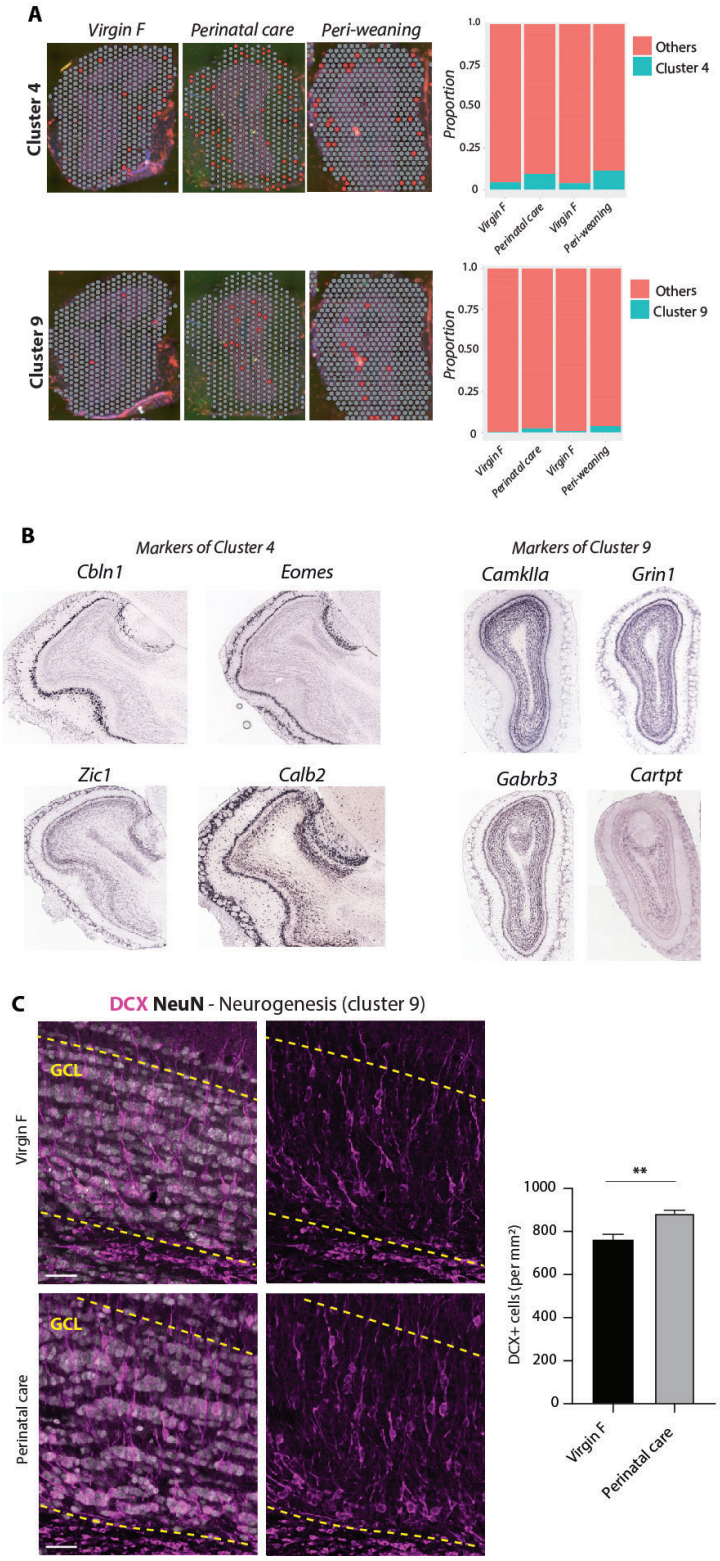

Fig. S 11 Molecular and functional characterization of mother-enriched clusters 4 and 9

(**A**) *Left:* Visium slides showing Cluster 4 and Cluster 9 spatial distribution in virgins and mothers. *Right:* Proportion of Cluster 4 and 9 spatial spots over total sequencing spots on slide. (**B**) Allen Brain ISH pictures of selected markers of cluster 4 and 9, confirming their regional enrichment.

(**C**) Immunostaining micrographs showing significant increase of DCX expression in the GCL at perinatal care. *DCX* is one of the top markers of Cluster 9 during perinatal care.

3 Oligodendrogenesis in the V-SVZ during pregnancy

3.1 Does pregnancy increase the production of oligodendrocytes in the V-SVZ?

In the previous chapter, we described how pregnancy recruits regionally-distinct stem cells in the V-SVZ at different phases of gestation, including stem cells in regions that are relatively quiescent in virgin females. Next, we examined whether pregnancy similarly increases generation of oligodendrocytes to the corpus callosum (or even to non-canonical target regions like the septum or main olfactory bulb), and whether V-SVZ oligodendrogenesis is regulated regionally, or globally.

3.2 Oligodendrogenesis around the V-SVZ

3.2.1 Proliferation of oligodendroglial cells during early pregnancy

As oligodendrocytes born in the V-SVZ do not migrate along the rostrocaudal axis (*42*), we hypothesized that if we pulsed pregnant mice with thymidine analogs and looked at the distribution of analog+ cells a few days later in coronal sections, we might observe labelled cells migrating radially away from the V-SVZ. In chapter two we described that in the medial wall, which is more oligodendrogenic compared to the lateral wall, proliferation rostrally was already increased at Gd 2.5, and caudally at Gd4.5. In the roof, which is located directly below the corpus callosum, stem cell proliferation peaked at Gd4.5. To examine potential increases in oligodendrogenesis from the roof to the corpus callosum and from the medial wall to the septum, we therefore pulsed mice with thymidine analogs once on Gd2.5 and on Gd4.5, and analyzed the distribution of analog+ cells at Gd4.5 (1h post last injection), Gd7.5 (3dpi) and Ppd12 (30dpi) (Fig. 3-1A) at bregma levels in which we previously had found increased stem cell recruitment during pregnancy (Fig. 1G chapter 2). For the analysis, the corpus callosum was divided into two domains, the domain located dorsally to the V-SVZ, which in virgin mice contains most of the V-SVZ-derived oligodendrocytes (Fig. 3-1B) (*43*, *47*); and the lateral domain of the corpus callosum, which is populated mainly by resident OPCs and only few V-SVZ-derived oligodendrocytes (*47*). The septum was divided in half into an area proximal and distal to the V-SVZ (Fig. 3-1B).

When we looked at the distribution of analog+ cells over time, we found them in virgin and pregnant mice in both areas of the corpus callosum, in the septal area proximal to the V-SVZ as well as distal to the V-SVZ at all studied timepoints (Fig. 3-1C). Interestingly, in the corpus callosum, numbers of analog+ cells in virgin females and mothers had dropped sharply by postpartum day 12. In the septum we made similar observations, but the decline was less dramatic (Fig. 3-1C).

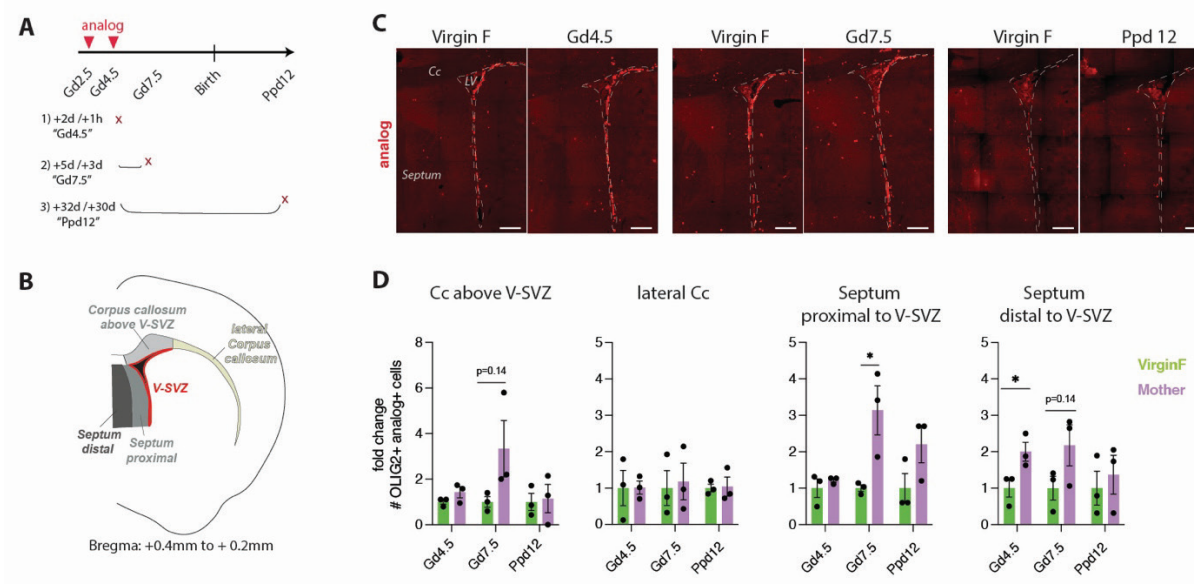

Figure 3-1 Oligodendrogenesis during early pregnancy in regions neighboring the V-SVZ

A Timeline of experiment: thymidine analogs were injected at Gd2.5 and Gd4.5. Mice were analyzed at three different points in time after the last injection: 1h (Gd4.5), 3d (Gd7.5) and 30d (Ppd12). **B** Schema of coronal brain section depicting regions analyzed. **C** Representatives images showing analog+ cells in the septum and corpus callosum above the V-SVZ at the three moments analyzed. **D** Fold change of OLIG2+ analog+ cells in mothers compared to virgin females, in the regions highlighted in B. **Abbreviations** Gd: gestation day; Ppd: Postpartum day; Cc: Corpus callosum; LV: lateral ventricle. **Scale bars** in B: 200µm.

BrdU is incorporated by any cell in S-phase, including cells of different lineages. To focus our analysis on cells of the oligodendroglial-lineage, we co-stained for analog and OLIG2, and quantified double-positive cells in the corpus callosum and in the septum (Fig. 3D).

At Gd4.5, the only area with more analog-labelled OLIG2+ cells in pregnant mice was the septum distal to the V-SVZ (Fig. 3-1D). Three days later, at Gd7.5, numbers of analog+ cells in mothers were three fold higher compared to virgins in the septum proximal to the V-SVZ. In the septum distal to the V-SVZ and the corpus callosum above the V-SVZ similar trends were observed, but the data was very variable (Fig. 3-1D). In the corpus callosum above the V-SVZ of both virgins and mothers, as seen in the staining for analog only, the number of OLIG2+ analog+ cells had decreased by the 30dpi timepoint (Fig. 3-1C). Importantly, numbers of OLIG2+ analog+ cells did not differ between virgin females and pregnant mice in the lateral part of the corpus callosum at any of the timepoints analyzed (Fig. 3-1D).

Together, we detected a transient increase of analog-labelled cells in the septum and corpus callosum during early pregnancy. The localized transient accumulation of analog+ cells in the corpus callosum above the V-SVZ but not in the lateral domain during pregnancy hints at a contribution of V-SVZ-oligodendrogenesis.

3.2.2 Maturation state of label-retaining oligodendroglial cells in motherhood

To examine whether the OLIG2+ cells dividing/generated during pregnancy differentiated into mature oligodendrocytes or remained immature in motherhood 30 days after analog injection (Fig. 3-2A), we stained for thymidine analogs, OLIG2 and CC1, a marker of cell bodies of maturing and mature oligodendrocytes (*118*). This combination allowed the positive identification of mature oligodendrocytes (OLIG2+ CC1+), while OLIG2+ CC1- cells are oligodendrocyte precursor cells (Fig. 3-2B). We analyzed the same domains as before, but this time for the septum, we followed anatomical landmarks. The septum proximal to the V-SVZ consisted of lateral septal nuclei, and the distal part contained both the medial septal nucleus and the septofimbrial nucleus, which are much richer in myelin (Fig. 3-2C).

Inspection of CC1 and OLIG2 -stained sections revealed differential distribution of CC1+ OLIG2+ cells, with many more co-labelled cells in the corpus callosum and the distal part of the septum, the myelin-rich domains (Fig. 3-2D). Based on this staining, we identified three classes of mature oligodendrocytes which showed different morphology and staining brightness ("bright, with processes", "almond shaped", "dim, diffuse"), and one CC1- class, likely oligodendrocyte precursor cells (Fig. 3-2D). We then quantified analog incorporation in these cell classes in virgins and mothers. Some cells in the white matter domains had indeed differentiated into mature oligodendrocytes, in both virgins and mothers (Fig. 3-2E).

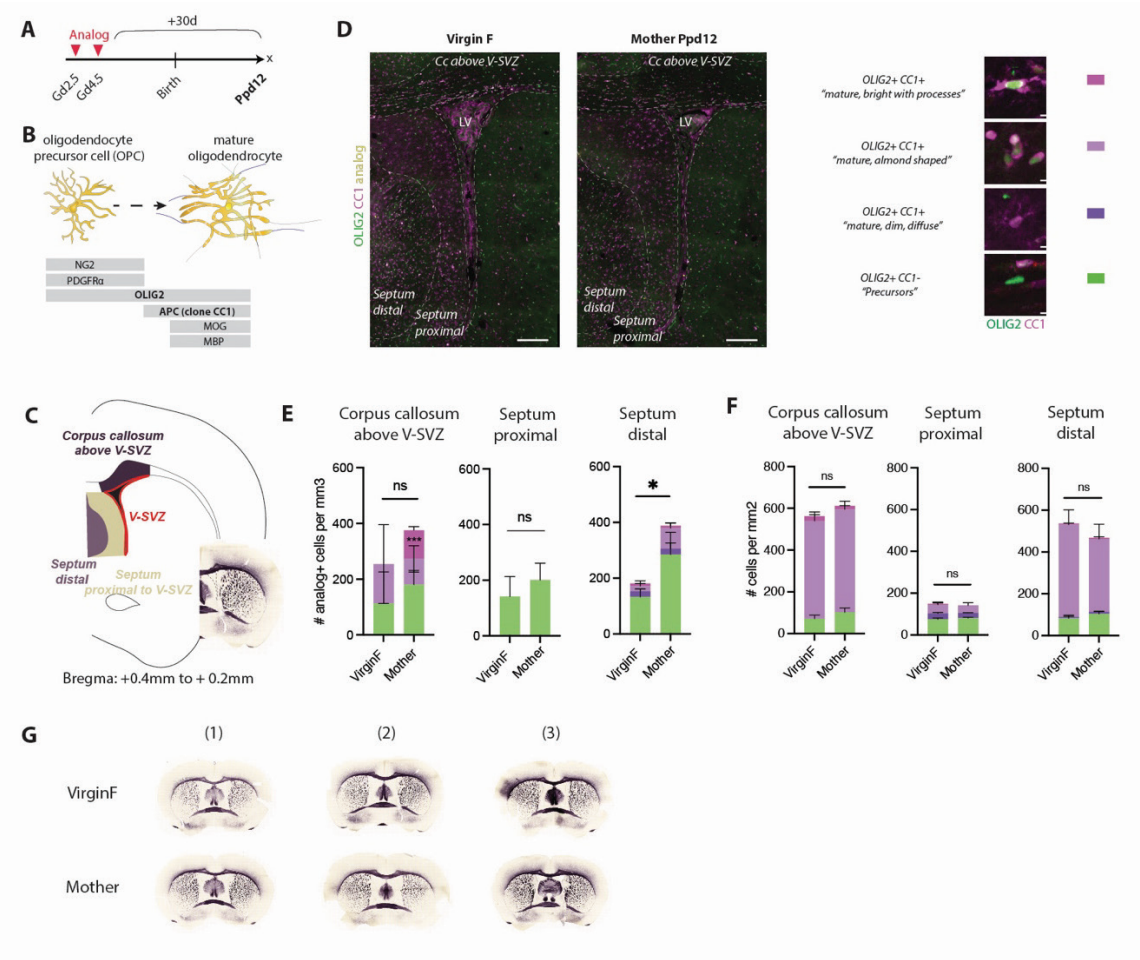

Figure 3-2 No lasting effect of increased oligodendrogenesis during pregnancy in motherhood

A Timeline of experiment: mice were given single pulses of thymidine analogs at Gd2.5 and Gd4.5, and sacrificed at Ppd12 after a chase of 30days. **B** Markers for oligodendrocyte precursor cells and mature oligodendrocytes, in bold those used in this experiment. **C** Schema highlighting the regions analyzed, and coronal section of the same level stained for myelin. **D** Left: representative images of virgin female and mother at Ppd12 showing differential distribution of CC1+ cells. Right: Classification of cells labelled with OLIG2 and CC1 based on staining intensity and morphology. **E** Quantification of OLIG2+ analog+ cells based on the subtypes described in D. **F** Characterization of total OLIG2+ population based on CC1 expression **G** Schmued's rapid myelin staining on coronal sections of three different mice per state. **Abbreviations** Gd: gestation day; Ppd: Postpartum day; NG2: Neural glial antigen2 = chondroitin sulphate proteoglycan 4; PDGFRα: Platelet derived growth factor alpha; APC: adenomatous polyposis coli; MOG: Myelin oligodendrocyte glycoprotein; MBP: Myelin basic protein. **Scale bars** in D: Overview images: 200µm. Blow-ups of different cell types/states:10µm.

Moreover, we detected significantly more analog+ OLIG2+ cells in the distal septum in mothers, and this was driven by slightly higher numbers of both oligodendrocyte precursor cells and mature oligodendrocytes (Fig. 3-2E). Few, but significantly more mature oligodendrocytes characterized

by bright cytoplasmic staining were found in the corpus callosum of mothers (Fig. 3-2E). Of note, in all regions analyzed, half or more of all analog+ OLIG2+ cells did not express CC1 and were therefore presumably oligodendrocyte precursor cells (Fig. 3-2E).

Due to the high proportions of oligodendrocyte precursor cells, we wondered whether dilution of the thymidine analog through continuous proliferation in mothers could affect the numbers of cells detected. We therefore assessed if the increase in oligodendrogenesis during early pregnancy had resulted in an expansion of the oligodendrocyte-lineage in mothers, by quantifying total numbers of OLIG2+ cells (analog+ and analog-) in the septum and corpus callosum. Neither CC1- nor CC1+ cell numbers were different between virgin females and mothers (Fig. 3-2F). Finally, we compared myelination in virgin females and mothers by performing Schmued's myelin stain protocol (*119*) on n=3 sections per state. It did not reveal any consistent differences detectable by eye (Fig. 3-2G).

Taken together, 30 days after pulsing with thymidine analog on Gd2.5 and Gd4.5, the remaining label-retaining cells in the septum and corpus callosum were composed of both oligodendrocyte precursor cells and mature oligodendrocytes. Increased proliferation in the oligodendrocyte-lineage during early pregnancy did not result in higher numbers of oligodendrocyte precursor cells or mature oligodendrocytes in motherhood.

3.3 Oligodendrogenesis in the V-SVZ

3.3.1 Acute analysis of thymidine analog incorporation revealed very few labelled cells of oligodendroglial lineage

The localized accumulation of analog+ cells in the corpus callosum above the V-SVZ, but not in the lateral corpus callosum, made us speculate that these cells were V-SVZ-derived. To identify potential domains in the V-SVZ with increased oligodendrogenesis during early pregnancy, we used a double thymidine analog paradigm (Fig. 3-3A), with a single pulse of CldU and IdU on Gd2.5 and Gd4.5, respectively, and quantified analog+ cells one hour post IdU injection, at different bregmas and in domains of the V-SVZ in which we had found increased stem cell proliferation during pregnancy (Fig. 3-3B & G). In general, numbers of analog+ cells in the V-SVZ were very low. Neither numbers of OLIG2+ CldU+ cells (in S-phase at Gd2.5), OLIG2+ IdU+ (in S-phase at Gd4.5) cells, nor total OLIG2+ analog+ (combined Gd2.5 and 4.5-labelled) changed in the analyzed domains in pregnancy, and not even a trend of increased OLIG2+ analog+ cells was detectable (Fig. 3-3C&H). Notably, we found more analog+ OLIG2- cells in the roof, dorsomedial corner, ventromedial and ventrolateral wall (Fig. 3-3D-F, I), reflecting the beginnings of increased stem cell division in these domains (see previous chapter on neurogenesis

during pregnancy), although not statistically significant here, likely due to the low number cells analyzed with this approach.

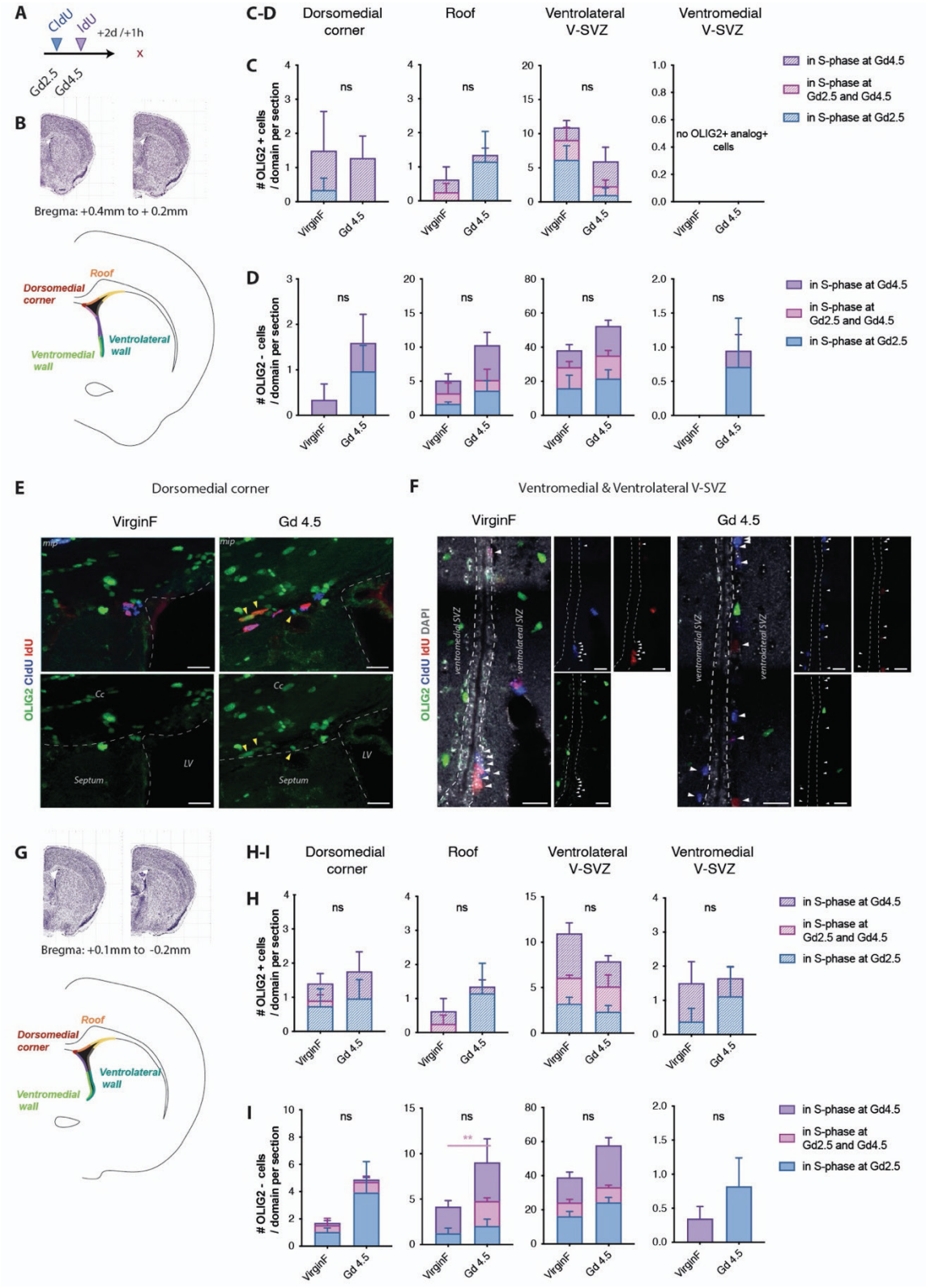

Figure 3-3 S-phase labelling during early pregnancy revealed no changes in proliferation in the OLIG2+ population in the V-SVZ, but strong trends in the OLIG2- fraction

A Experimental paradigm: mice were pulsed once on Gd2.5 with CldU, and two days later on Gd4.5 with IdU. Mice were sacrificed 2h after the IdU injection. **B** Levels on the rostrocaudal axis and domains analyzed in the analysis shown in C-F. **C** Quantification of analog+ OLIG2+ cells. **D** Quantification of analog+ OLIG2- cells. **E** Representative images of the dorsomedial corner. Arrowheads point to analog+ OLIG2+ cells. **F** Representative images of the ventromedial wall. Arrowheads point to analog+ OLIG2- cells. **G** Levels on the rostrocaudal axis and domains analyzed in the analysis shown in H-I. **H** Quantification of analog+ OLIG2+ cells. **I** Quantification of analog+ OLIG2- cells. **Abbreviations** Gd: gestation day; CldU: 5-chloro-2'-deoxyuridine; IdU: 5-iodo-2'-deoxyuridine. **Scale bars** in E&F: 20μm.

3.3.2 Characterization of oligodendrocyte progenitors in the V-SVZ revealed two different types with differential distribution

To increase the power of the analysis, we next stained for MCM2 to label all cells in cell cycle, instead of just those in S-phase, and combined it with immunostainings for OLIG2 and PDGFRα, markers for the entire oligodendroglial lineage and oligodendrocyte precursor cells, respectively (Fig. 3-2B). With this combination we identified two types of cycling OLIG2+ cells in the V-SVZ itself. One of them was, as expected, the typical branchy PDGFRα+ oligodendrocyte precursor cell (OPC) that is found brain-wide. OPCs appeared evenly distributed over the V-SVZ and existed in MCM2+ and MCM2- states (Fig. 3-4A, arrowheads). In addition, we also observed MCM2+ OLIG+ cells negative for PDGFRα, located primarily in the lateral wall, the roof and dorsomedial corner (Fig. 3-4A, arrows). These cells likely corresponded to EGFR+ OLIG2+ Ki67+ transit amplifying cells (TACs), as they show a similar distribution upon visual inspection (Fig. 3-4B).

3.3.3 Oligodendrogenesis in the V-SVZ does not change over pregnancy

We proceeded with quantifying those two types between bregma +0.4mm to -0.2mm in all domains of the V-SVZ in virgin females and during early, mid and late pregnancy, specifically at Gd2.5, Gd4.5, Gd7.5, Gd12.5 and Gd18.5 (Fig. 3-4C, D, H). Transit-amplifying OLIG2+ cells showed highest density in the dorsolateral wedge, followed by the lateral wall, the roof and the dorsomedial corner. In the medial wall, however, these cells were rare (Fig. 3-4 E& I). The numbers of these cells within any of the analyzed domains, however, remained unaltered over pregnancy as tested with one-way ANOVA. The exception was an isolated significant increase in the dorsolateral V-SVZ at Gd12.5, but only at the more caudal level analyzed (Fig. 3-4I). Finally, in the roof and dorsomedial corner, a trend towards a transient increase at Gd4.5 was observed (Fig. 3-4E).

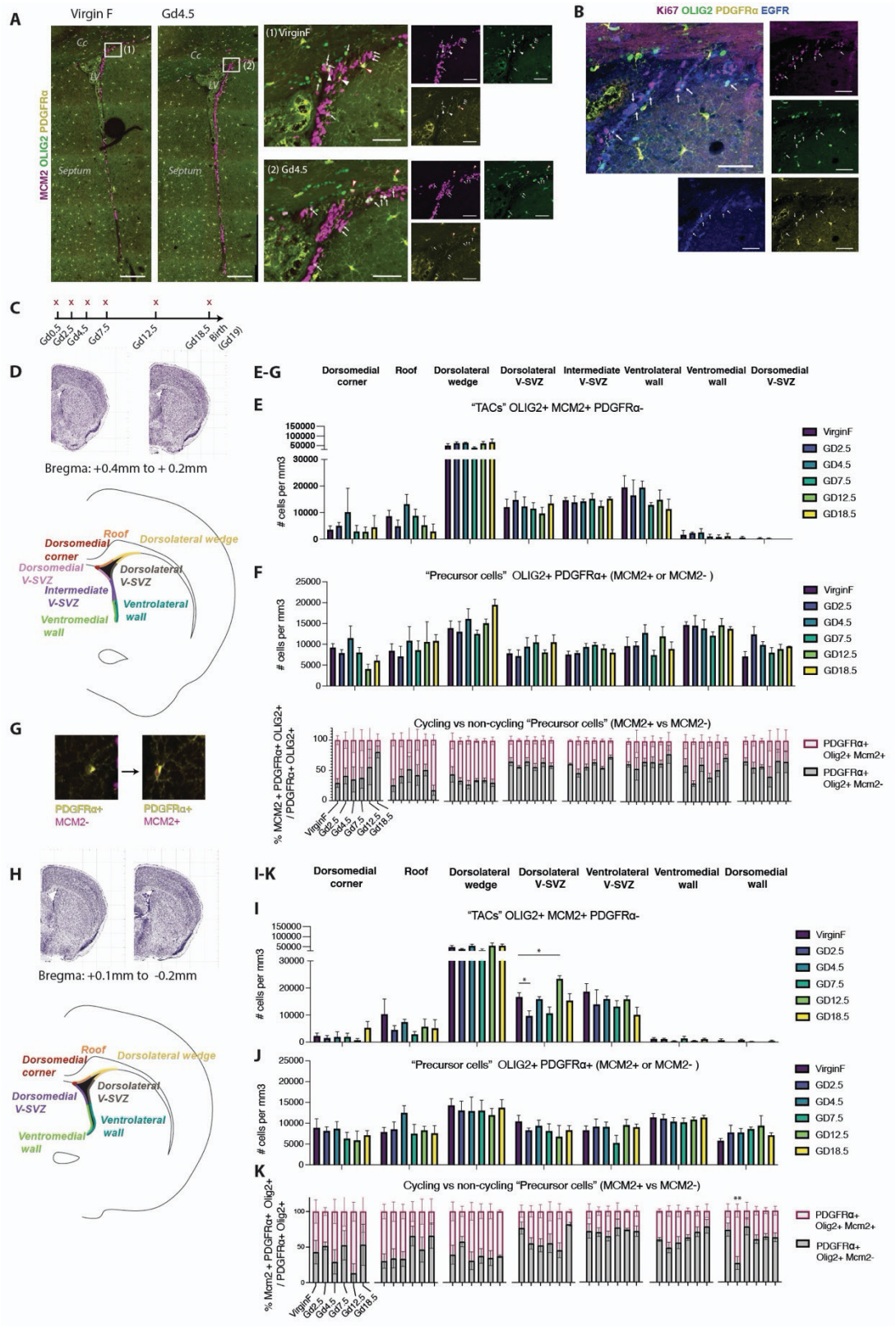

Figure 3-4 Analysis of OLIG2+ transit-amplifying cells and oligodendrocyte precursor cells in the V-SVZ during pregnancy

A Representative images of OLIG2, PDGFRα and MCM2 in the V-SVZ of a virgin female and a Gd4.5 mouse. Arrows point to OLIG2+ MCM2+ PDGFRα- cells (TACs), arrowheads to OLIG2+ PDGFRα+

cells (OPCs). Arrowheads with red border point to MCM2+ OPCs. **B** Exemplary images of TACs identified with immunostainings against EGFR and OLIG2. **C** Experimental paradigm: Mice were sacrificed at different timepoints during early, mid and late pregnancy, namely Gd0.5 (morning of copulatory plug), Gd2.5, Gd4.5, Gd7.5, Gd12,5 and Gd18.5. **E** Quantifications of TACs, **F** OPCs and **G** proportions of OPCs in cell cycle, in the bregma and domains shown in **D**. **I-K**: like E-F, but on more caudal bregma (**H**). **Abbreviations** Gd: gestation day, TAC: transit amplifying cell; OPC: oligodendrocyte precursor cell. **Scale bars** Low power images in A: 200µm. All other in A and B: 50µm.

Unlike transit-amplifying OLIG2+ cells, branched PDGFRα+ oligodendrocyte precursor cells occurred in highly similar densities in all domains analyzed. However, also their numbers did not change during pregnancy (Fig. 3-4F&J), and this result was also reflected in the mostly unchanging proportions of MCM2- vs MCM2+ oligodendrocyte precursor cells (Fig. 3-4G&K). Between bregma +0.1mm and -0.2mm in the dorsomedial wall, a higher proportion of MCM2+ cells was detected at Gd2.5 (Fig. 3-4K). The meaning of this was unclear, as it did not result in higher numbers of oligodendrocyte precursor cells at Gd4.5 as a consequence (Fig. 3-4J).
The same analysis as shown in figure 4 was also performed on a more rostral level of the V-SVZ, around bregma + 1.1mm, with similar results (data not shown).

3.3.3.1 Enriched OLIG2+ transit-amplifying cells in the lateral end of the dorsolateral wedge

Of all domains, the dorsolateral wedge showed the highest density of OLIG2+ MCM2+ PDGFRα- transit amplifying cells, and given the location right below the corpus callosum, these cells might give rise to or differentiate into oligodendrocytes destined for the corpus callosum. We therefore examined the dorsolateral wedge more closely (Fig. 3-5A). Upon visual inspection we noticed that PDGFRα- OLIG2+ transit amplifying cells were distributed differentially within this domain, with a bias towards the lateral aspect (Fig. 3-5B, arrows). As potential changes in the more proliferative part of the wedge might have been masked by less proliferative side, we reanalyzed the two types of OLIG2+ progenitors in the dorsolateral wedge, splitting it into medial and lateral subdomains (Fig. 3-5C&G). Indeed, the medial and the lateral domain proved to harbor significantly different numbers of transit-amplifying OLIG2+ cells, in both virgin and pregnant mice (Fig. 3-5E&I). PDGFRα+ oligodendrocyte precursor cells were distributed evenly. However, neither in the medial nor the lateral part of the dorsolateral wedge did numbers of transit amplifying OLIG2+ cells or oligodendrocyte precursor cells change during pregnancy, and the proportions of cycling versus non-cycling oligodendrocyte precursor cells remained unaltered as well (Fig. 3-5 E-G, I-K).

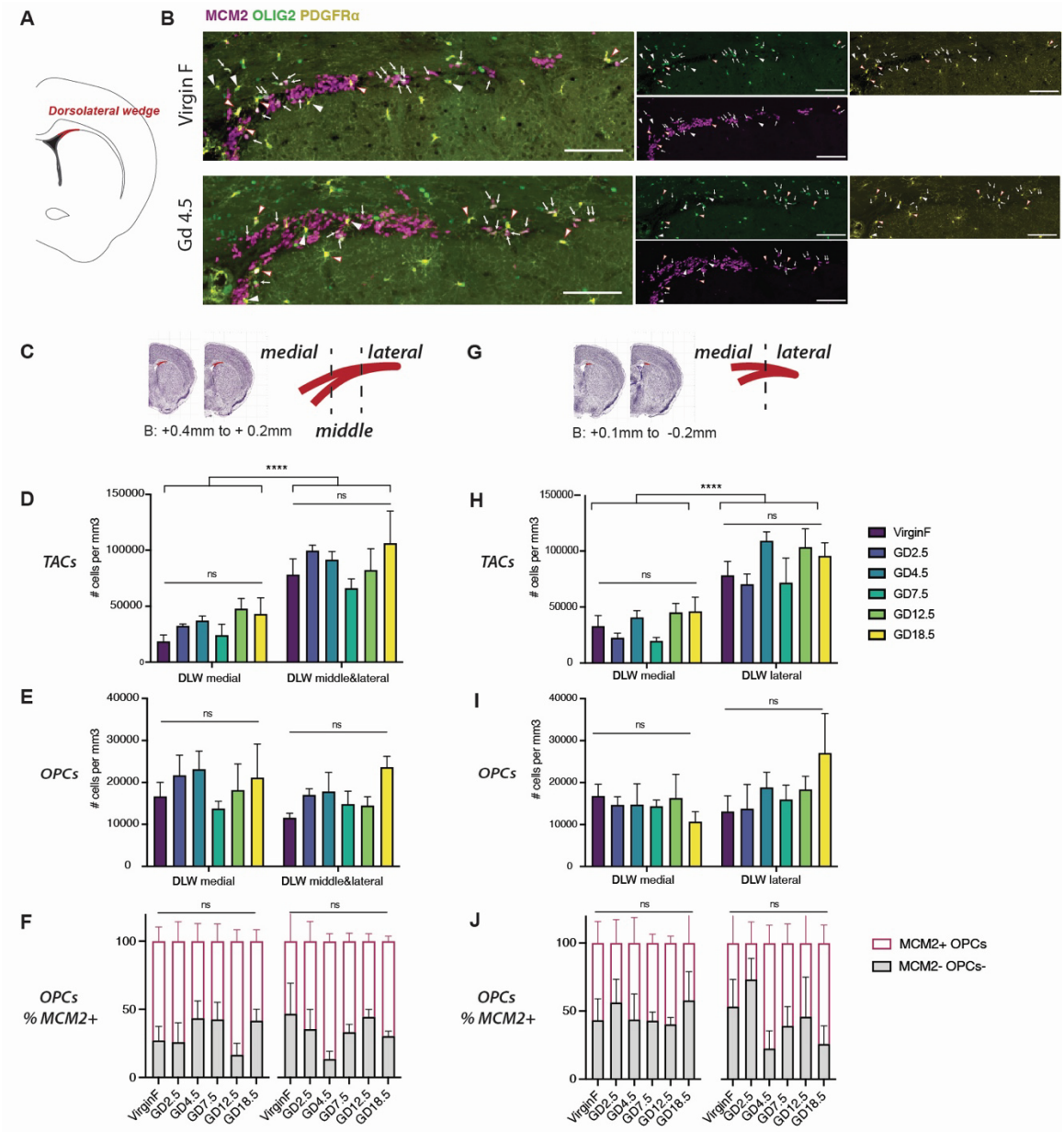

Figure 3-5 Analysis of OLIG2+ transit-amplifying cells and oligodendrocyte precursor cells in the dorsolateral wedge of the V-SVZ during pregnancy

A Location of the dorsolateral wedge. **B** Representative images of staining for OLIG2+ MCM2+ PDGFRα in the dorsolateral wedge. Arrows point to TACs, white arrowheads to non-cycling OPCs and arrowheads with a red border to cycling, MCM2+ OPCs. **C** Coronal sections showing the Bregma analyzed in D-F, and the division in three subdomains. **D-F** Quantifications of TACs **(D)**, OPCs **(E)** and the proportion of cycling OPCs **(F)**. **G** Coronal sections showing the Bregma analyzed in H-J, and the division in three subdomains. **H-J** Quantifications of TACs **(H)**, OPCs **(I)** and the proportion of cycling OPCs **(J)**. **Abbreviations** Gd: gestation day, B: Bregma; TAC: transit amplifying cell; OPC: oligodendrocyte precursor cell; DLW: dorsolateral wedge. **Scale bars** 100µm.

Taken together, we identified two different types of oligodendroglial precursors in the V-SVZ, PDGFRα-transit amplifying cells and PDGFRα + oligodendrocyte precursor cells, but neither was increased over pregnancy in the analyzed domains at the timepoints examined.

3.4 Temporary increase of OPCs in the main olfactory bulb during perinatal care period

In the olfactory bulb, when we quantified neurons born during early pregnancy during the perinatal care period (Fig. 3-6A), we also analyzed the generation of glial cells, including microglia (IBA1+), GFAP+ astrocytes and oligodendroglial cells (OLIG2+). In virgins, 98% of all analog+ cells were putative neurons (OLIG2- IBA1-), a bit over 1.5% of the labelled cells were of the oligodendrocyte lineage, and an even smaller fraction were microglia (Fig. 3-6B). In mothers, the percentage of newborn glial cells was even lower, due to the increased number of newborn neurons (Fig.3-6B). In both virgin females and mothers, no analog+ GFAP+ astrocytes were detected. Although the fraction of newborn oligodendroglial cells among all analog+ cells was smaller in mothers, the raw numbers were actually higher in mothers (Fig. 3-6C, stacked bars). Co-staining of OLIG2 and NG2 revealed that this was due to higher numbers of analog+ NG2+ oligodendrocyte precursor cells (Fig. 3-6C; green bars), but not mature oligodendrocytes (analog+ OLIG2+ NG2-cells) (Fig. 3-6C, magenta bars). Importantly, when we analyzed total numbers of OLIG2+ NG2+ cells during late pregnancy and in the postpartum period, we found them only transiently increased during the perinatal care period (Fig. 3-6D,E). These oligodendrocyte precursor cells could be the result of increased division of other resident oligodendrocyte precursor cells, or they could originate from outside the bulb.

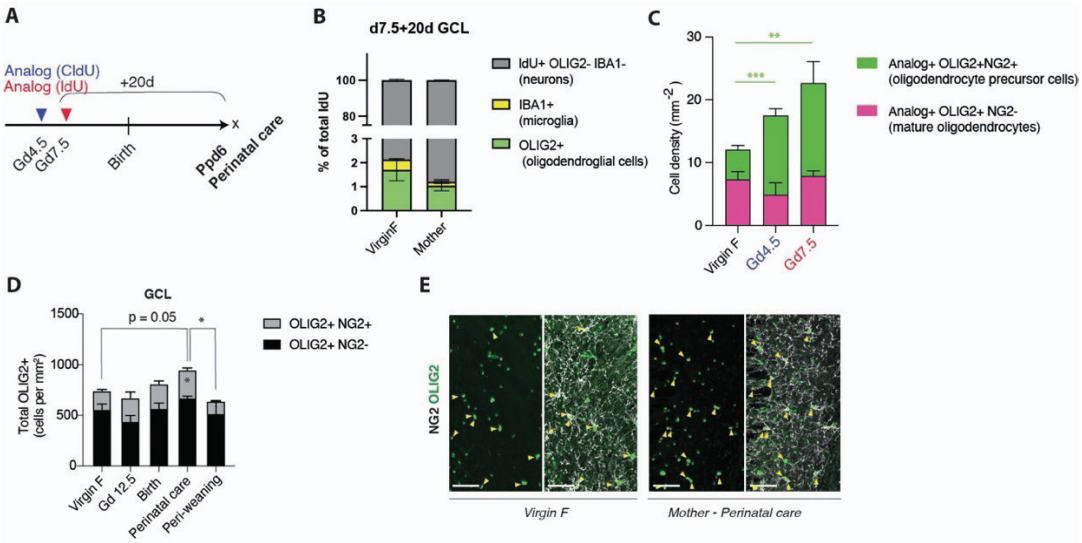

Figure 3-6 Temporary increase in oligodendrocyte precursors in the main olfactory bulb in the perinatal care period

A Experimental paradigm **B** Composition of analog+ cells in the granule cell layer of the MOB at perinatal care **C** Quantification of analog+ mature oligodendrocytes and analog+ oligodendrocyte precursor cells (OPCs) at perinatal care **D** Quantification of total OPCs (OLIG2+ NG2+) and putative mature oligodendrocytes (OLIG2+ NG2-) in the granule cell layer over time. **E** Representative images of OPCs during the perinatal care period. **Scale bar** in E: 50µm. **Abbreviations** Gd: gestation day; Ppd: postpartum day; MOB: main olfactory bulb; GCL: granule cell layer

3.5 Oligodendrogenesis in the rostral migratory stream

As discussed in the introduction, stem cells can also be found along the rostral migratory stream (RMS) (*49*). When compared to V-SVZ stem cells or stem cells in the rostral RMS (RE2), progenitors isolated from the caudal RMS (RE1) exhibit the highest oligodendrogenic potential in culture (Fig. 1-4A) (*49*), but their lineage *in vivo* is unclear. Moreover, it was shown that the abundance of NG2 cells within the RMS increases with proximity to the olfactory bulb, and is highest in the olfactory bulb (*120*). NG2 density and maturation state of newborn neurons in the RMS and olfactory bulb are correlated, and it was suggested that oligodendrocyte precursor cells may regulate maturation of young neurons in a contact-dependent mechanism (*120*).

We therefore hypothesized that in pregnancy, progenitors in the caudal RMS may give rise to NG2 cells migrating to the olfactory bulb, which could help pregnancy-associated neurons mature.

3.5.1 Pregnancy does not increase oligodendrogenesis in the caudal RMS

We analyzed the effect of pregnancy on the oligodendroglial lineage in the caudal RMS at Gd4.5 and Gd7.5 (Fig. 3-7A), again with the marker combination OLIG2, MCM2 and PDGFRα. As in the V-SVZ, neither transit amplifying OLIG2+ cells nor PDGFRα oligodendrocyte precursor cells, or their proportion in cell cycle were altered in comparison the virgin females (Fig. 3-7B&C). We challenged this result using an alternative approach, pulsing mice at Gd4.5 with IdU, and studied incorporation one hour later (Fig. 3-6D), this time staining for OLIG2, EGFR and IdU to identify transit amplifying cells of oligodendroglial lineage (EGFR+ OLIG2+) , and their proportions in S-phase (EGFR+, OLIG2+, IdU+). Quantification of transit amplifying cells showed a highly similar picture to when studied with the first marker combination (Fig. 3-7E, F), with no statistically significant change in oligodendrogenesis at Gd4.5. To conclude, pregnancy did not increase local oligodendrogenesis in the caudal RMS.

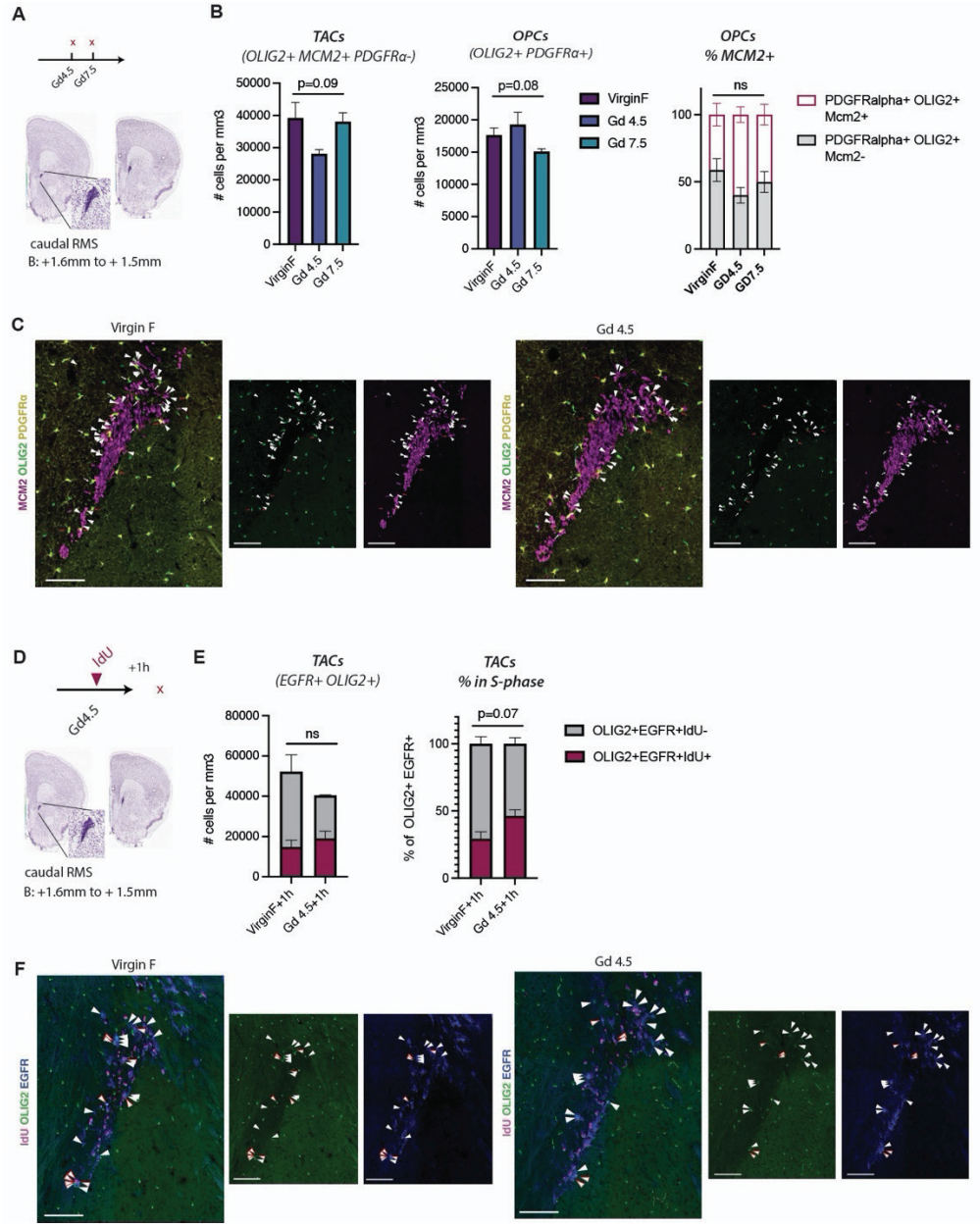

Figure 3-7 Analysis of OLIG2+ transit-amplifying cells and oligodendrocyte precursor cells in the caudal RMS during early pregnancy

A Mice were sacrificed at Gd4.5 and Gd7.5. **B** Quantification of transit amplifying oligos, oligodendrocyte precursor cells and their proportion in cell cycle, assessed with immunostaining for OLIG2, PDGFRα and MCM2. **C** Representative images to quantification shown in E. Arrowheads: TACs. White arrows: MCM2- OPCs. Red arrows: MCM2+ OPCs. **D** Mice were pulsed with a single injection of IdU at Gd4.5 and sacrificed 1h later. Analyzed was the caudal RMS. **E** Quantification of transit amplifying oligos (TACs) and their proportion in S-phase, assessed with immunostaining for EGFR, OLIG2 and IdU. **F** Representative images to quantification shown in B. White arrowheads point to Olig2+ EGFR+ IdU- cells; arrowheads with a red border point to Olig2+ EGFR+ IdU+ cells. **Abbreviations** IdU: 5-iodo-2'-deoxyuridine; Gd: gestation day; RMS: rostral migratory stream; TAC: transit amplifying cell; OPC: oligodendrocyte precursor cell. **Scale bars** in C and F: 100μm.

3.6 Summary

Early pregnancy increased oligodendrogenesis in the septum, in both myelin-rich and grey matter areas. In the corpus callosum, a trend for increased oligodendrogenesis was observed, but regionally limited to the domain above the V-SVZ. These newborn oligodendroglial cells appeared to be short-lived.

Some oligodendroglial cells born during pregnancy became mature oligodendrocytes in the postpartum period, while others remained oligodendrocyte precursor cells. Enhanced oligodendrogenesis during pregnancy did not increase total numbers of mature oligodendrocytes or oligodendrocyte precursor cells in motherhood in the corpus callosum or septum. In contrast, in the granule cell layer of the olfactory bulb, we observed a temporary increase in oligodendrocyte precursor cells in the early postpartum period, accompanying the wave of young neurons born during early gestation.

In the V-SVZ and RMS, we characterized two cycling populations of oligodendroglial cells with unknown lineage relationship, branchy PDGFRα+ oligodendrocyte precursor cells and PDGFRα- transit-amplifying cells. However, pregnancy neither affected PDGFRα+ oligodendrocyte precursor cells nor PDGFRα- transit-amplifying cells in any of the analyzed domains.

4 Discussion

4.1 Conclusions

Neural stem cells (NSCs) in the V-SVZ generate neurons and a small number of glia throughout life. Recent advances in the field have unveiled an astonishing regional heterogeneity among V-SVZ stem cells and interneurons they generate. The functional relevance of stem cell- and interneuron heterogeneity for olfaction is unknown. We hypothesized that adult V-SVZ neural stem cells comprise a mosaic of cells, and that different physiological states regulate stem cells in regionally distinct domains, modulating neuro- and gliogenesis on-demand, in preparation of future need. Here, we show that pregnancy recruits multiple regionally-distinct NSCs with different temporal dynamics (Fig. 4-1A), resulting in the generation of sequential waves of olfactory bulb interneurons added transiently to the olfactory bulb during the perinatal care period (Fig.4-1B,C). Moreover, our data suggest that different subtypes of pregnancy-associated interneurons are involved in distinct aspects of maternal behaviour. Spatial transcriptomics revealed layer-specific olfactory bulb remodeling during motherhood, and identified neuropeptide Y interneurons as a new type of adult-generated neuron, whose generation (among others) dynamically changes in pregnancy. Interestingly, in the granule cell layer of the main olfactory bulb, a transient increase in oligodendrocyte precursor cells in the early postpartum period occurs simultaneously to the functional addition of young pregnancy-associated interneurons (Fig.4-1C).

Oligodendrogenesis in the corpus callosum was described to be increased during pregnancy, but it remained an open question whether V-SVZ-derived oligodendrocytes contribute to this increase. Here, we identify two cycling populations of oligodendroglial cells in the V-SVZ with unknown lineage relationship, branchy PDGFRα+ oligodendrocyte precursor cells and PDGFRα- transit-amplifying cells. Oligodendrogenesis increases during early pregnancy in both white and grey matter around the V-SVZ. In the corpus callosum, newborn oligodendroglial cells are predominantly found in the area above the V-SVZ, suggesting a contribution of V-SVZ-derived oligodendrocytes. However, pregnancy neither affects PDGFRα+ oligodendrocyte precursor cells nor PDGFRα- transit-amplifying cells in any of the analyzed domains.

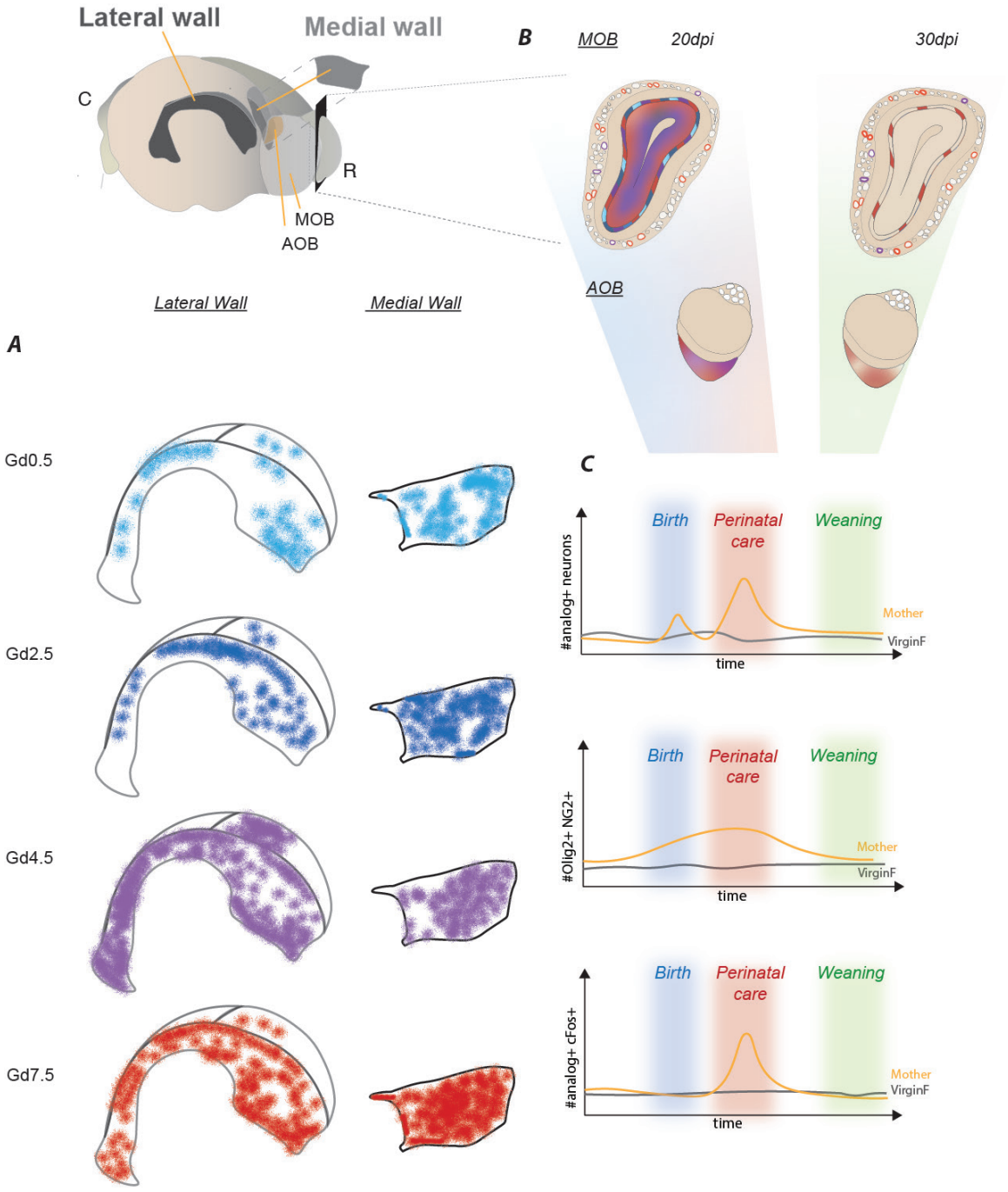

Figure 4-1 Summary schema

Top left: Schema of mouse brain showing location of V-SVZ stem cell niche with the lateral and medial wall, as well as the main and accessory olfactory bulb (MOB/AOB). **A** Expanded view of the lateral wall (left) and medial wall (right). Shaded areas highlight domains that showed more stem cell recruitment and/or proliferation in pregnant mice compared to virgin females. **B** Summary schemas of main and accessory olfactory bulbs and showing layers with increased neuronal addition in the perinatal care period (20dpi) of cells labeled at Gd0.5 (turquoise), Gd2.5 (blue), Gd4.5 (lila) and Gd7.5 (red). The majority of these cells are only transiently present and functional in the olfactory bulb, and are culled by the weaning period (30dpi) **C** Schematic graphs summarizing the temporal dynamics of pregnancy-associated interneurons and oligodendrocyte precursor cells in the OB, and transient increase in c-fos expression of the newly generated neurons.

4.2 Spatio-temporal recruitment of adult neural stem cells in the V-SVZ for transient neurogenesis

4.2.1 Potential mechanisms leading to spatiotemporal recruitment of stem cells during gestation

Many years ago it was shown that pregnancy increases stem cell proliferation on gestation day seven (*94*). We showed that pregnancy changes the behaviour of neural stem cells in different domains with distinct temporal dynamics. Stem cell proliferation in the dorsolateral wedge increases already the morning after the mating, in the roof it peaks on the day of embryo implantation, and in the ventromedial and ventrolateral wall stem cell proliferation is highest on gestation day seven. What are possible mechanisms behind this finely orchestrated stem cell recruitment during gestation? As discussed in the introduction, V-SVZ stem cells reside in a highly specialized niche. Possible mediators therefore include systemic signals and hormones, factors released into the cerebrospinal fluid, neurotransmitters and neuropeptides.

4.2.1.1 Hormones

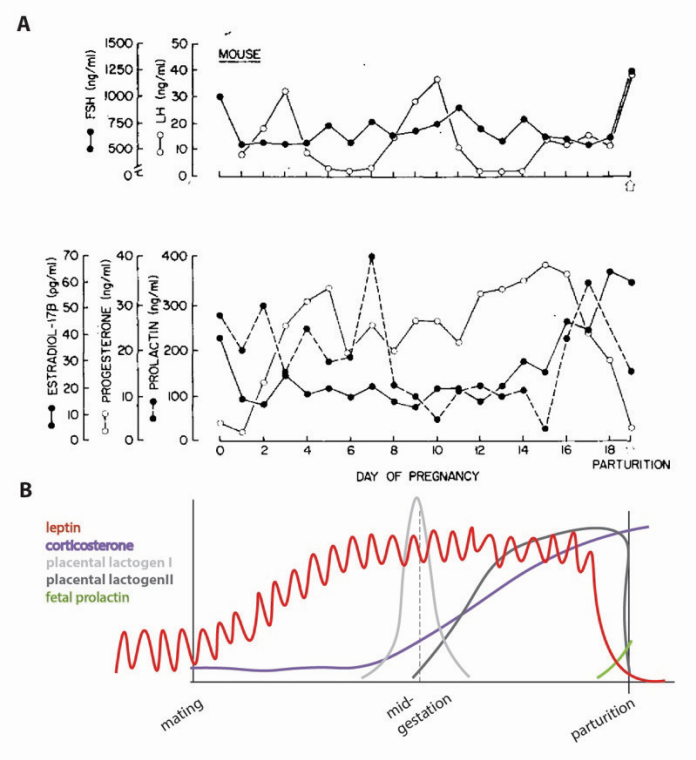

Figure 4-2 Circulating levels of pregnancy hormones over gestation

A Serum levels of pregnancy hormones in the mouse. Image source: (*121*) Reprinted with permission of edpsciences. **B** Further pregnancy hormones. Data on mouse/rat, collected from (*122*, *123*)

Prolactin has been described as a mediator of pregnancy-associated neurogenesis (*94*, *95*), and expression of prolactin receptor (PRLR) was reported to be restricted to the dorsolateralwedge (*94*). We found that pregnancy recruited stem cells also in other domains, with different temporal dynamics. Moreover, on mRNA level, *Prlr* expression was broad, and not restricted to the dorsolateral wedge. Serum levels of prolactin rise during the first week of pregnancy, with peaks at gestation days five and seven, after which its levels decrease until rising again towards the end of pregnancy (Fig. 4.2A). Our results show that in the first days of pregnancy, stem cell proliferation dynamics in the ventral walls, but not in the roof or

in the dorsolateral wedge, mimic prolactin levels. Moreover, in none of the analyzed domains we detected increased stem cell proliferation on gestation day 18, on which prolactin levels are high again. Thus, prolactin is beyond doubt a major regulator of stem cells during pregnancy, however, it seems unlikely that prolactin alone mediates the distinct temporal dynamics in stem cell proliferation observed in different domains. Other hormones fluctuating over pregnancy include follicle stimulating hormone, luteinizing hormone, estradiol, progesterone, more lactogenic hormones, leptin and corticosterone (Fig. 4.2 A, B). They all show distinct temporal expression patterns and might influence stem cell behavior alone or in combination with other hormones. Of note, progesterone and estradiol were ruled out as activators. Infusion of the hormones separately or in combination did not increase neurogenesis in the V-SVZ (*94*), however, the response was not analyzed in a regional manner. Careful analysis of hormone fluctuations over time and receptor expression in the V-SVZ is needed to understand stem cell regulation by hormones.

4.2.1.2 Other niche components: Innervation and cerebrospinal fluid

Other niche components including innervation and the cerebrospinal fluid might also be involved in the dynamic stem cell regulation during pregnancy (Fig.1 and Fig.S1 in chapter 2). A preliminary in-silico mapping (data not shown) made using the Allen Brain Atlas revealed that the V-SVZ is regionally innervated by hypothalamic POMC neurons and neurons in the nucleus raphe, the substantia nigra and the ventral tegmental area, as shown before (*23*, *30–32*), as well as by neurons in other hypothalamic nuclei, septal nuclei, the striatum, thalamus, visual cortex, and the hippocampus. Whether these axons are just passing the V-SVZ or also ending in the V-SVZ, and if they recruit regionally distinct stem cell pools similar to hypothalamic POMC neurons, is subject to future studies. Neuropeptides or neurotransmitters released could affect the behavior and proliferation of stem cells directly or indirectly.

Quiescent neural stem cells extend a cilium into the cerebrospinal fluid (CSF), which is made by the choroid plexuses, highly vascularized structures floating inside the ventricles. The choroid plexus of the lateral ventricle changes its secretome over life, which modulates stem cell behaviour (*124*). It is highly likely that is alters the composition of the CSF also during other physiological states, including pregnancy. As such, the altered choroid plexus secretome may also contribute to the regionalized recruitment of adult NSCs during gestation.

Ultimately, multiple layers of stem cell regulation likely underlie the observed dynamic stem cell recruitment during pregnancy.

4.2.2 Pregnancy leads to generation of common and rarer interneurons transiently populating the olfactory bulb during perinatal care period

The finely orchestrated recruitment of stem cells in different domains during pregnancy led to increased generation of multiple olfactory bulb interneuron subtypes to the accessory olfactory bulb and to all layers of the main olfactory bulb except the external plexiform layer. This included common types, but also interneurons that are produced in low numbers in the adult, such as interneurons localized in the mitral cell layer. Intriguingly, most newborn periglomerular cells were preserved into the weaning period, but in mothers, numbers of interneurons in the mitral cell layer and granule cell layer born during early pregnancy dropped. The mode of this neuronal loss is worth investigating in the future. Apoptosis is a demonstrated mode of cell death for granule cells in the olfactory bulb, and is promoted in the postprandial period (*125*). Apoptotic cells release soluble "find-me" signals and express specific "eat -me" signals that are displayed on the cell surface to be recognized by phagocytes (*126*). Interestingly, our spatial transcriptomics analysis in the olfactory bulb did not reveal increased expression of any of the caspase genes, but indicated increased expression of certain "find-me" and "eat-me" signals in the perinatal care period, the timepoint before we observed a decline in newborn neurons in mothers. These preliminary findings merit further investigation.

4.2.3 Transient addition of functionally distinct interneurons for different aspects of maternal care

Many interneurons generated during pregnancy were only transiently added to the olfactory bulb and were culled by the periweaning period, while numbers of newborn interneurons stayed stable in virgin females.

From an energetic perspective, the tightly controlled production of thousands of young neurons, of which many are culled within a short period of time, raises questions about costs and benefits. On a circuit level, granule cells in the OB sharpen mitral cell output via lateral inhibition. Young, newly integrated neurons with dendritic trees unshaped by experience serve as sources for new synapses, and are more excitable compared to older neurons in the circuit. Like their older counterparts, young neurons provide lateral inhibition to mitral and tufted cells, but it is proposed that they do so with higher efficiency. That way, continuous adult neurogenesis increases discriminatory power in mitral cells (*127*). However, the need for more olfactory discrimination power alone does not explain why pregnancy alters the balance of interneuron subtypes made, and why many of these should be short-lived.

Our model suggests that regional stem cell pools are recruited on-demand by distinct physiological states to generate specific interneurons needed in the near future. It would fit nicely with the observed dynamics of pregnancy-associated neurogenesis. Neurons born in the V-SVZ during early pregnancy should be mature and integrated into the olfactory bulb circuit by the early postpartum period, which is characterized by lactation and intense maternal care. With our cross-fostering experiment we demonstrated that continuous exposure to newborn pups prolonged the survival of granule cell neurons, whereas interneurons in the mitral cell layer were lost rapidly despite the presence of foster pups. Inversely, pup removal in donor mothers accelerated the loss of interneurons in the mitral cell layer, while granule cell were not sensitive to pup removal. The different behavior of these two interneuron classes hints to different functions during the perinatal period. Conjecturing, granule cells could be involved in mediating interactions with pups, including nurturing and lactation, while interneurons in the mitral cell layer potentially form of an olfactory memory of the biological pups in the first couple of hours after birth. In the female accessory olfactory bulb, a similar function has been described for adult-born granule cells. They are necessary for learning and imprinting the odour of mating partners within the first few hours after mating. In the absence of adult-born neurons, if a female is exposed to the smell of its mating partner in the first days following the mating, its smell is not recognized as familiar, which prevents blastocyst implantation, a reflex called pregnancy block or Bruce effect (*100*, *128*).

Together, our results suggest that pregnancy recruits distinct stem cells quasi "on-demand" for the generation of functionally distinct interneurons that are used for different aspects of perinatal care, and that neurons which are generated as a response to changing physiology, are removed from the circuit as soon as they are no longer needed.

4.2.4 Pregnancy-a potential activator of neurogenesis in humans?

The study of adult neurogenesis in humans is difficult, as no prospective labelling methods can be used due to their often mutagenic or toxic nature, and therefore research is mostly based on immunostaining, comparisons between atmospheric and genomic ^{14}C levels and mathematical modelling.

Human V-SVZ architecture differs from mice, and is yet similar. In adult humans, ribbons of GFAP expressing astrocytes are separated from the ependymal layer by a hypocellular gap (*129*). When cultured as neurospheres in the presence of epidermal growth factor (EGF) and fibroblast growth factor (FGF), these V-SVZ astrocytes behave as multipotent stem cells, giving rise to neurons, astrocytes and oligodendrocytes. When grown on a layer of cortical astrocytes, they generate neurons, direct evidence that adult human V-SVZ GFAP+ astrocytes can function as

stem cells in the absence of exogenous growth factors (*129*). Occasionally, dividing (Ki67+) GFAP+ stem cells can be detected *in situ*, but there is no evidence of chain migration of newborn neurons (*129*). In infants however, doublecortin-positive cells can be detected in the niche (*130*). Some have been observed in chains seemingly migrating towards the medial prefrontal cortex, others, like in rodents, have been detected in the rostral migratory stream (*130*). However, there are no means to determine whether these cells ever differentiate into mature neurons (*131*). Doublecortin expression and proliferation almost cease after the age of six to nine months (*130*), and mathematical modelling suggest that in the human olfactory bulb, which is much smaller compared to mice, maximum 1% of neurons get replaced in 100 years (*131*). Several lines of evidence however indicate that some neurons in the striatum, a neighboring region of the ventricular zone, are generated in the adult brain, and strikingly, some of these express the interneuron markers neuropeptide Y and calretinin (*131*, *132*). Our results show that both of these are also markers for adult-generated and pregnancy-associated OB interneurons in mice. As we show that physiological states, in this particular case pregnancy, dynamically regulate proliferation of stem cells in different domains of the rodent V-SVZ, it is a highly interesting question whether pools of adult neural stem cells are released from quiescence during a human pregnancy. Indeed, many pregnant women self-report a heightened sense of smell during pregnancy. However, scientific evidence for lowered olfactory thresholds and superior odour recognition in pregnant women is sparse and contradictive, surprising given all the anecdotal evidence (*133*). Adult neurogenesis may bring light into the darkness. Pregnancy may recruit quiescent stem cells for the generation of interneurons for the adult human olfactory bulb for a transient period. In addition, if underlying activating signals were deciphered, avenues would be opened for endogenous brain repair.

4.3 Oligodendrogenesis during pregnancy

4.3.1 Pregnancy increases oligodendrogenesis in grey and white matter around the V-SVZ

After pulsing with thymidine analogs on Gd2.5 and Gd4.5 we observed trends for higher fold changes of analog+ OLIG2+ cells in pregnant mice at Gd7.5 compared to virgin mice in both white and grey matter areas around the V-SVZ. In the corpus callosum at the 30 dpi timepoint, most analog-labelled cells in both virgin and mothers had disappeared. In general, the data were very variable, not allowing any major conclusions. It will be important to add more timepoints to our analysis, and to increase the cohort size and synchronize the estrous cycle of virgin females to reduce variability.

Higher fold changes in analog+ OLIG2+ cells during pregnancy in the areas around the V-SVZ could have resulted from increased proliferation of resident oligodendrocyte precursor cells, increased V-SVZ oligodendrogenesis or a combination of both. In the septum, increases in analog+ OLIG2+ cells became first apparent in the septum distal to the V-SVZ, favoring local proliferation of oligodendrocytes rather than an origin in the V-SVZ. Moreover, the high fraction of CC1- oligodendrocyte precursor cells among the remaining analog+ cells in motherhood in both the septum and corpus callosum points to local division of oligodendrocyte precursor cells. In the corpus callosum however, the transient increase of OLIG2+ analog+ cells during early pregnancy in the domain above the V-SVZ but not more lateral, hinted at a contribution of V-SVZ neurogenesis. Only lineage tracing would tell for certain. Inducible Cre reporter mice are unsuitable for our experiments, with tamoxifen being an antagonist of estrogen receptors, and estrogen being important in maintaining pregnancy. Administration of tamoxifen to mice in early gestation can perturb embryonic development (*134*), and we found that injecting virgin females with a single dose of tamoxifen (120mg/kg) prevented them from becoming pregnant for several weeks. To avoid tamoxifen-induced side effects, viral labelling strategies or other systems for controlling Cre activity could be used.

Interestingly, increased oligodendrocyte precursor cell division during early pregnancy did not lead to an expansion of mature or immature oligodendroglial cells during motherhood (Ppd15), and a rapid myelin stain revealed no obvious differences in myelination between virgin females and mothers at Ppd6. Previous findings on the expression of myelin protein MBP in the genu of the corpus callosum (most rostral part) by western blot showed significantly increased levels in mothers at Ppd7 and Ppd14 compared to virgins, and the number of myelinated axons (but not total number of axons) was increased at Ppd14 (*109*). Histochemical myelin stainings are useful to compare myelination over different ages (*135*), or to visualize demyelinated lesions (*47*), but may not be sensitive enough to reveal subtle changes in myelination. Electron microscopy for assessing myelin sheet thickness, internode length and number and percentage of axons myelinated would be a more powerful approach.

4.3.2 Is there a domain for pregnancy-associated oligodendrogenesis?

In the V-SVZ and RMS, we characterized two dividing types of the oligodendrocyte lineage. PDGFRα+ oligodendrocyte precursor cells (OPCs) and PDGFRα- MCM2+ transit-amplifying cells. While OPCs are evenly distributed across domains, transit amplifying OLIG2+ cells are rarely found on the medial wall, and have the highest density in the dorsolateral wedge. We do not know whether these two types share a direct lineage relationship, but their differential distribution in the V-SVZ makes it unlikely. Moreover, one of them may give rise to callosal oligodendrocytes.

Given the high density of transit amplifying cells in the dorsolateral wedge, they seem the more likely candidates. Surprisingly, we found that neither these nor the oligodendrocyte precursor cells amplified on any of the analyzed gestation days, not even on the medial wall, which has been shown to have high gliogenic potential (*34*). In the dorsolateral corner and the roof, there were slightly more OLIG2+ TACs at gestation day 4.5, but these were only trends. Interestingly, on the more caudal brain level analyzed, we detected a pregnancy-associated increase in OLIG2+ transit amplifying cells in the lateral wall at Gd12.5. In mice in which stem cells are released from quiescence, these caudal domains in the lateral wall are more oligodendrogenic than more rostral domains, suggesting that these may also be recruited during pregnancy (*34*).

Remarkably, pregnancy increases the ability to repair white matter lesions, and it was speculated that V-SVZ- derived oligodendrocytes may contribute to regeneration (*109*). Our data suggest that while V-SVZ neurogenesis is modulated during pregnancy, V-SVZ oligodendrogenesis is not. Importantly, in virgin mice that ingested a demyelinating agent over a period of several weeks, the density of NSC-derived oligodendroglia recruited to the corpus callosum varied along the rostrocaudal axis (*47*). We analyzed oligodendrogenesis during pregnancy solely on coronal sections at three bregma levels, which allowed us to simultaneously study all three walls of the V-SVZ, including the V-SVZ roof and the dorsolateral wedge, at the cost of resolution along the rostrocaudal axis. It will therefore be important to complement our analysis with quantifications on wholemount preparations, as we did for MCM2 in chapter 2. Ultimately, B1 stem cells in the walls of the V-SVZ might not be the origin of callosal oligodendrocytes, but GFAP+ stem cells that generate intraventricular OPCs, whose fate and function is still unknown. While it remains important to analyze further domains, it is a possibility that a demyelinating injury is needed in the first place to trigger a response from the V-SVZ, before the effect of pregnancy can unfold, or alternatively, that pregnancy does not modulate V-SVZ oligodendrogenesis at all.

4.3.3 Do NG2 oligodendrocyte precursor cells regulate maturation of pregnancy-associated neurons?

In the granule cell layer of the olfactory bulb we detected a temporary increase of NG2+ cells in the perinatal care period, paralleling the temporary rise in newborn neurons. The origin of these cells is still unknown. They could have been made locally in the olfactory bulb, or migrated there from other brain areas. Our data suggest that oligodendrogenesis in the RMS and V-SVZ are not changing with pregnancy, which makes is unlikely they originate from there. However, it is a possibility that these oligodendrocyte precursor cells are intraventricular oligodendrocyte

precursor cells that migrated to the olfactory bulb. The behavior of these intraventricular oligodendrocyte precursor cells during pregnancy is currently being analyzed in the lab.

Another exciting possibility is that these cells are derived from the fetuses. Fetal microchimerism has been described in the brain, and strikingly, fetal cells were found with higher densities in the olfactory bulb compared to the rest of the brain (*136*). Another study found that fetal cells were only detectable starting P0, but not yet during gestation, and showed that the distribution of fetal cells within the brain was variable between mothers (*137*). Interestingly, fetal cells can adopt neuronal and glial identity, including the oligodendrocyte lineage (*136*).

A concomitant arrival of new neurons and increase in oligodendrocyte precursor cells in the olfactory bulb could hint to an interaction between NG2 cells and newborn neurons. The best known function of NG2+ cells is to differentiate into myelinating oligodendrocytes. However, adult-born olfactory bulb neurons do not get myelinated (*138*). Indeed, we found that these oligodendrocyte precursor cells did not differentiate into mature oligodendrocytes in motherhood, suggesting they were generated for another function.

NG2 cells are unique from other glial cells in the sense that they receive synaptic input from neurons (*139*). Moreover, there is increasing evidence that oligodendrocyte precursors cells do not only respond to, but also regulate neurons via different mechanisms (*140*, *141*). As contacts between young neurons and oligodendrocyte precursor cells increase with the maturation state of neurons (*120*), pregnancy-associated NG2 cells increased at perinatal care may help neurons to mature. In the future, it would be interesting to study whether regional ablation of oligodendrocyte precursors impedes maturation of neurons and their integration into the circuit. This could be achieved by injection of AAVs expressing diphtheria toxin fragment A in a Cre-dependent manner into the granule cell layer of NG2-Cre mice, however, this could induce injury in the olfactory bulb, which could affect neuronal maturation and survival. Alternatively, one could cross NG2-CreER^{T2} mice with mice in which diphtheria toxin fragment A gene is preceded by a lox-stop-lox (lsl) cassette knocked into the ubiquitously expressed Rosa26locus. NG2 cells all over the brain would be ablated, but this approach would leave the olfactory bulb uninjured.

4.4 Closing remarks

A pregnancy induces many changes in a female's physiology, endocrinology, immune system and behavior. The maternal brain undergoes rewiring and shows remarkable plasticity (*142*). T2-weighted MRI allows to detect and follow morphometrical changes in the brain over the course of pregnancy and lactation (*113*, *143*). In mice, mesoscopic changes appear in centers for olfactory- and somatosensory processing, memory and reward. Strikingly, the levels of grey matter

concentration change in the olfactory system during late pregnancy predict maternal performance in the postpartum period (*113*, *143*). Modifications in grey matter concentration can result from changes in blood flow, synaptic changes, cell death, and cell addition (*143*).

We studied one specific layer of brain plasticity, the de-novo generation of olfactory bulb neurons and oligodendrocytes. Our results suggest that pregnancy, or more globally physiological states, dynamically regulate regionally distinct stem cell pools for the generation of different interneuron subtypes in anticipation of future need. The general principle of transient neurogenesis at different time scales for future physiological demand may be conserved across evolution, including in humans.

5 Materials & Methods

5.1 Animal use

Two to three month-old heterozygous *hGFAP::GFP* mice (*144*) were used for timed-matings. Mice of each pregnancy cohort were compared to age-matched virgin controls, injected and processed at the same time. Females from different litters were randomized to form the control virgin and pregnancy/lactation groups. Virgin females were housed in cages of three to four. To set up the timed mating, two females were placed in a cage together with one male 30min before onset of the dark cycle. On the morning of the copulatory plug, mated females were transferred into fresh cages and housed in pairs until the end of experiment. The females spent on average 2-3 days with a male before separation, which is important in our context, as male pheromones have been described to have an effect on V-SVZ neurogenesis after seven but not two days of exposure (*93*). Mice kept for the 30dpi timepoints were housed alone with their litter shortly after giving birth. The morning of the plug is defined as Gd 0.5. This mouse strain gives birth between gestation days 18.5-19.5.

For experiments assessing c-fos in the OB, three groups were used: virgins with no contact to pups, virgins exposed to pups for 1 hour, and mothers with their pups. All groups (virgins and mothers with pups) were transferred to fresh cages and allowed to acclimate for 1 hour. For the virgins exposed to pups for 1 hour group, pups were added to the cage for 1 hour. All mice were sacrificed after 1 hour.

For the cross-fostering experiment, mice were divided into groups of donor mothers, foster mothers, and virgin female controls for both groups. Staggered timed-matings were set up, beginning with prospective foster mothers, and 6 and 11 days later with prospective pup donor mothers. All groups were injected on Gd 4.5 and Gd 7.5 with 43mg/kg CldU and 58mg/kg IdU respectively. On the day donor mothers gave birth, their pups were removed and given to foster mothers for adoption. Donor mothers were housed in pairs with other donor mothers or virgin females, and sacrificed on the day corresponding to their postpartum day 6 (matching the 20dpi/perinatal care timepoint). Foster mothers were housed with their own pups until Ppd6, when they were replaced with newborn pups from donor mothers. 6 days later, the alien pups from the first adoption were replaced again with newborn alien pups from another donor mother. Foster mothers were sacrificed on the day on which their biological pups would have been weaned (matching the 30dpi mice /peri-weaning period).

Mice were housed in a 12:12h dark/light cycle with ad libitum access to food. All experimental

cohorts were sacrificed at the same time of the day, i.e the morning. All experiments were performed under a license approved by the veterinary office of canton Basel-Stadt.

5.2 Thymidine analog injection

Virgin control females, pregnant and lactating mice were pulsed with a single intraperitoneal injection of thymidine analog on specific days of gestation and mice sacrificed 20 or 30 days later. All injections were performed in the morning. The following timepoints were investigated: Gd 0.5 (morning of copulatory plug), Gd 2.5, Gd 4.5 (day of blastocyst implantation), Gd 7.5. Three different thymidine analogs were used at equivalent stochiometric doses: 1) 5-bromo-2'deoxyuridine (BrdU; Sigma B5002-5G; 50mg/kg body weight), 2) 5-Chloro-2'deoxyuridine (CldU; Sigma C6981-100MG; 43mg/kg body weight), and 3) 5-Iodo-2'deoxyuridine (IdU; Sigma I7125-5G; 58mg/kg body weight). For all three thymidine analogs, 10mg/ml stock solutions were prepared in sterile 0.9% NaCl. A few drops of 5M NaOH were added to the IdU solution to dissolve it. Aliquots of each solution were stored at -20°C (BrdU, CldU) or refrigerated (IdU) up to 6 months. Solutions were vortexed at 37°C for 10-15min prior to injection.

All pregnant mice were compared to matched controls injected with the same thymidine analogs. Gd 0.5/Gd 2.5 + 20 dpi cohorts and their matched virgin control mice were co-injected with CldU at Gd0.5 and IdU at Gd 2.5. Similarly, Gd 4.5/Gd 7.5 + 20 dpi cohorts and their matched virgin control mice were co-injected with CldU at Gd4.5 and IdU at Gd 7.5. For the 30dpi time point, Gd 2.5/Gd 4.5 cohorts and their matched virgin control mice were co-injected with CldU at Gd2.5 and IdU at Gd 4.5. Gd 0.5+ 30 dpi (CldU) and Gd7.5 + 30 dpi (IdU or BrdU) cohorts were single injected. Mice were sacrificed 20 or 30 days after the last injection of analog.

5.3 Tissue preparation

Mice were deeply anaesthetized with pentobarbital and perfused with 0.9% saline followed by ice-cold 3.2% paraformaldehyde (PFA, Electron Microscopy Sciences) in 0.1M phosphate buffer (PB). Brains were postfixed in 3.2% PFA for 24h at 4°C, washed 3x in PBS over a day and subsequently stored at 4°C in 0.05% PBS-azide until processing. Coronal sections were cut on a vibrating microtome (Leica VT10006). Olfactory bulbs were sectioned at 30µm (OB) and the rest of the brain at 25µm.

V-SVZ sections were serially collected in sequential wells of a twelve-well plate and stored in 0.05% PBS-azide until processing. Olfactory bulb sections were cut at 30µm thickness between Bregma +5.2 mm to +3.0 mm and were serially collected in different wells.

5.4 Immunostaining

Immunostaining of virgin and pregnant /lactating groups was performed on bregma-matched sections. Floating sections were blocked for 1h at RT in PBS with 0.3-0.5% Triton-X 100, 10% normal donkey serum (Gene Tex, #GTX73245). For wholemounts, blocking solution contained 3% bovine serum albumin (Sigma, A7030) in 1.6% Triton-X 100. Sections and wholemounts were incubated in the primary antibody solution prepared in the same blocking solution at 4°C (1 overnight for sections, 2 overnights for wholemounts), washed 3x15min in 1X PBS before incubating for 1-2h at RT in the secondary antibody prepared in blocking solution. Finally, the sections were washed 3x15min, and counterstained with DAPI. Sections were mounted on glass slides using Aqua-Poly/Mount (Polysciences #18606-20) and wholemounts were mounted with FluorSave (Merck, 345789).

When combining thymidine analog detection with other immunostaining, other antibodies were immunostained first, sections fixed for 10 min at RT in 3.2% PFA, and washed 3x15min in PBS. Sections were then incubated for 20 to 30 min in 2M HCl at 37°C. After removing the HCL, the pH was neutralized using a 0.1M Borax pH 8.5 solution for 10min at RT, followed by 3x15min wash in 1X PBS. Detection of the thymidine analogs was performed with the following antibodies: Anti-BrdU rat (abcam) for detecting BrdU and CldU, and anti-BrdU mouse (clone B44, BD-Bioscience) for IdU. In mice co-injected with both CldU and IdU, we distinguished the two analog types following the protocol described in Podgorny et al. 2018 (*145*), except we shortened the DNA denaturation step to 20-30 min. Single injected controls were processed in parallel to set the imaging settings and thresholds.

5.4.1 Antibodies

The following primary antibodies were used: anti-BrdU (rat, 1:500-1:1000, abcam #ab6326); anti-BrdU (mouse clone B44, BD-Bioscience), anti-Calbindin (rabbit, 1:1000, Chemicon, #AB1778), anti-Calretinin (rabbit, 1:1000, SWANT, #7697), anti-Calretinin goat, 1:1000, Labome Millipore, #ab1550), anti-Tyrosine Hydroxylase (sheep, 1:500, Millipore, #AB1542), anti-doublecortin, DCX (goat, 1:100, Santa Cruz, discontinued); anti-doublecortin, DCX (guinea pig, 1:1000, MerckMillipore, #ab2253), anti-GFAP (chicken, 1:600, Millipore, #MAB5541), anti GFAP (rat, 1:600, Invitrogen, #13-0300), anti-Ki67 (rabbit, 1:100, abcam, #ab15580), anti-NeuN (mouse, 1:100, Millipore, #MAB377); anti-NeuN (rabbit, abcam, #ab177487); anti-c- fos (rabbit, 1:1000, Synaptic Systems, 226003), anti-neuropeptide Y (rabbit, 1:200, abcam, ab30914), anti-APC (clone CC1; mouse; 1:100, Millipore; #OP80, anti-NG2 (rabbit, 1:100, Millipore, #AB5320); anti-Olig2 (rabbit, 1:150, Millipore, #ab9610); anti-Olig2 (goat, 1:150, R&D, #AF2418, anti-PDGFRα (goat, 1:100, R&D Systems, #AF1062.

.

The following secondary antibodies were used: Alexa Fluor-conjugated (405, 488 and 647; 1:200-1:600, Invitrogen) and Cy3-conjugated (1:600-1:1000, Jackson ImmunoResearch) Fab2 fragments raised in donkey.

5.5 RNAscope

Brains were snap frozen in liquid nitrogen and stored at -80°C. 10µm thick sections were cut on a cryostat and collected on Superfrost slides (Biosystems, Cat. 85-0551-00). Tissue sections were fixed in pre-chilled 4% PFA at 4°C for 30min and washed 5 times in 1x PBS. Sections were dehydrated in 50% EtOH, 70% EtOH and twice in 100% EtOH for 5min each, treated with Peroxidase (RNAscope Multiplex Fluorescent Assay Kit (Advanced Cell Diagnostics) for 10min at RT and submitted to antigen retrieval (Cat. 322000) in the steamer at 100°C for 10min. Sections were washed with dH2O, followed by 20min permeabilization with Protease Plus (Cat. 322330) at 40°C and a wash in 1x PBS. Probes targeting Elp3 (Cat.400941), Egr1 (Cat. 423371), Klf9 (Cat. 488371) and Nr4a3 (Cat. 483411) were preheated to 40°C, and incubated onto the sections in probe solutions for 2h at 40°C. Sections were washed 2x for 2min in wash buffer before signal amplification (Kit Cat. 320851), incubating in RNAscope AMP-1(30min, 40°C), AMP-2 (15min, 40°C), RNAscope AMP-3 (30min, 40°C), and AMP-4-FL (15min, 40°C). After each amplification step, sections were washed 2x 2min in wash buffer. Finally, sections were stained for DAPI for 30s and mounted in Aqua-Poly/Mount (Polysciences #18606-20).

5.6 Schmued's myelin gold stain

The protocol for frozen sections (*119*) was applied on fixed tissue. Coronal brain sections were prepared as described in the section "tissue preparation".

A 0.2% gold chloride solution was prepared freshly in glassware. For 250ml: 0.5g crystalline gold chloride (Gold(III) chloride trihydrate >99.9% trace metal basis; Sigma, #520918), 82mg sodium phosphate monobasic monohydrate, 0.9g sodium phosphate dibasic anhydrous, 2.25g sodium chloride in distilled water. The solution was stirred at RT until all salts had dissolved, and was adjusted to pH7.4. Sections were stained floating in glassware at RT on an orbital shaker. The staining progress was monitored under a dissection scope, and stopped for all brain sections simultaneously when the staining was of dark purple color (after a few hours). The sections were washed for 5min in 0.9% NaCl, fixed for 5min in 2.5% sodium thiosulfate (RT) and washed for

30min in tap water. Ultimately, the sections were mounted in Aqua-Poly/Mount (Polysciences #18606-20) and imaged with the Zeiss AxioScanZ1.

5.7 Image acquisition and quantification

Images were acquired using LSM700, LSM800 and LSM880 confocal microscopes (Zeiss), the Olympus confocal spinning disk microscopes SpinSR(CSU-W1) and SpinD(CSU-W1) or the Zeiss AxioScan Z1. On the LSM700 and LSM800, images were acquired with PLAN APO 25x/0.80NA and PLAN APO 40x/1.3NA objectives. On the LSM880, a PLAN APO 40x/1.2 NA objective was used, and on the SpinSR a UPL S APO 30x/1.05NA in combination with Silicon oil. On the SpinSR and SpinD, images were acquired with 2x2 binning, and a resolution of 1152x1152. Tile scans of the entire OB and V-SVZ were acquired, with z-stacks encompassing the entire thickness of the sections. Individual z step sizes were 1-2µm, depending on the staining. Images of the same immunostaining were acquired on the same microscope. Individual tiles acquired on the SpinSR were stitched using the Fiji plugin *recursive olympus vsi stitcher* provided by the local Imaging Core Facility.

Analysis of proliferating NSCs was performed on sections between Bregma +0.3 mm and 0 mm. For each bregma, two to four sections per mouse were analyzed for n=3-6 mice per group. Cells were quantified manually using the counter tool in Fiji. Data are presented as densities (cells per mm3 for NSCs in the V-SVZ, or cells per mm2 for MOB and AOB sections).

Counts in the OB were performed on entire olfactory bulb sections. For the quantification of cells in the main olfactory bulb GCL and GL, two sections were used per mouse for n=3-7 mice per group. For the MCL and AOB, four to five sections per animal were sampled due the low number of total analog cells incorporated in these regions. For quantification of NeuN+ analog+ cells in the superficial and deep GCL only (Fig. S6B), two separate strips on the medial and lateral olfactory bulbs capturing the entire dorsal-ventral length were quantified.

Quantifications of oligodendroglial cells in the septum and corpus callosum in Fig. 3-1 are reported as raw numbers in the analyzed domain per section, not normalized to the area analyzed due to the low cell number.

Analog+(OLIG2+ or OLIG2-) cells in Fig. 3-3 are reported as the number of cells found in a domain per section, normalized to the average size of the domain.

All other cell counts in chapter 3 are reported as densities, per mm^3 when cells were analyzed in a volume, per mm^2 when cells were counted on a single plane.

5.7.1 Wholemount analysis

Whole mount preparations of the entire lateral wall and entire medial wall were analyzed (n=3-7 mice per group). Images of each whole mount were stitched using the recursive olympus vsi stitcher in Fiji. A pseudo flat-field correction was applied onto maximum intensity projections to correct for uneven illumination and facilitate analysis: The channel containing MCM2 was duplicated. On the duplicate, a gaussian blur with a sigma (radius) of 100 was applied, and the resulting image was converted into a 32-bit image. This image was divided by the intensity value of its brightest pixel (process>math>divide). The image calculator (process> image calculator) was used to divide the original image by the processed image. The resulting flat-field corrected image was saved and analyzed using the software Qu-Path 2.3 (*146*). Quantification of nuclear MCM2 staining was done semi-automatically. The wholemounts were divided into three (medial wall) or four (lateral wall) areas for quantification. For the medial wall these were the area rostral to where the lateral and medial walls fuse (1), the fusion area (2) and the area caudal to the fused area (3). Rostrally, the lateral wall was divided into the same bins. The part of the lateral wall caudal to the fused walls was divided in two areas (3&4). These regions of interest were drawn manually, and for a more accurate analysis further subdivided into more ROIs in order to adjust the detection settings (threshold and sigma) to local background and signal intensity. The applied cell detection parameters were the following:

Set up parameter:

- requested pixel size= 0.5µm

Nucleus parameter:

- Background radius = 8µm
- Median filter radius = 0µm
- Sigma: 1.5µm for low density areas, 1.3µm for high density areas
- Minimum area 10µm2
- Maximum area 400µm2

Intensity Parameters:

- Threshold: adjusted manually for each ROI until the result was satisfying

Only when the cell detection was accurate as determined by visual validation, cell number and area of each region of interest were noted. The number of Mcm2 cells is given per mm2.

Density maps were created based on the cell detections using the density map tool in QuPath 0.3, using a density radius of 50µm and interpolation mode "nearest neighbor". The lateral walls were imaged in two files, rostral and caudal. The density maps of the rostral and caudal part of each

lateral wall were fused in Fiji using the plug-in TrakEM2. Three medial and three lateral walls were aligned to templates of the walls using the ec-clem plug-in in Icy, by first using the rigid and then the non-rigid mode for fine alignment. For both the lateral and the medial walls, three density maps per state / timepoint were averaged in Fiji. The averaged pregnancy timepoint maps were then each divided by the averaged virgin female density map in order to obtain the fold change. We used thresholding to select and highlight only those areas in which pregnant mice showed higher proliferation compared to virgin females (values>1). Infinity values (value 0 in averaged virgin females because there were no cells in those regions) are shown in white. Pixels <1 and =1 and non-assigned numbers (no value or not any Mcm2 cell in both virgins and pregnant mice) are shown in black, comprising non-changing areas and areas in which the virginF showed higher proliferation. The most caudal part in the lateral wall is shown in dashed lines, as the dissection was variable, and the density map therefore not precise in this caudal-most part of the wholemount. Values are shown on a log scale, and the look-up-tables "fire" was applied for better visualization.

5.7.2 RNAscope signal quantification

Sections stained with the same probe were all imaged with the same settings. In Fiji, for each section, background staining was determined by measuring mean intensity of a rectangle in an unstained region and subtracting this value from the entire image. A line with the length of 685µm and width of 1000 pixels was drawn to span the GCL to the GL, and the average intensity profile along the line plotted in Prism. Shown are smoothened curves, generated by a restricted cubic spline analysis with 25knots.The area under the (unsmoothened) curve and standard error of mean were calculated and plotted as bar graphs. The analysis was done with n=3 for virgin females, n=3 for mothers during perinatal care and n=2 for mothers in the peri-weaning period.

5.8 Spatial transcriptomics

Four brain samples were used for spatial transcriptome analyses: (i) one mother during perinatal care, (ii) one mother at peri-weaning, (iii) two age-matched virgins. Brains were snap frozen in liquid nitrogen and stored at -80°C. RNA quality of all samples was assessed through RIN measurement, and only brains with a RIN > 8 were processed for sequencing. 10µm thick olfactory bulb sections were cut on a cryostat and placed on pre-chilled Visium Tissue Optimization Slides or Visium Spatial Gene Expression Slides. Tissue sections were then fixed for 30 minutes in methanol at -20°C and processed for a short immunofluorescence staining (CG000312 Rev C, 10x Genomics), using NeuN (ms) and DAPI. Tissue permeabilization time was set to 9 minutes, as

evaluated by the maximal yield of fluorescent cDNA according to Visium Spatial Tissue Optimization User Guide (CG000238 Rev D, 10x Genomics). Immunofluorescence images were acquired using a 10x objective on a Leica DMI8 inverted microscope with a Leica DFC9000 GTC VSC-11972 camera. mRNA extraction and library preparation were performed according to 10x Genomics protocols (CG000239 Rev D, 10x Genomics).

The resulting libraries were sequenced by the Genomics Facility Basel. The sequencing was performed in a paired-end manner with dual indexing on a NovaSeq 6000 (Illumina) with SP 100 kits. 100µl of library mix at a concentration of 1.8nM with a 1% PhiX spike-in was loaded by the core facility. Libraries were then sequenced with the following cycle settings: Read1 28 cycles, i7 10 cycles, i5 10 cycles, Read2 82 cycles. The resulting Bcl files were demultiplexed with Space Ranger 1.2.0 (10x Genomics) using the mkfastq command.

Immunofluorescence images in TIFF format were processed with ImageJ (*147*), and manually aligned to the fiducial frames with Loupe Browser 5.1.0 (10x Genomics) to generate a .json file. The 10x Genomics Space Ranger 1.2.0 count pipeline was run with the FASTQ files, images and .json files on the ETH Euler cluster. The mouse reference mm10-2020-A (GENCODE vM23/Ensemk 98) was used for read alignment (10x Genomics).

Raw Space Ranger output files of the four 10x Visium capture areas were normalized using the SCTransform (*148*) with default parameters in Seurat v4.0 (*149*). Principal component analysis (PCA) was performed on the normalized dataset, and the top 20 components were used for neighbor finding, Louvain-based cluster analysis, and uniform manifold approximation and projection (UMAP) visualization. Data subsets were defined based on clusters of interest (anatomical and marker genes). The resulting data subsets were normalized the same way and merged with the merge() function to enable a joint dimensional reduction and clustering. Integrated dimensional reduction was then performed with 20 dimensions from PCA and clusters were identified with FindClusters() at a resolution of 0.5.

For the identification of differentially-expressed genes, the Seurat function FindMarkers() was used with a Wilcoxon rank sum test on the log normalized data. Differential gene expression analysis across states (perinatal care, peri-weaning and virgins) was performed was performed both globally and also stratified within the corresponding spot clusters. To visualize and compare genes across states in a qualitative manner the maximal cutoff settings of the SpatialFeaturePlot() were set for each gene individually.

Gene ontology analysis and gene regulatory networks

Whole bulb analyses

We first performed whole bulb (main and accessory bulb) differentially expressed gene analysis, comparing "virgins (n=2)" to "perinatal care mother-20dpi", and "perinatal care mother-20dpi" to "peri-weaning mother-30dpi". Genes with a log2(FC) > 0.10 and adjusted p-value < 0.05 were considered significantly up-regulated. From this analysis, three distinct gene sets were identified.

(1) A first set comprising all up-regulated genes in mothers at perinatal care compared to virgins.

(2) A "transient" set: composed of the up-regulated genes at perinatal care, excluding those that remained high through peri-weaning.

(3) A "maintained" set: composed of commonly up-regulated genes at both perinatal care and peri-weaning compared to virgins.

Cluster-based analyses

We performed differentially-expressed gene analysis for each cluster obtained, comparing mothers (during perinatal care and at peri-weaning) to the two virgin samples. Genes with a log2(FC) > 0.25 and adjusted p-value < 0.05 were considered significantly up-regulated. The log2(FC) threshold is more stringent for cluster-based comparison than for whole bulb analysis because the lower number of spatial dots per layer. In each cluster, up-regulated genes at perinatal care were compared to those up-regulated at peri-weaning, and GO process analysis was run on overlapping sets, as well as perinatal- or peri-weaning-specific gene sets.

GO process analyses

We used EnrichR and Metacore (Clarivate Analytics) to explore GO biological functions of each dataset of interest. GO terms with P-value < 0.05 were considered significant. Results from EnrichR are ranked by the combined enrichment score, and those from Metacore are ranked based on $-\log_{10}$ (P-value).

Gene network analysis

Gene networks in Fig. S9 were obtained with the STRING software, using differentially expressed gene lists as input, and applying k-means clustering on network components.

5.9 Statistical analysis

Significance was established using two-tailed student's *t*-tests for pair-wise comparisons. 1-way ANOVA was used to assess the effect of pregnancy time in all quantifications included in the paper, followed by multiple comparisons using t-tests. All ANOVAs were significant ($p<0.05$), except for MCM2 counts in the medial wall-region2 (Fig1H), and GFAP/Ki67 counts in the dorsomedial corner (Fig.S1A). Significance was established at *$p<0.05$, **$p<0.01$, ***$p<0.001$, ****$p<0.0001$. Error bars indicate the standard error of the mean (SEM). Statistics were performed using Prism 6 software.

For figures 2C to F (fold change quantifications), significance was calculated on raw values relative to the matched virgin control group. In figures 3A and B (c-fos quantifications), statistical tests were comparing "plain mothers with pups" to "virgin females exposed to pups" as controls.

5.10 Image Credit for ISH images: Allen Institute

Figure S7:

Nrgn: https://mouse.brain-map.org/experiment/show/736

Pcp4: https://mouse.brain-map.org/experiment/show/79912613

Uchl1: https://mouse.brain-map.org/experiment/show/1088

Trh: https://mouse.brain-map.org/experiment/show/71016631

Doc2g: https://mouse.brain-map.org/experiment/show/74881341

Slc20a1: https://mouse.brain-map.org/experiment/show/1571

Necab2: https://mouse.brain-map.org/experiment/show/73788010

Doc2b: https://mouse.brain-map.org/experiment/show/72283810

Figure S11:

CamkIIa: https://mouse.brain-map.org/experiment/show/79490122

Grin1: https://mouse.brain-map.org/experiment/show/1585

Gabrb3: https://mouse.brain-map.org/experiment/show/75551468

Carpt: https://mouse.brain-map.org/experiment/show/72077479

Cbln1: https://mouse.brain-map.org/experiment/show/100145395

Eomes: https://mouse.brain-map.org/experiment/show/100142505

Calb2: https://mouse.brain-map.org/experiment/show/75492430

Zic1: https://mouse.brain-map.org/experiment/show/79677351

6 References

1. J. M. W. Slack, *The science of stem cells* (2018).
2. H. Bindu A, S. B, Potency of Various Types of Stem Cells and their Transplantation. *J. Stem Cell Res. Ther.* **01**, 1–6 (2011).
3. H. Clevers, F. M. Watt, Defining Adult Stem Cells by Function , not by Phenotype. *Annu. Rev. Biochem.* **87**, 1–13 (2018).
4. L. Li, T. Xie, Stem Cell Niche : Structure and Function. *Annu. Rev. Cell Dev. Biol.* **21**, 605–634 (2005).
5. A. Rezza, R. Sennett, M. Rendl, in *Current Topics in Developmental Biology* (2014), vol. 107, pp. 333–372.
6. M. V. Sofroniew, H. V. Vinters, Astrocytes: Biology and pathology. *Acta Neuropathol.* **119**, 7–35 (2010).
7. M. Götz, S. Sirko, J. Beckers, M. Irmler, Reactive astrocytes as neural stem or progenitor cells: In vivo lineage, In vitro potential, and Genome-wide expression analysis. *Glia.* **63**, 1452–1468 (2015).
8. R. A. Hill, A. Nishiyama, NG2 cells (polydendrocytes): Listeners to the neural network with diverse properties. *Glia.* **62**, 1195–1210 (2014).
9. S. Owji, M. M. Shoja, The History of Discovery of Adult Neurogenesis. *Clin. Anat.* **33**, 41–55 (2020).
10. A. M. Bond, G. Ming, H. Song, Adult Mammalian Neural Stem Cells and Neurogenesis: Five Decades Later. *Cell Stem Cell.* **17**, 385–395 (2015).
11. A. Kriegstein, A. Alvarez-Buylla, The glial nature of embryonic and adult neural stem cells. *Annu. Rev. Neurosci.* **32**, 149–184 (2009).
12. L. C. Fuentealba, S. B. Rompani, J. I. Parraguez, K. Obernier, R. Romero, C. L. Cepko, A. Alvarez-Buylla, Embryonic Origin of Postnatal Neural Stem Cells. *Cell.* **161**, 1644–1655 (2015).
13. S. Furutachi, H. Miya, T. Watanabe, H. Kawai, N. Yamasaki, Y. Harada, I. Imayoshi, M. Nelson, K. I. Nakayama, Y. Hirabayashi, Y. Gotoh, Slowly dividing neural progenitors are an embryonic origin of adult neural stem cells. *Nat. Neurosci.* **18**, 657–665 (2015).
14. N. Urbán, I. M. Blomfield, F. Guillemot, Quiescence of Adult Mammalian Neural Stem Cells: A Highly Regulated Rest. *Neuron.* **104**, 834–848 (2019).
15. F. Doetsch, I. Caille, D. A. Lim, J. M. Garcia-Verdugo, A. Alvarez-Buylla, Subventricular Zone Astrocytes Are Neural Stem Cells in the Adult Mammalian Brain. *Cell.* **97**, 703–716 (1999).

16. Z. Mirzadeh, F. T. Merkle, M. Soriano-Navarro, J. M. Garcia-Verdugo, A. Alvarez-Buylla, Neural Stem Cells Confer Unique Pinwheel Architecture to the Ventricular Surface in Neurogenic Regions of the Adult Brain. *Cell Stem Cell.* **3**, 265–278 (2008).
17. K. Sawamoto, H. Wichterle, O. Gonzalez-Perez, J. A. Cholfin, M. Yamada, N. Spassky, N. S. Murcia, J. M. Garcia-Verdugo, O. Marin, J. L. R. Rubenstein, M. Tessier-Lavigne, H. Okano, A. Alvarez-Buylla, New Neurons Follow the Flow of Cerebrospinal Fluid in the Adult Brain. *Science (80-.).* **311**, 629–632 (2006).
18. F. Doetsch, J. M. García-Verdugo, A. Alvarez-Buylla, Regeneration of a germinal layer in the adult mammalian brain. *Proc. Natl. Acad. Sci. U. S. A.* **96**, 11619–11624 (1999).
19. P. Khatri, K. Obernier, I. K. Simeonova, A. Hellwig, G. Hölzl-Wenig, C. Mandl, C. Scholl, S. Wölfl, J. Winkler, J. A. Gaspar, A. Sachinidis, F. Ciccolini, Proliferation and cilia dynamics in neural stem cells prospectively isolated from the SEZ. *Sci. Rep.* **4**, 3803 (2015).
20. P. Codega, V. Silva-Vargas, A. Paul, A. R. Maldonado-Soto, A. M. DeLeo, E. Pastrana, F. Doetsch, Prospective Identification and Purification of Quiescent Adult Neural Stem Cells from Their In Vivo Niche. *Neuron.* **82**, 545–559 (2014).
21. M. Tavazoie, L. Van der Veken, V. Silva-Vargas, M. Louissaint, L. Colonna, B. Zaidi, J. M. Garcia-Verdugo, F. Doetsch, A Specialized Vascular Niche for Adult Neural Stem Cells. *Cell Stem Cell.* **3**, 279–288 (2008).
22. R. Daneman, A. Prat, The Blood–Brain Barrier. *Cold Spring Harb. Perspect. Biol.* **7**, 1–23 (2015).
23. C. K. Tong, J. Chen, A. Cebrián-Silla, Z. Mirzadeh, K. Obernier, C. D. Guinto, L. H. Tecott, J. M. García-Verdugo, A. Kriegstein, A. Alvarez-Buylla, Axonal control of the adult neural stem cell niche. *Cell Stem Cell.* **14**, 500–511 (2014).
24. A. Kerever, E. Arikawa-Hirasawa, Optimal Extracellular Matrix Niches for Neurogenesis: Identifying Glycosaminoglycan Chain Composition in the Subventricular Neurogenic Zone. *Front. Neuroanat.* **15**, 4–10 (2021).
25. A. Kerever, F. Nagahara, K. Keino-Masu, M. Masu, T. H. van Kuppevelt, R. R. Vivès, E. Arikawa-Hirasawa, Regulation of fractone heparan sulfate composition in young and aged subventricular zone neurogenic niches. *Glycobiology.* **31**, 1531–1542 (2021).
26. F. Mercier, J. T. Kitasako, G. I. Hatton, Anatomy of the brain neurogenic zones revisited: Fractones and the fibroblast/macrophage network. *J. Comp. Neurol.* **451**, 170–188 (2002).
27. J. Kjell, J. Fischer-Sternjak, A. J. Thompson, C. Friess, M. J. Sticco, F. Salinas, J. Cox, D. C. Martinelli, J. Ninkovic, K. Franze, H. B. Schiller, M. Götz, Defining the Adult Neural

Stem Cell Niche Proteome Identifies Key Regulators of Adult Neurogenesis. *Cell Stem Cell.* **26**, 277–293 (2020).

28. P. Paez-Gonzalez, B. Asrican, E. Rodriguez, C. T. Kuo, Identification of distinct ChAT+ neurons and activity-dependent control of postnatal SVZ neurogenesis. *Nat. Neurosci.* **17**, 934–942 (2014).
29. S. Z. Young, C. A. Lafourcade, J.-C. Platel, T. V. Lin, A. Bordey, GABAergic striatal neurons project dendrites and axons into the postnatal subventricular zone leading to calcium activity. *Front. Cell. Neurosci.* **8**, 1–9 (2014).
30. G. U. Höglinger, P. Rizk, M. P. Muriel, C. Duyckaerts, W. H. Oertel, I. Caille, E. C. Hirsch, Dopamine depletion impairs precursor cell proliferation in Parkinson disease. *Nat. Neurosci.* **7**, 726–735 (2004).
31. J. B. Lennington, S. Pope, A. E. Goodheart, L. Drozdowicz, S. B. Daniels, J. D. Salamone, J. C. Conover, Midbrain dopamine neurons associated with reward processing innervate the neurogenic subventricular zone. *J. Neurosci.* **31**, 13078–13087 (2011).
32. A. Paul, Z. Chaker, F. Doetsch, Hypothalamic regulation of regionally distinct adult neural stem cells and neurogenesis. *Science (80-.).* **356**, 1383–1386 (2017).
33. D. A. Lim, A. Alvarez-Buylla, Adult neural stem cells stake their ground. *Trends Neurosci.* **37**, 563–571 (2014).
34. A. C. Delgado, A. R. Maldonado-Soto, V. Silva-Vargas, D. Mizrak, T. Von Känel, K. R. Tan, A. Paul, A. Madar, H. Cuervo, J. Kitajewski, C. S. Lin, F. Doetsch, Release of stem cells from quiescence reveals gliogenic domains in the adult mouse brain. *Science (80-.).* **372**, 1205–1209 (2021).
35. K. Obernier, A. Cebrian-Silla, M. Thomson, J. I. Parraguez, R. Anderson, C. Guinto, J. Rodas Rodriguez, J.-M. Garcia-Verdugo, A. Alvarez-Buylla, Adult Neurogenesis Is Sustained by Symmetric Self-Renewal and Differentiation. *Cell Stem Cell.* **22**, 221-234.e8 (2018).
36. G. Ponti, K. Obernier, C. Guinto, L. Jose, L. Bonfanti, A. Alvarez-Buylla, Cell cycle and lineage progression of neural progenitors in the ventricular-subventricular zones of adult mice. *Proc. Natl. Acad. Sci. U. S. A.* **110**, E1045–E1054 (2013).
37. S. Nagayama, R. Homma, F. Imamura, Neuronal organization of olfactory bulb circuits. *Front. Neural Circuits.* **8**, 1–19 (2014).
38. C. Lois, A. Alvarez-Buylla, Long-distance neuronal migration in the adult mammalian brain. *Science (80-.).* **264**, 1145–1148 (1994).
39. L. Bonfanti, P. Peretto, A. Merighi, A. Fasolo, Newly-generated cells from the rostral

migratory stream in the accessory olfactory bulb of the adult rat. *Neuroscience.* **81**, 489–502 (1997).

40. F. Doetsch, A. Alvarez-Buylla, Network of tangential pathways for neuronal migration in adult mammalian brain. *Proc. Natl. Acad. Sci. U. S. A.* **93**, 14895–14900 (1996).
41. X. Zhu, D. E. Bergles, A. Nishiyama, NG2 cells generate both oligodendrocytes and gray matter astrocytes. *Development.* **135**, 145–157 (2008).
42. B. Menn, J. M. Garcia-Verdugo, C. Yaschine, O. Gonzalez-Perez, D. Rowitch, A. Alvarez-Buylla, Origin of oligodendrocytes in the subventricular zone of the adult brain. *J. Neurosci.* **26**, 7907–7918 (2006).
43. I. Kazanis, K. A. Evans, E. Andreopoulou, C. Dimitriou, C. Koutsakis, R. T. Karadottir, R. J. M. Franklin, Subependymal Zone-Derived Oligodendroblasts Respond to Focal Demyelination but Fail to Generate Myelin in Young and Aged Mice. *Stem Cell Reports.* **8**, 685–700 (2017).
44. B. Nait-Oumesmar, L. Decker, F. Lachapelle, V. Avellana-Adalid, C. Bachelin, A. Baron-Van Evercooren, Progenitor cells of the adult mouse subventricular zone proliferate, migrate and differentiate into oligodendrocytes after demyelination. *Eur. J. Neurosci.* **11**, 4357–4366 (1999).
45. N. Picard-Riera, L. Decker, C. Delarasse, K. Goude, B. Nait-Oumesmar, R. Liblau, D. Pham-Dinh, A. Baron-Van Evercooren, Experimental autoimmune encephalomyelitis mobilizes neural progenitors from the subventricular zone to undergo oligodendrogenesis in adult mice. *Proc. Natl. Acad. Sci. U. S. A.* **99**, 13211–13216 (2002).
46. J. M. Parent, N. von dem Bussche, D. H. Lowenstein, Prolonged seizures recruit caudal subventricular zone glial progenitors into the injured hippocampus. *Hippocampus.* **16**, 321–328 (2006).
47. Y. L. Xing, P. T. Röth, J. A. S. Stratton, B. H. A. Chuang, J. Danne, S. L. Ellis, S. W. Ng, T. J. Kilpatrick, T. D. Merson, Adult neural precursor cells from the subventricular zone contribute significantly to oligodendrocyte regeneration and remyelination. *J. Neurosci.* **34**, 14128–14146 (2014).
48. C. Guglielmetti, J. Praet, J. R. Rangarajan, R. Vreys, N. De Vocht, F. Maes, M. Verhoye, P. Ponsaerts, A. Van der Linden, Multimodal imaging of subventricular zone neural stem/progenitor cells in the cuprizone mouse model reveals increased neurogenic potential for the olfactory bulb pathway, but no contribution to remyelination of the corpus callosum. *Neuroimage.* **86**, 99–110 (2014).
49. A. Gritti, L. Bonfanti, F. Doetsch, I. Caille, A. Alvarez-Buylla, D. A. Lim, R. Galli, J. M.

G. Verdugo, D. G. Herrera, A. L. Vescovi, Multipotent neural stem cells reside into the rostral extension and olfactory bulb of adult rodents. *J. Neurosci.* **22**, 437–445 (2002).

50. B. Malnic, P. A. Godfrey, L. B. Buck, The human olfactory receptor gene family. *Proc. Natl. Acad. Sci. U. S. A.* **101**, 2584–2589 (2004).
51. C. Mucignat-Caretta, M. Redaelli, A. Caretta, One nose, one brain: Contribution of the main and accessory olfactory system to chemosensation. *Front. Neuroanat.* **6**, 1–9 (2012).
52. T. Imai, Construction of functional neuronal circuitry in the olfactory bulb. *Semin. Cell Dev. Biol.* **35**, 180–188 (2014).
53. G. M. Shepard, W. R. Chen, C. A. Greer, in *The Synaptic Organization of the Brain* (Oxford Scholarship Online, 2004).
54. M. Apostolopoulou, T. R. Kiehl, M. Winter, E. Cardenas De La Hoz, N. C. Boles, C. S. Bjornsson, K. L. Zuloaga, S. K. Goderie, Y. Wang, A. R. Cohen, S. Temple, Non-monotonic Changes in Progenitor Cell Behavior and Gene Expression during Aging of the Adult V-SVZ Neural Stem Cell Niche. *Stem Cell Reports.* **9**, 1–17 (2017).
55. L. Oboti, G. Savalli, C. Giachino, S. De Marchis, G. C. Panzica, A. Fasolo, P. Peretto, Integration and sensory experience-dependent survival of newly-generated neurons in the accessory olfactory bulb of female mice. **29**, 679–692 (2009).
56. K. Mori, K. Kishi, H. Ojima, Distribution of Dendrites of Mitral, Displaced Mitral, Tufted, and Granule Cells in the Rabbit Olfactory Bulb. *J. Comp. Neurol.* **219**, 339–355 (1983).
57. M. T. Shipley, M. Ennis, Functional organization of olfactory system. *J. Neurobiol.* **30**, 123–176 (1996).
58. F. Imamura, H. Nagao, H. Naritsuka, Y. Murata, H. Taniguchi, K. Mori, A leucine-rich repeat membrane protein, 5T4, is expressed by a subtype of granule cells with dendritic arbors in specific strata of the mouse olfactory bulb. *J. Comp. Neurol.* **495**, 754–768 (2006).
59. H. Naritsuka, K. Sakai, T. Hashikawa, K. Mori, M. Yamaguchi, Perisomatic-targeting granule cells in the mouse olfactory bulb. *J. Comp. Neurol.* **515**, 409–426 (2009).
60. F. T. Merkle, L. C. Fuentealba, T. A. Sanders, L. Magno, N. Kessaris, A. Alvarez-Buylla, Adult neural stem cells in distinct microdomains generate previously unknown interneuron types. *Nat. Neurosci.* **17**, 207–214 (2014).
61. F. T. Merkle, Z. Mirzadeh, A. Varez-Buylla, Mosaic organization of neural stem cells in the adult brain. *Science (80-.).* **317**, 381–384 (2007).
62. T. Guo, G. Liu, H. Du, Y. Wen, S. Wei, Z. Li, G. Tao, Z. Shang, X. Song, Z. Zhang, Z. Xu, Y. You, B. Chen, J. L. Rubenstein, Z. Yang, Dlx1/2 are Central and Essential

Components in the Transcriptional Code for Generating Olfactory Bulb Interneurons. *Cereb. Cortex.* **29**, 4831–4849 (2019).

63. R. Batista-Brito, J. Close, R. Machold, G. Fishell, The Distinct Temporal Origins of Olfactory Bulb Interneuron Subtypes. **28**, 3966–3975 (2008).
64. S. Gribaudo, S. Bovetti, D. Garzotto, A. Fasolo, S. De Marchis, Expression and localization of the calmodulin-binding protein neurogranin in the adult mouse olfactory bulb. *J. Comp. Neurol.* **517**, 683–694 (2009).
65. M. S. Brill, J. Ninkovic, E. Winpenny, R. D. Hodge, I. Ozen, R. Yang, A. Lepier, S. Gascón, F. Erdelyi, G. Szabo, C. Parras, F. Guillemot, M. Frotscher, B. Berninger, R. F. Hevner, O. Raineteau, M. Götz, Adult generation of glutamatergic olfactory bulb interneurons. *Nat. Neurosci.* **12**, 1524–1533 (2009).
66. L. Petreanu, A. Alvarez-Buylla, Maturation and Death of Adult-Born Olfactory Bulb Granule Neurons: Role of Olfaction. *J. Neurosci.* **22**, 6106–6113 (2002).
67. M. Yamaguchi, K. Mori, Critical period for sensory experience-dependent survival of newly generated granule cells in the adult mouse olfactory bulb. *Proc. Natl. Acad. Sci. U. S. A.* **102**, 9697–9702 (2005).
68. A. Carleton, L. T. Petreanu, R. Lansford, A. Alvarez-Buylla, P. M. Lledo, Becoming a new neuron in the adult olfactory bulb. *Nat. Neurosci.* **6**, 507–518 (2003).
69. F. Lazarini, M. A. Mouthon, G. Gheusi, F. de Chaumont, J. C. Olivo-Marin, S. Lamarque, D. N. Abrous, F. D. Boussin, P. M. Lledo, Cellular and behavioral effects of cranial irradiation of the subventricular zone in adult mice. *PLoS One.* **4**, 1–11 (2009).
70. B. Winner, C. M. Cooper-Kuhn, R. Aigner, J. Winkler, H. G. Kuhn, Long-term survival and cell death of newly generated neurons in the adult rat olfactory bulb. *Eur. J. Neurosci.* **16**, 1681–1689 (2002).
71. J. C. Platel, A. Angelova, S. Bugeon, J. Wallace, T. Ganay, I. Chudotvorova, J. C. Deloulme, C. Béclin, M. C. Tiveron, N. Coré, V. N. Murthy, H. Cremer, Neuronal integration in the adult mouse olfactory bulb is a non-selective addition process. *Elife.* **8**, 1–21 (2019).
72. R. Fiorelli, K. Azim, B. Fischer, O. Raineteau, Adding a spatial dimension to postnatal ventricular-subventricular zone neurogenesis. *Development.* **142**, 2109–2120 (2015).
73. D. Mizrak, H. M. Levitin, A. C. Delgado, V. Crotet, J. Yuan, Z. Chaker, V. Silva-Vargas, P. A. Sims, F. Doetsch, Single-Cell Analysis of Regional Differences in Adult V-SVZ Neural Stem Cell Lineages. *Cell Rep.* **26**, 394-406.e5 (2019).
74. A. M. Falcão, J. A. Palha, A. C. Ferreira, F. Marques, N. Sousa, J. C. Sousa, Topographical

analysis of the subependymal zone neurogenic niche. *PLoS One.* **7**, 1–12 (2012).

75. R. E. Ventura, J. E. Goldman, Dorsal radial glia generate olfactory bulb interneurons in the postnatal murine brain. *J. Neurosci.* **27**, 4297–4302 (2007).
76. M. A. Hack, A. Saghatelyan, A. De Chevigny, A. Pfeifer, R. Ashery-Padan, P. M. Lledo, M. Götz, Neuronal fate determinants of adult olfactory bulb neurogenesis. *Nat. Neurosci.* **8**, 865–872 (2005).
77. M. Kohwi, N. Osumi, J. L. R. Rubenstein, A. Alvarez-Buylla, Pax6 is required for making specific subpopulations of granule and periglomerular neurons in the olfactory bulb. *J. Neurosci.* **25**, 6997–7003 (2005).
78. R. N. Delgado, D. A. Lim, Embryonic Nkx2.1-expressing neural precursor cells contribute to the regional heterogeneity of adult V-SVZ neural stem cells. *Dev. Biol.* **407**, 265–274 (2015).
79. K. M. Young, M. Fogarty, N. Kessaris, W. D. Richardson, Subventricular zone stem cells are heterogeneous with respect to their embryonic origins and neurogenic fates in the adult olfactory bulb. *J. Neurosci.* **27**, 8286–8296 (2007).
80. A. López-Juárez, J. Howard, K. Ullom, L. Howard, A. Grande, A. Pardo, R. Waclaw, Y. Y. Sun, D. Yang, C. Y. Kuan, K. Campbell, M. Nakafuku, Gsx2 controls region-specific activation of neural stem cells and injury-induced neurogenesis in the adult subventricular zone. *Genes Dev.* **27**, 1272–1287 (2013).
81. A. Alvarez-Buylla, M. Kohwi, T. M. Nguyen, F. T. Merkle, The heterogeneity of adult neural stem cells and the emerging complexity of their niche. *Cold Spring Harb. Symp. Quant. Biol.* **73**, 357–365 (2008).
82. M. Lemasson, A. Saghatelyan, J. C. Olivo-Marin, P. M. Lledo, Neonatal and adult neurogenesis provide two distinct populations of newborn neurons to the mouse olfactory bulb. *J. Neurosci.* **25**, 6816–6825 (2005).
83. I. Imayoshi, M. Sakamoto, T. Ohtsuka, K. Takao, T. Miyakawa, M. Yamaguchi, K. Mori, T. Ikeda, S. Itohara, R. Kageyama, Roles of continuous neurogenesis in the structural and functional integrity of the adult forebrain. *Nat. Neurosci.* **11**, 1153–1161 (2008).
84. M. Sakamoto, N. Ieki, G. Miyoshi, D. Mochimaru, H. Miyachi, T. Imura, M. Yamaguchi, G. Fishell, K. Mori, R. Kageyama, I. Imayoshi, Continuous postnatal neurogenesis contributes to formation of the olfactory bulb neural circuits and flexible olfactory associative learning. *J. Neurosci.* **34**, 5788–5799 (2014).
85. H. Takahashi, S. Yoshihara, A. Tsuboi, The Functional Role of Olfactory Bulb Granule Cell Subtypes Derived From Embryonic and Postnatal Neurogenesis. *Front. Mol. Neurosci.*

11, 1–11 (2018).

86. Y. Adam, A. Mizrahi, Long-term imaging reveals dynamic changes in the neuronal composition of the glomerular layer. *J. Neurosci.* **31**, 7967–7973 (2011).
87. C. Mirescu, J. D. Peters, L. Noiman, E. Gould, Sleep deprivation inhibits adult neurogenesis in the hippocampus by elevating glucocorticoids. *Proc. Natl. Acad. Sci. U. S. A.* **103**, 19170–19175 (2006).
88. Y. Zhao, L. Zhang, M. Wang, J. Yu, J. Yang, A. Liu, H. Yao, X. Liu, Y. Shen, B. Guo, Y. Wang, S. Wu, Anxiety Specific Response and Contribution of Active Hippocampal Neural Stem Cells to Chronic Pain Through Wnt/β-Catenin Signaling in Mice. *Front. Mol. Neurosci.* **11**, 1–11 (2018).
89. J. Brown, C. M. Cooper-Kuhn, G. Kempermann, H. Van Praag, J. Winkler, F. H. Gage, H. G. Kuhn, Enriched environment and physical activity stimulate hippocampal but not olfactory bulb neurogenesis. *Eur. J. Neurosci.* **17**, 2042–2046 (2003).
90. N. M. Unda, W. Portillo, R. Corona, R. G. Paredes, Sexual Stimulation Increases the Survival of New Cells in the Accessory Olfactory Bulb of the Male Rat. **10**, 1–8 (2016).
91. B. Leuner, E. R. Glasper, E. Gould, Sexual experience promotes adult neurogenesis in the hippocampus despite an initial elevation in stress hormones. *PLoS One.* **5** (2010), doi:10.1371/journal.pone.0011597.
92. R. Corona, S. Retana-Márquez, W. Portillo, R. G. Paredes, Sexual behavior increases cell proliferation in the rostral migratory stream and promotes the differentiation of the new cells into neurons in the accessory olfactory bulb of female rats. *Front. Neurosci.* **10**, 1–15 (2016).
93. G. K. Mak, E. K. Enwere, C. Gregg, T. Pakarainen, M. Poutanen, I. Huhtaniemi, S. Weiss, Male pheromone – stimulated neurogenesis in the adult female brain : possible role in mating behavior. *Nat. Neurosci.* **10**, 1003–1012 (2007).
94. T. Shingo, C. Gregg, E. Enwere, H. Fujikawa, R. Hassam, C. Geary, J. C. Cross, S. Weiss, Pregnancy-stimulated neurogenesis in the adult female forebrain mediated by prolactin. *Science (80-.).* **299**, 117–120 (2003).
95. C. M. Larsen, D. R. Grattan, Prolactin-induced mitogenesis in the subventricular zone of the maternal brain during early pregnancy is essential for normal postpartum behavioral responses in the mother. *Endocrinology.* **151**, 3805–3814 (2010).
96. L. Wei, M. J. Meaney, R. S. Duman, A. Kaffman, Affiliative behavior requires juvenile, but not adult neurogenesis. *J. Neurosci.* **31**, 14335–14345 (2011).
97. C. E. Feierstein, F. Lazarini, S. Wagner, M. M. Gabellec, F. de Chaumont, J. C. Olivo-

Marin, F. D. Boussin, P. M. Lledo, G. Gheusi, Disruption of adult neurogenesis in the olfactory bulb affects social interaction but not maternal behavior. *Front. Behav. Neurosci.* **4**, 1–17 (2010).

98. S. Bragado Alonso, J. K. Reinert, N. Marichal, S. Massalini, B. Berninger, T. Kuner, F. Calegari, An increase in neural stem cells and olfactory bulb adult neurogenesis improves discrimination of highly similar odorants. *EMBO J.* **38**, 1–13 (2019).
99. M. Sakamoto, I. Imayoshi, T. Ohtsuka, M. Yamaguchi, K. Mori, R. Kageyama, Continuous neurogenesis in the adult forebrain is required for innate olfactory responses. *Pnas*. **108**, 8479–8484 (2011).
100. L. Oboti, R. Schellino, C. Giachino, P. Chamero, M. Pyrski, T. Leinders-Zufall, F. Zufall, A. Fasolo, P. Peretto, Newborn Interneurons in the Accessory Olfactory Bulb Promote Mate Recognition in Female Mice. *Front. Neurosci.* **5**, 1–14 (2011).
101. L. M. Silver, *Mouse Genetics* (1995; http://www.informatics.jax.org/silver/chapters/6-2.shtml#6.2.3).
102. L. M. Silver, *Mouse Genetics* (1995; http://www.informatics.jax.org/silver/chapters/4-3.shtml).
103. R. F. Seegal, V. H. Denenberg, Maternal experience prevents pup-killing in mice induced by peripheral anosmia. *Physiol. Behav.* **13**, 339–341 (1974).
104. F. Lévy, A. Loctelli, V. Piketty, Y. Tillet, P. Poindron, Involvement of the Main But Not the Accessory Olfactory System in Maternal Behavior of Primiparous and Multiparous Ewes. *Physiol. Behav.* **57**, 97–104 (1975).
105. P. D. Morgan, C. A. P. Boundy, G. W. Arnold, D. R. Lindsay, The roles played by the senses of the ewe in the location and recognition of lambs. *Appl. Anim. Ethol.* **1**, 139–150 (1975).
106. J. J. Lepri, C. J. Wysocki, J. G. Vandenbergh, Mouse vomeronasal organ: Effects on chemosignal production and maternal behavior. *Physiol. Behav.* **35**, 809–814 (1985).
107. R. Corona, M. Meurisse, F. Cornilleau, C. Moussu, M. Keller, F. Lévy, Disruption of adult olfactory neurogenesis induces deficits in maternal behavior in sheep. *Behav. Brain Res.* **347**, 124–131 (2018).
108. C. Confavreux, M. Hutchinson, M. M. Hours, P. Cortinovis-Tourniaire, T. Moreau, Rate of Pregnancy-Related Relapse in Multiple Sclerosis. *Surv. Anesthesiol.* **339**, 285–291 (1999).
109. C. Gregg, V. Shikar, P. Larsen, G. Mak, A. Chojnacki, V. W. Yong, S. Weiss, White Matter Plasticity and Enhanced Remyelination in the Maternal CNS. *J. Neurosci.* **27**, 1812–1823 (2007).

110. K. Obernier, A. Alvarez-Buylla, Neural stem cells: origin, heterogeneity and regulation in the adult mammalian brain. *Development.* **146**, dev156059 (2019).

111. Z. Chaker, P. Codega, F. Doetsch, A mosaic world : puzzles revealed by adult neural stem cell heterogeneity. *WIREs Dev. Biol.* **5** (2016), doi:10.1002/wdev.248.

112. B. Winner, C. M. Cooper-Kuhn, R. Aigner, J. Winkler, H. G. Kuhn, Long-term survival and cell death of newly generated neurons in the adult rat olfactory bulb. *Eur. J. Neurosci.* **16**, 1681–1689 (2002).

113. D. A. Barrière, A. Ella, F. Szeremeta, H. Adriaensen, W. Même, E. Chaillou, M. Migaud, S. Même, F. Lévy, M. Keller, Brain orchestration of pregnancy and maternal behavior in mice: A longitudinal morphometric study. *Neuroimage.* **230** (2021), doi:10.1016/j.neuroimage.2021.117776.

114. L. Belnoue, S. Malvaut, E. Ladevèze, D. N. Abrous, M. Koehl, Plasticity in the olfactory bulb of the maternal mouse is prevented by gestational stress. *Sci. Rep.* **6**, 1–11 (2016).

115. P. Peretto, R. Schellino, S. De Marchis, A. Fasolo, The interplay between reproductive social stimuli and adult olfactory bulb neurogenesis. *Neural Plast.* **2014**, 1–11 (2014).

116. F. Nottebohm, The neural basis of birdsong. *PLoS Biol.* **3**, 0759–0761 (2005).

117. D. F. Sherry, J. S. Hoshooley, Seasonal hippocampal plasticity in food-storing birds. *Philos. Trans. R. Soc. B Biol. Sci.* **365**, 933–943 (2010).

118. J. M. Bin, S. N. Harris, T. E. Kennedy, The oligodendrocyte-specific antibody 'CC1' binds Quaking 7. *J. Neurochem.* **139**, 181–186 (2016).

119. L. C. Schmued, A rapid, sensitive histochemical stain for myelin in frozen brain sections. *J. Histochem. Cytochem.* **38**, 717–720 (1990).

120. M. Komitova, X. Zhu, D. R. Serwanski, A. Nishiyama, NG2 cells are distinct from neurogenic cells in the postnatal mouse subventricular zone. *J. Comp. Neurol.* **512**, 702–716 (2009).

121. J. S. Rosenblatt, Hormonal and nonhormonal regulation of maternal behavior: A theoretical survey. *Reprod. Nutr. Dev.* **20**, 791–800 (1980).

122. M. J. Soares, The prolactin and growth hormone families: Pregnancy-specific hormones/cytokines at the maternal-fetal interface. *Reprod. Biol. Endocrinol.* **2** (2004), doi:10.1186/1477-7827-2-51.

123. R. A. Augustine, S. R. Ladyman, D. R. Grattan, Introduction : metabolic adaptation to pregnancy Neuroendocrine regulation of body weight Leptin action in the CNS Mechanisms of leptin resistance Physiological regulation of leptin responses Changes in leptin action during pregnancy The melanocortin syst. *J. Physiol.* **586**, 387–397 (2008).

124. V. Silva-Vargas, A. R. Maldonado-Soto, D. Mizrak, P. Codega, F. Doetsch, Age-Dependent Niche Signals from the Choroid Plexus Regulate Adult Neural Stem Cells. *Cell Stem Cell*. **19**, 643–652 (2016).
125. T. K. Yokoyama, D. Mochimaru, K. Murata, H. Manabe, K. Kobayakawa, R. Kobayakawa, H. Sakano, K. Mori, M. Yamaguchi, Elimination of adult-born neurons in the olfactory bulb is promoted during the postprandial period. *Neuron*. **71**, 883–897 (2011).
126. K. S. Ravichandran, Beginnings of a Good Apoptotic Meal: The Find-Me and Eat-Me Signaling Pathways. *Immunity*. **35**, 445–455 (2011).
127. H. Shani-Narkiss, A. Vinograd, I. D. Landau, G. Tasaka, N. Yayon, S. Terletsky, M. Groysman, I. Maor, H. Sompolinsky, A. Mizrahi, Young adult-born neurons improve odor coding by mitral cells. *Nat. Commun.* **11**, 1–16 (2020).
128. P. Peretto, R. G. Paredes, *Social Cues, Adult Neurogenesis, and Reproductive Behavior* (2014; http://www.ncbi.nlm.nih.gov/pubmed/24830028).
129. N. Sanai, A. D. Tramontin, A. Quin˜ones-Hinojosa, N. M. Barbaro, N. Gupta, S. Kunwar, M. T. Lawton, M. W. McDermott, A. W. Parsa, Manuel-Garcia, M.-G. Verdugo, M. S. Berger, A. Alvarez-Buylla, Unique Astrocyte Ribbon in Adult Human Brain Contains Neural Stem Cells But Lacks Chain Migration. *Lett. to Nat.* **427**, 740–744 (2004).
130. N. Sanai, T. Nguyen, R. A. Ihrie, Z. Mirzadeh, H. H. Tsai, M. Wong, N. Gupta, M. S. Berger, E. Huang, J. M. Garcia-Verdugo, D. H. Rowitch, A. Alvarez-Buylla, Corridors of migrating neurons in the human brain and their decline during infancy. *Nature*. **478**, 382–386 (2011).
131. O. Bergmann, K. L. Spalding, J. Frisén, Adult Neurogenesis in Humans. *Cold Spring Harb Perspect Biol*. **7** (2015), doi:10.1101/cshperspect.a018994.
132. A. Ernst, K. Alkass, S. Bernard, M. Salehpour, S. Perl, J. Tisdale, G. Possnert, H. Druid, J. Frisén, Neurogenesis in the striatum of the adult human brain. *Cell*. **156**, 1072–1083 (2014).
133. E. L. Cameron, Pregnancy and olfaction: A review. *Front. Psychol.* **5**, 1–11 (2014).
134. X. Tian, B. Zhou, Strategies for site-specific recombination with high efficiency and precise spatiotemporal resolution. *J. Biol. Chem.* **296** (2021), doi:10.1016/j.jbc.2021.100509.
135. L. Hammelrath, S. Škokić, A. Khmelinskii, A. Hess, N. van der Knaap, M. Staring, B. P. F. Lelieveldt, D. Wiedermann, M. Hoehn, Morphological maturation of the mouse brain: An in vivo MRI and histology investigation. *Neuroimage*. **125**, 144–152 (2016).
136. X. Tan, H. Liao, L. Sun, M. Okabe, Z. Xiao, G. S. Dawe, Fetal Microchimerism in the

Maternal Mouse Brain: A Novel Population of Fetal Progenitor or Stem Cells Able to Cross the Blood–Brain Barrier? *Stem Cells*. **23**, 1443–1452 (2005).

137. X. X. Zeng, K. H. Tan, A. Yeo, P. Sasajala, X. Tan, Z. C. Xiao, G. Dawe, G. Udolph, Pregnancy-Associated Progenitor Cells Differentiate and Mature into Neurons in the Maternal Brain. **19** (2010).
138. M. O'Rourke, R. Gasperini, K. M. Young, Adult myelination: Wrapping up neuronal plasticity. *Neural Regen. Res.* **9**, 1261–1264 (2014).
139. R. A. Hill, A. Nishiyama, NG2 cells (polydendrocytes): Listeners to the neural network with diverse properties. *Glia*. **62**, 1195–1210 (2014).
140. D. Sakry, A. Neitz, J. Singh, R. Frischknecht, D. Marongiu, F. Binamé, S. S. Perera, K. Endres, B. Lutz, K. Radyushkin, J. Trotter, T. Mittmann, Oligodendrocyte Precursor Cells Modulate the Neuronal Network by Activity-Dependent Ectodomain Cleavage of Glial NG2. *PLoS Biol.* **12** (2014), doi:10.1371/journal.pbio.1001993.
141. X. Zhang, Y. Liu, X. Hong, X. Li, C. K. Meshul, C. Moore, Y. Yang, Y. Han, W. G. Li, X. Qi, H. Lou, S. Duan, T. Le Xu, X. Tong, NG2 glia-derived GABA release tunes inhibitory synapses and contributes to stress-induced anxiety. *Nat. Commun.* **12**, 1–18 (2021).
142. C. H. Kinsley, K. G. Lambert, Reproduction-induced neuroplasticity: Natural behavioural and neuronal alterations associated with the production and care of offspring. *J. Neuroendocrinol.* **20**, 515–525 (2008).
143. D. A. Barrière, A. Ella, F. Szeremeta, H. Adriaensen, W. Même, E. Chaillou, M. Migaud, S. Même, F. Lévy, M. Keller, Brain orchestration of pregnancy and maternal behavior in mice. *bio*R*xiv*, 1–43 (2020).
144. L. Zhuo, B. Sun, C. Zhang, A. Fine, Live Astrocytes Visualized by Green Fluorescent Protein in Transgenic Mice. *Dev. Biol.* **187**, 36–42 (1997).
145. O. Podgorny, N. Peunova, J. H. Park, G. Enikolopov, Triple S-Phase Labeling of Dividing Stem Cells. *Stem Cell Reports*. **10**, 615–626 (2018).
146. P. Bankhead, M. B. Loughrey, J. A. Fernández, Y. Dombrowski, D. G. McArt, P. D. Dunne, S. McQuaid, R. T. Gray, L. J. Murray, H. G. Coleman, J. A. James, M. Salto-Tellez, P. W. Hamilton, QuPath: Open source software for digital pathology image analysis. *Sci. Rep.* **7**, 1–7 (2017).
147. C. T. Rueden, J. Schindelin, M. C. Hiner, B. E. DeZonia, A. E. Walter, E. T. Arena, K. W. Eliceiri, ImageJ2: ImageJ for the next generation of scientific image data. *BMC Bioinformatics*. **18**, 1–26 (2017).

148. C. Hafemeister, R. Satija, Normalization and variance stabilization of single-cell RNA-seq data using regularized negative binomial regression. *bioRxiv*, 1–15 (2019).

149. Y. Hao, S. Hao, E. Andersen-Nissen, W. M. Mauck, S. Zheng, A. Butler, M. J. Lee, A. J. Wilk, C. Darby, M. Zager, P. Hoffman, M. Stoeckius, E. Papalexi, E. P. Mimitou, J. Jain, A. Srivastava, T. Stuart, L. M. Fleming, B. Yeung, A. J. Rogers, J. M. McElrath, C. A. Blish, R. Gottardo, P. Smibert, R. Satija, Integrated analysis of multimodal single-cell data. *Cell*. **184**, 3573-3587.e29 (2021).

Acknowledgement

For the last 5 1/2 years I have been able to work in a fantastic work environment.
-First and foremost, I am very grateful to my PhD advisor Prof. Dr. Fiona Doetsch, for giving me the opportunity to together explore the world of adult neural stem cells in the V-SVZ, for the supervision and for giving me room to grow.

-Special thanks go to my thesis committee members, Prof. Dr. Peter Scheiffele and Prof. Dr. Sebastian Jessberger, for their guidance and precious suggestions during the advisory meetings, and on other occasions.

-Dr. Zayna Chaker has a special place in my heart in her role as mentor, collaborator and colleague.

-Many thanks go to my colleagues Dr. Violeta Silva Vargas, Dr. Ana C. Delgado Fumero, Dr. Fabrizio Favaloro, Luca von Allmen, Thomas von Känel, Dr. Karol Kaiser, Valérie Crotet and Melvin Alappat for the honest and constructive feedback in lab meetings, and the many cheerful moments we spent together in- and outside the lab.

-Many thanks go to my collaborators abroad, Dr. Hunki Paek and Prof. Juan Tapia.

-Special thanks to go to Dr. Oliver Biehlmaier, Dr. Kai Schleicher, Dr. Sébastien Herbert, Dr. Alexia Loynton-Ferrand, Nikolaus Ehrenfeuchter, Laurent Guerard, Dr. Wolf Heusermann and Dr. Sara Roig., who go above and beyond to make image acquisition and analysis as smooth as possible.

-Many thanks to all the animal facility personnel for taking such good care of my mice, especially Zoe Grünig, Cassie Liss, Nicole Mosimann, David Überschlag and all those who work so hard in the background.

-I would also like to thank our administrative assistant, Nadine Iberl; Hafiza Shams of "Labware and Media preparation" and our floor managers Markus Meier and Markus Hämmerle for their daily work.

-Finally, I would like to thank my parents for enabling me to pursue a higher education and career of my choice, and for always believing in me.